# *In vivo* regulation of oligodendrocyte precursor cell proliferation and differentiation by AMPA-receptor subunit GluA2

Dissertation

zur Erlangung des Grades eines

Doktors der Naturwissenschaften

der Mathematisch-Naturwissenschaftlichen Fakultät

und

der Medizinischen Fakultät

der Eberhard-Karls-Universität Tübingen

vorgelegt

von

Ting-Jiun Chen
Taipei, Taiwan

19 March 2018

Tag der mündlichen Prüfung: .....

Dekan der Math.-Nat. Fakultät: Prof. Dr. W. Rosenstiel

Dekan der Medizinischen Fakultät: Prof. Dr. I. B. Autenrieth

1. Berichterstatter: Dr. M. Kukley

2. Berichterstatter: Prof. Dr. B. Antkowiak

Prüfungskommission: Dr. M. Kukley

Prof. Dr. B. Antkowiak

Prof. Dr. C. Schwarz

Dr. I. Ehrlich

**Erklärung / Declaration:**

Ich erkläre, dass ich die zur Promotion eingereichte Arbeit mit dem Titel:

"*In vivo* regulation of oligodendrocyte precursor cell proliferation and differentiation by AMPA-receptor subunit GluA2"

selbständig verfasst, nur die angegebenen Quellen und Hilfsmittel benutzt und wörtlich oder inhaltlich übernommene Stellen als solche gekennzeichnet habe. Ich versichere an Eides statt, dass diese Angaben wahr sind und dass ich nichts verschwiegen habe. Mir ist bekannt, dass die falsche Abgabe einer Versicherung an Eides statt mit Freiheitsstrafe bis zu drei Jahren oder mit Geldstrafe bestraft wird.

*I hereby declare that I have produced the work entitled "In vivo regulation of oligodendrocyte precursor cell proliferation and differentiation by AMPA-receptor subunit GluA2", submitted for the award of a doctorate, on my own (without external help), have used only the sources and aids indicated and have marked passages included from other works, whether verbatim or in content, as such. I swear upon oath that these statements are true and that I have not concealed anything. I am aware that making a false declaration under oath is punishable by a term of imprisonment of up to three years or by a fine.*

Tübingen, den ..... .....

Datum / Date Unterschrift /Signature

**Acknowledgments.**

I would like to thank my supervisor Dr. Maria Kukley for giving me the opportunity to pursue the doctoral study in her group. I appreciate Dr. Kukley's guidance and advice regarding the study, career and life experience. I would like to thank Dr. Ingrid Ehrlich for her helpful discussions. I also want to thank Andrea Gall for giving me the support in molecular biology.

I would also like to thank all the members of my group: Daniela, Nicole, Anahit, Balint, Ruxandra, Ramazan, Bartosz, and Friederike for your support and suggestion. I have a lot of fun with you and enjoy the time working with you.

Finally, I would like to thank my parents, my sisters, and my friends. I think I would not make it without their supports.

**Contributions.**

The major part of this thesis has been submitted as a manuscript. Several people contributed to this work and their contributions are listed below in detail.

I performed all the molecular biology with the initial help from Andrea Gall. I performed all the *in vivo* stereotaxic retroviral injection. For the electrophysiological recording, there are 76 cells included in this thesis. I recorded 63 cells, Bartosz Kula recorded 11 cells, and Balint Nagy recorded 2 cells. For electrophysiological analysis, Dr. Maria Kukley analyzed 12 cells, Bartosz Kula analyzed 16 cells, and I analyzed 48 cells.

I also performed all immunohistochemical experiments and confocal image acquisition. Whole immunohistochemistry analysis was performed by me. Part of the immunohistochemistry analysis was re-examined as a control by Ruxandra Barzan (10 animals) and Balint Nagy (4 animals).

**Content**

**List of Figures**

**List of Tables**

**Abstract.**

Oligodendrocyte precursor cells (OPCs), also known as NG2 cells, are widespread in the grey and white matter regions throughout the entire central nervous system. OPCs express functional 3-hydroxy-5-methyl-4-isoxazolepropionate receptors (AMPARs) and receive glutamatergic synaptic input from neurons. Transition of OPCs to the pre-myelinating stage is accompanied by the rapid removal of glutamatergic synaptic input, including downregulation of AMPARs. However, the functional role of AMPARs mediated synaptic signaling between neurons and OPCs remains unclear. The goal of my study was to alter the AMPARs mediated signaling between neurons and OPCs in the mouse corpus callosum *in vivo*, and to study the consequences of these alterations for proliferation and differentiation of OPCs. To reach this goal, I perturbed the properties of GluA2-containing AMPARs in callosal OPCs during the 2-3 postnatal weeks. Expression of $Ca^{2+}$-permeable or pore-dead GluA2-containing AMPARs altered $Ca^{2+}$ permeability of AMPARs in OPCs, and resulted in the increased proliferation and reduced differentiation of OPCs. Expression of GluA2 carboxyl-terminus, which is expected to affect the interaction between GluA2 subunit and AMPARs-binding-proteins and to perturb the trafficking of GluA2-containing AMPARs, did not change the $Ca^{2+}$ permeability of AMPARs but suppressed the differentiation of OPCs into OLs. The results of my study suggest that properties of AMPARs-mediated signaling between neurons and OPCs in the mouse corpus callosum are important for regulation of differentiation and proliferation of OPCs.

## 1. Introduction.

### *1.1. Oligodendrocytes (OLs) in the central nervous system (CNS).*

OLs were discovered by Pío del Río Hortega [1] and are considered as one type of glial cells in CNS. OLs produce large amount of membrane called myelin, which contains high proportion of lipids (70-80% dry mass) and small proportion of proteins (15-30% dry mass) [2]. Myelin wraps the axons multiple times, and these wraps are called internodes. The neighboring internodes on the same axon are separated by the nodes of Ranvier (Fig. 1-1). Myelin sheath acts as insulation. This insulation can reduce the attenuation of electrical signal due to its high electrical resistance and low electrical capacitance [3]. Therefore, myelination increases the conduction velocity of action potential propagating along the myelinated axon.

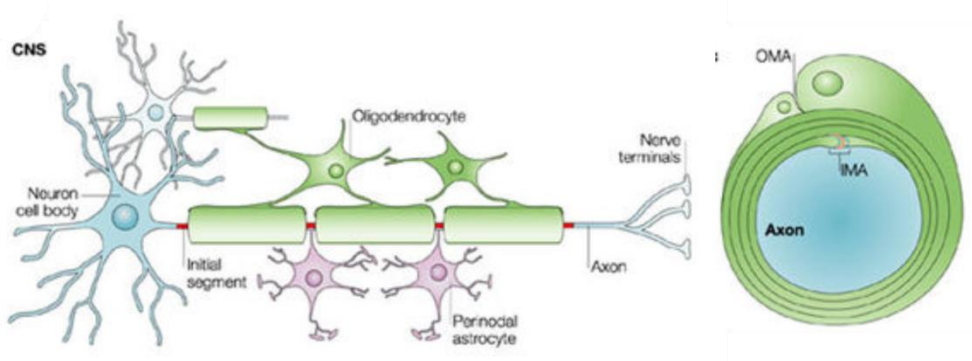


**Figure 1-1. Myelination from OLs in CNS.**

(*Left*) Myelin enwraps axon into several segments. (*Right*) Cross-section of myelinated axon. IMA: inner mesaxons; OMA: outer mesaxons. From [4], modified.

### *1.2. Development and molecular markers of the oligodendrocyte lineage cells.*

OLs are generated from the oligodendrocyte precursor cells (OPCs), also called NG2-cells and polydendrocytes. During development of the oligodendrocyte lineage, OPCs first differentiate into pre-myelinating OLs, which then further mature into OLs (Fig. 1-2). In brain slices, cells at each of these three developmental stages can be distinguished using different

immunohistochemical markers. OPCs are usually distinguished using labelling for neuron-glial antigen 2 (NG2, a product of chondroitin sulphate proteoglycan 4, *CSPG4* gene) and α-receptor for platelet-derived growth factor (PDGFR α) [5] (Fig. 1-2). Of note, in the brain the expression of NG2 is also found in pericytes, which are cellular components of bold vessels [6]. However, pericytes are morphologically different from OPCs: they are surrounded by basement membrane and extend their processes along and around the microvasculature [7]. With this typical morphological feature of NG2-positive pericytes, it is easily distinguished from OPCs which have complex morphology.

In rodents, differentiation of OPCs into pre-myelinating and subsequently into myelinating OLs starts from the early postnatal stage, reaches its peak during the second postnatal week (P7-P14), and continues till adulthood, in both gray and white matter areas of the brain [8-14] although the differentiation rate from OPCs to OLs declines with age [8, 14]. When OPCs start undergoing differentiation into pre-myelinating OLs, i.e. the intermediate stage in the lineage cells, NG2 and PDGFR α start getting downregulated, and the expression of these markers gets lost when the cells become OLs. At the same time, during the process of differentiation, other markers such as proteolipid protein (PLP)/DM20, immature OL antigen O4, galactocerebroside O1, and CC1 (adenomatous polyposis coli, CC1 clone) appear in the pre-myelinating OLs and OLs [15] (Fig. 1-2). In the final stage of OLs maturation, myelinating OLs express myelin basic protein (MBP), myelin associated glycoprotein (MAG), and myelin oligodendrocyte glycoprotein (MOG) [15-17]. Majority of the myelin proteins are restricted to the myelin sheaths, and therefore, anti-MBP, anti-MAG and anti-MOG antibodies are often used to label myelin sheathes in immunohistochemical experiments [15]. For quantification of OLs, other antibodies are usually used, e.g. anti-APC, which is a protein expressed in the cell body of OL.

Pre-myelinating OLs represent an intermediate stage between OPC and OLs. One approach to distinguish them in brain slices is to perform co-labelling for NG2 and CC1. Both markers are co-expressed in pre-myelinating OLs, but the labelling for NG2 is weaker than in OPCs and labelling for CC1 is weaker than in OLs [18]. Recently, a new maker for newly forming OLs, ecto-nucleotide pyrophosphatases/phosphodiesterases 6 (Enpp6), was discovered [19, 20]. Enpp6 is mainly found in early developing OLs. Enpp6 start to express in the cell after the maker of

OPCs extinguishes and expression of Enpp6 overlaps with the onset of OLs marker [19, 21]. Therefore, Enpp6 may be useful for the detection of pre-myelinating OLs.

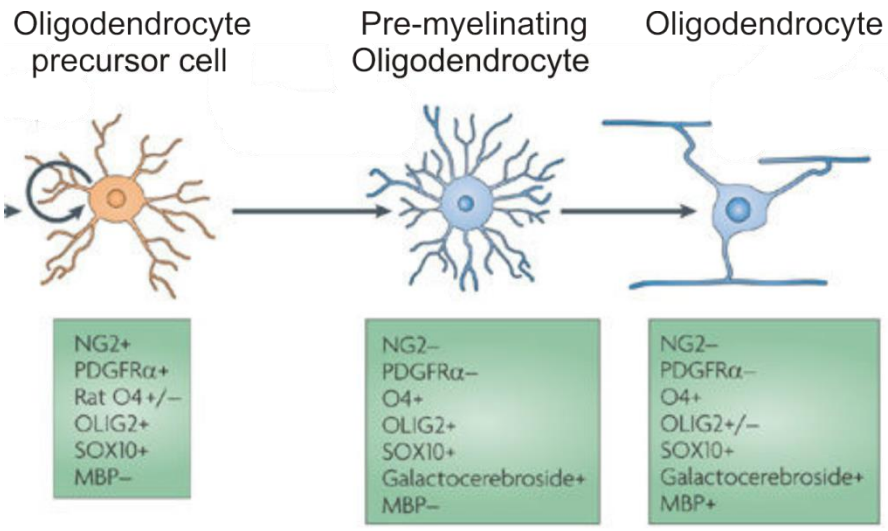


**Figure 1-2. Schematic drawing showing the development of OL lineage.**

The markers in different stages of lineage cells are listed in the rectangles below each stage of cells. From [22], modified.

*1.3. OPCs possess electrophysiological properties.*

OPCs are considered special within the oligodendrocyte lineage because they combine properties of proliferating progenitors, mature glial cells, and neurons. OPCs are widely spread in the white and grey matter area of the CNS and constitute 2-9 % of total cells in the adult rodent brain [23]. The discovery of OPCs goes back to 1983, when it has been demonstrated that oligodendrocyte-type-2 astrocyte (O-2A) progenitor cells purified from rat optic nerve were capable of differentiating into oligodendrocytes in culture system [24]. O-2A progenitors in culture co-express NG2 proteoglycan and PDGFR α, and later on it has been found that these markers are expressed by OPCs in brain slices [5].

Many studies demonstrated that OPCs possess ion channels including voltage-gate $K^+$ and $Na^+$ channels [25]. According to the RNA-sequencing transcriptome data, the mRNA level of $Kir_{4.1}$ is high in OPCs [20]. $Kir_{4.1}$ is an inwardly rectifying $K^+$ channel and expressed predominantly in glial cells in CNS [26]. Indeed, when the hyperpolarizing voltage steps were recorded from

OPCs, inward $K^+$ currents were observed [27-29]. The density of inward $K^+$ currents in subcortical white matter OPCs was lower than in cortical OPCs although the variations of inward $K^+$ currents density in cortical OPCs was high [28]. The functional role of $Kir_{4.1}$ in OPCs is unknown. Apart from inward $K^+$ currents, voltage-gated outward $K^+$ currents were also recorded in OPCs when depolarizing voltage steps were applied [27, 29-32]. The outward $K^+$ currents contained two components: sustained $K^+$ currents sensitive to tetraethylammonium [25, 29, 30, 32] and transient $K^+$ currents sensitive to 4-aminopyridine [25, 29, 32]. Voltage-gated $K^+$ channels have been suggested to contribute to the regulation of OPCs proliferation [33, 34].

Similar to neurons, OPCs also express voltage-gated $Na^+$ channels [28, 31, 32, 35-37]. Furthermore, when depolarizing currents were injected to OPCs during current clamp recording, the "immature" spike-like events with small amplitude could be recorded [28, 37]. The study of Karadottir et al. [36] revealed that OPCs were heterogeneous with respect to the expression of voltage-gated $Na^+$ channels. One group of OPCs was devoid of voltage-gated $Na^+$ channels; another group of OPCs expressed voltage-gated $Na^+$ channels and generated action potentials upon depolarizing current injection [36]. Heterogeneity of OPCs with respect to the expression of voltage-gated $Na^+$ channels was also reported by another group [38]. The authors showed that one-third of non-dividing OPCs generated action potential when depolarized the cell [38]. In the population of dividing OPCs, the majority of cells (75.9%) generated spike-like events with small amplitude, 18.9% of cells generated true action potentials, and the remaining 5.2% of cells did not produce any spikes even depolarized the cell to 0 mV [38].

Functional role of ion channels in OPCs is still not fully understood. Interestingly, voltage-gated ion channels were not detected in mature OLs [31, 37], suggesting that ion channels are likely involved in OPCs development and/or survival.

*1.4. Glutamate receptor in OPCs.*

In addition to expression of complex set of voltage-gated ion channels, OPCs also express functional glutamate receptors (see below). Two groups of glutamate receptors are known: ionotropic and metabotropic. Ionotropic glutamate receptors are the ion channels which are directly activated by the glutamate binding to the receptors. Metabotropic glutamate receptors are G-protein-coupled receptor which are also activated by glutamate binding but transduce the

signals via G-proteins. Ionotropic glutamate receptors encompass three types of receptors named by their selective agonist: N-methyl-D-aspartate (NMDA), 3-hydroxy-5-methyl-4-isoxazolepropionate (AMPA), and kainate receptor. Metabotropic glutamate receptors are composed of 8 subtypes and are categorized into 3 groups according to their sequencing homology, signaling pathway, and pharmacology [39-41].

OPCs express both ionotropic and metabotropic receptors for glutamate, but the ionotropic glutamate receptors have been most extensively studied in these cells so far. Ionotropic glutamate receptors have been discovered in OPCs in 1990 using whole-cell patch-clamp recordings combined with pressure-application of glutamate onto O-2A progenitors acutely isolated from P7 rat optic nerve [42]. In these experiments inward currents were recorded in O-2A cells (clamped at -80 mV) upon application of 200 µM glutamate (Fig. 1-3 a). Glutamate-induced inward currents were blocked by 20 µM 6-cyano-7-nitroquinoxaline-2,3-dione (CNQX), a competitive AMPA/kainate receptor antagonist (Fig. 1-3 a). Furthermore, inward currents could also be activated in O-2A cells upon application of 100 µM kainate (agonist for kainate receptor) or 100 µM quisqualate (a potent AMPARs agonist) (Fig. 1-3 b, c). At positive holding potentials of 20, 40, and 60 mV, application of 100 µM glutamate resulted in outward currents in O-2A cells (Fig. 1-3 b, c) and the reversal potential of the current was close to zero mV. These data suggested that O-2A progenitors express functional AMPA/kainate receptors [42].

In the follow-up studies, functional glutamate receptors were found in OPCs (at that time called "complex glial cells") from mouse hippocampal slices [43]. In these experiments, application of 1 mM glutamate or 1mM kainate to the bath activated inward currents in "complex glial cells"clamped at -70 mV [43]. However, application of 5 mM NMDA via the bath failed to elicit the response [43]. In another study, it has been shown that glial precursor cells, presumably OPCs, in the rat corpus callosum also express AMPA-type glutamate receptors [44]. Co-application of 30 µM AMPA and 100 µM cyclothiazide (CTZ), a blocker for AMPARs desensitization [45, 46], resulted in the enhancement of AMPA-induced currents in these cells [44]. Taken together, these findings from different research groups showed that functional AMPARs are expressed in OPCs in various brain regions and can be activated by their agonists.

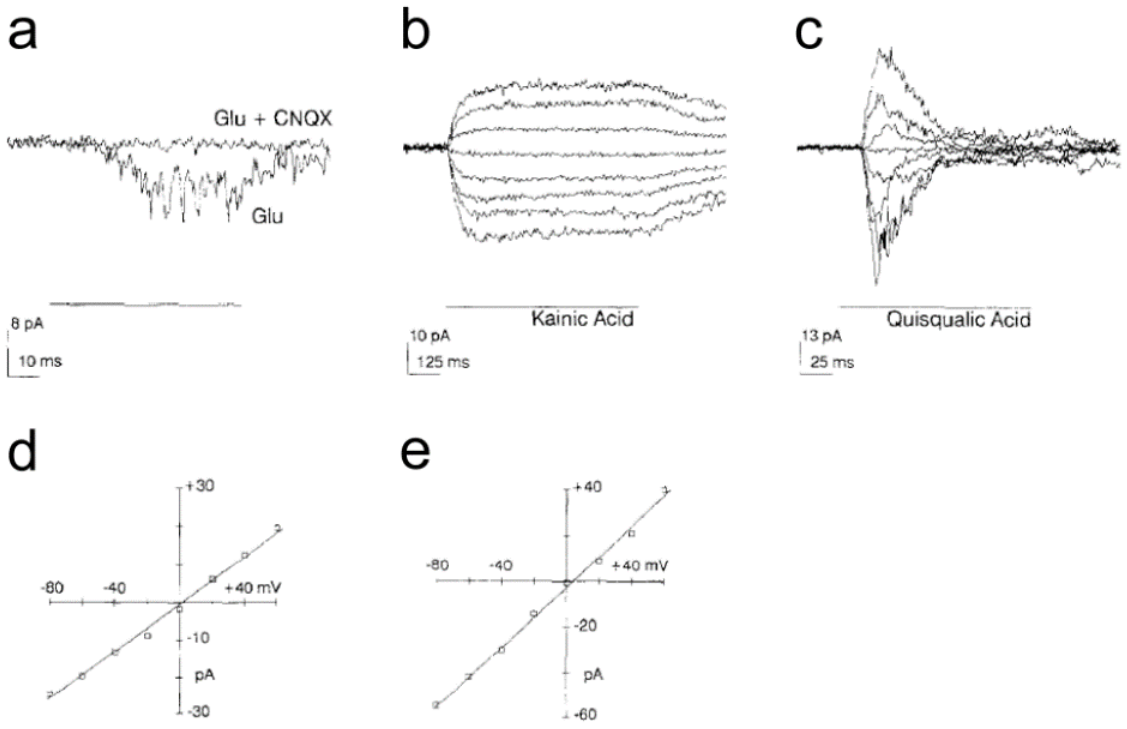


**Figure 1-3. Activation of glutamate receptors in O-2A progenitors.**

(a) Acutely isolated O-2A progenitors are whole-cell voltage-clamped at -80 mV and inward currents are elicited by glutamate puff. (b and c) Currents responses are elicited by kainite and quisqualate puff from -80 mV to +60 mV in 20 mV increments. (d and e) Elicited peak currents in (b) and (c) are plotted to the corresponding voltage. From [42], modified.

*1.5. Properties and subunit composition of AMPARs in OPCs.*

In neurons, AMPARs are tetramers and composed of four subunits: GluA1, GluA2, GluA3, and GluA4 (also called GluR1-4 or GluRA-D) [47]. Each of the subunit contains an extracellular N-terminus, an intracellular C-terminus, and four transmembrane domains (Fig. 1-4 a). The majority of AMPARs is hetero-tetramers and is assembled from a combination of GluA1/GluA2 or GluA2/GluA3 subunits [48, 49]. The RNA for GluA2 subunit of AMPARs can be edited at the Q/R site resulting in substitution of glutamine (Q) with arginine (R) in the transmembrane domain II of the GluA2 subunit (Fig. 1-4 a). GluA2 subunit determines many important properties of AMPARs including kinetic of the channels, single-channel conductance, and $Ca^{2+}$

permeability [50]. Edited GluA2 subunit forms heteromers with other subunits of AMPARs, these receptors are impermeable to $Ca^{2+}$ (Fig. 1-4 b); while AMPARs containing un-edited/no GluA2 subunit are permeable to $Ca^{2+}$ and $Zn^{2+}$ [51-54].

GluA2-lacking AMPARs or AMPARs containing unedited GluA2 subunit show inwardly rectifying current-voltage (I-V) relationship (Fig. 1-5 a). This effect is attributed to the intracellular polyamines which block the ionic flow through the channels at positive potentials [55-58]. On the contrary, due to the positive charge of arginine residue at the Q/R editing site of the GluA2 subunit, AMPARs containing edited GluA2 limit the passage of divalent ions through the channels, rendering the receptors $Ca^{2+}$-impermeable. I-V relationship of these receptors displays linearity (Fig. 1-5 b). Therefore, recording AMPAR-mediated currents and constructing the I-V relationship allow estimating the presence of edited GluA2 subunit within AMPARs in a given cell. To compare the changes in the rectification of I-V relationship of AMPARs in the cells under different conditions (e.g. different age of animals), the calculation of rectification index is widely used. In general, rectification index is calculated: (1) the peak amplitude of AMPARs EPSCs at positive holding potential (+40 mV or +50 mV) divided by the peak amplitude of AMPARs EPSCs at negative holding potential (from -60 mV to -90 mV); (2) the peak amplitude of AMPARs EPSCs at negative holding potential (from -60 mV to -90 mV) divided by the peak amplitude of AMPARs EPSCs at positive holding potential (+40 mV or +50 mV).

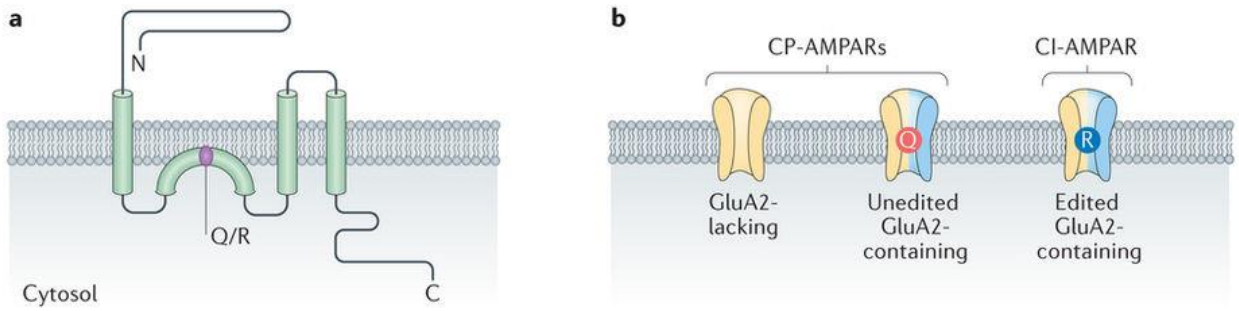


**Figure 1-4. Structure of AMPARs and the property of AMPARs**

(a) Schematic drawing showing a topology of the AMPAR subunit. Purple circle denotes Q607R editing in the GluA2 subunit. (b) (*Left*) AMPARs lacking GluA2 subunit (receptor showing in light yellow represent non-GluA2 subunits). (*Middle*) AMPARs containing GluA2 subunits (light blue) in unedited from (Q in red) also permeates to $Ca^{2+}$. (*Right*) AMPARs containing GluA2 subunits with RNA edited at 607 to arginine (R in dark blue) are $Ca^{2+}$-impermeable. From [59].

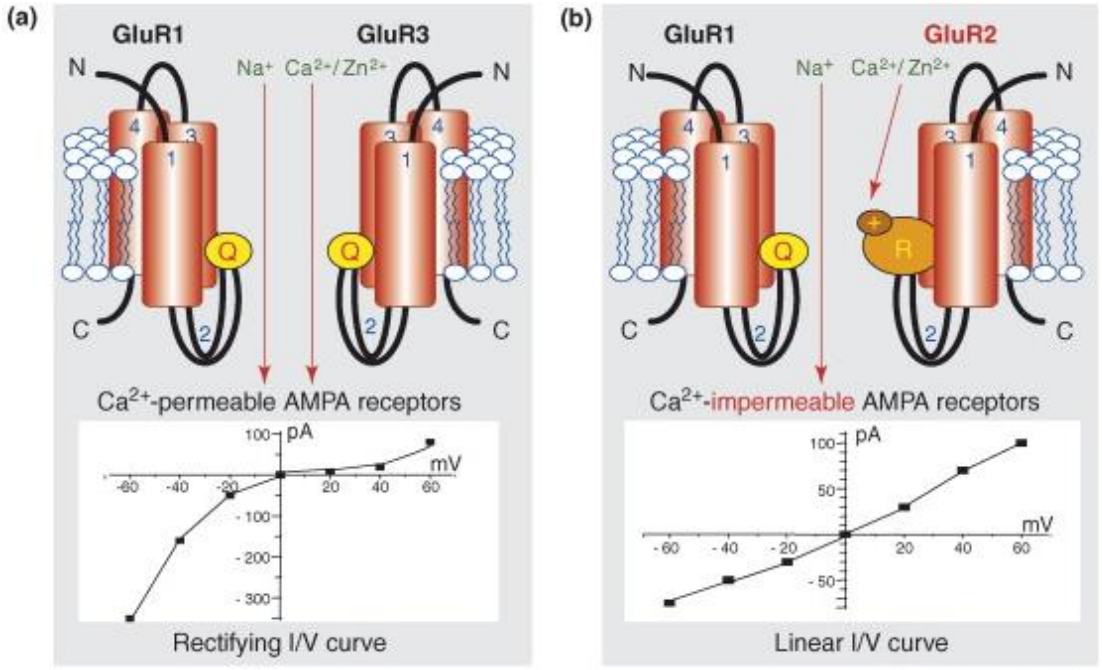


**Figure 1-5. $Ca^{2+}$ permeability of AMPARs is examined by the I-V relationship.**

(a) GluA2-lacking AMPARs permeate to $Ca^{2+}$ and displays inward rectifying I-V relationship while polyamine is present. (b) GluA2-containing AMPARs are $Ca^{2+}$ permeable and exhibits the linear I-V relationship. The heteromeric GluA2 AMPAR channels restrain the ionic flow of $Ca^{2+}$ and $Zn^{2+}$ resulting from the positive charge of R at the Q/R RNA editing site. From [60].

Up to date, several studies have reported the subunits of AMPARs at the messenger ribonucleic acid (mRNA) and protein level in OPCs. Northern blot, real-time polymerase chain reaction (Real-Time PCR), reverse transcription polymerase chain reaction (RT-PCR), RT-PCR combining Southern blot, RNA-Sequencing, and in situ hybridization (ISH) provided the evidence that mRNA of GluA1-GluA4 are present in the purified O-2A progenitor cells and oligodendroglial lineage from mouse or rat, CG-4 progenitor cell line, rat forebrain, or mouse subcortical white matter [20, 61-65]. Some reports indicated that GluA2-4 mRNA were present in OPCs at the high level [61, 64] but the GluA1 mRNA was low [61, 64, 65], or not detected at all [61]. Furthermore, immunolabeling, Western blot, and immunoprecipitation combined with Western blot showed that GluA1-GluA4 proteins were present in purified O-2A progenitor cells, and in OPCs purified from the developing rodent brain [66-71], mouse cerebellum, and several other regions of rat brain [70, 72]. Consistent with the low level of mRNA for GluA1 subunit, the GluA1 protein level was also low [69].

GluA2 subunit of AMPARs is critical subunit because it determines the properties of AMPARs as mentioned above (introduction part of 1.5). Currents induced in cultured purified OPCs by fast application of 500 µM kainate displayed linear I-V relationship suggesting that edited GluA2 subunit is present in the tetrameric AMPARs [73]. Currents triggered in purified O-2A progenitor cells by pressure ejection of 100 µM kainate or 100 µM quisqualate also showed linear I-V relationship (Fig. 1-3 c). These findings are in agreement with the results of RT-PCR showing that purified OPCs contain mRNA for edited GluA2 subunit [66]. Taken together, GluA1-GluA4 subunits of AMPARs are present in OPCs but likely differ in their expression level.

*1.6. OPCs form synaptic connections with neurons and receive glutamatergic synaptic input from neurons.*

When AMPARs were first discovered in OPCs, AMPARs-mediated currents were activated by the application of AMPARs agonists via the bath or using pressure-induced application systems [42, 66, 73]. However, it was still unclear how AMPARs in OPCs are activated *in vivo*. The first discovery illustrating that these receptors are activated by glutamate which is synaptically released from was published by Bergels et al. in 2000 [74]. The authors performed whole-cell

voltage clamp recordings from NG2-positive OPCs in hippocampal slices and recorded inward currents upon afferent excitatory axonal stimulation. These evoked currents were blocked by 5 μM 2,3-dihydroxy-6-nitro-7-sulfamoyl-benzo [f] quinoxaline (NBQX), a competitive antagonist for AMPA/kainate receptors (Fig. 1-6 a), and by 10 μM **(**1-(4-Aminophenyl)-4-methyl-7,8-methylenedioxy-5H-2,3-benzodiazepine hydrochloride (GYKI 52466), a non-competitive antagonist of AMPARs. These evoked currents were enhanced by the application of 100 μM CTZ, a substance potentiating AMPAR-mediated currents by preventing desensitization of AMPARs [45, 46]. The results of these experiments indicated that recorded axon-OPC currents were mediated by AMPARs, and therefore these currents were called neuron-glia excitatory postsynaptic currents, EPSCs [74]. In addition to evoked EPSCs, AMPARs-mediated miniature EPSCs (mEPSCs) could be recorded in hippocampal OPCs, similarly to neurons. These currents occur in response to the release of single neurotransmitter-filled vesicles from the presynaptic axons and subsequent binding of the neurotransmitter to the postsynaptic receptors in OPCs (Fig. 1-6 b). Both evoked EPSCs and mEPSCs (Fig. 1-6 c) recorded in hippocampal OPCs had fast rise and decay time constant: rise time: 259±15 μs (20-80%) for mEPSCs and 1.21±0.09 ms for evoked EPSCs [74]; decay time constant: 985±58 μs (range from 700-1250 μs) for mEPSCs [74], as expected for synaptic currents.

In addition to electrophysiological evidence for synaptic input from neurons to OPCs, data from electron microscopy also revealed that OPCs form synapses with neurons [74]. Thus, it has been demonstrated that processes of OPCs filled with biocytin are directly opposed to the vesicle-filled axonal terminals (Fig. 1-7).

Taken together, electrophysiological and ultrastructural data demonstrated that OPCs in hippocampus establish synaptic structures with neurons and receive excitatory glutamatergic AMPAR-mediated synaptic input from neurons.

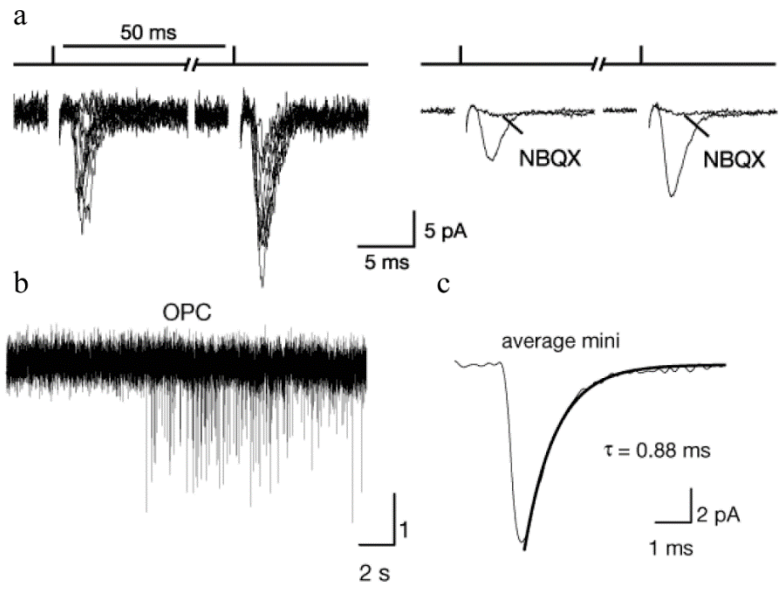


**Figure 1-6. EPSCs in OPCs are mediated by AMPARs.**

(a) (*Left*) Paired stimuli evoked inward currents in OPCs. (*Right*) These currents are blocked by NBQX. (b) Bursts of mEPSCs observed in OPCs are elicited by application of neurotoxin pardaxin. (c) Averaged time course of mEPSC obtained from OPCs. The averaged rise time is 295±15 μs and decaying constant is 983±58 μs. From [74], modified.

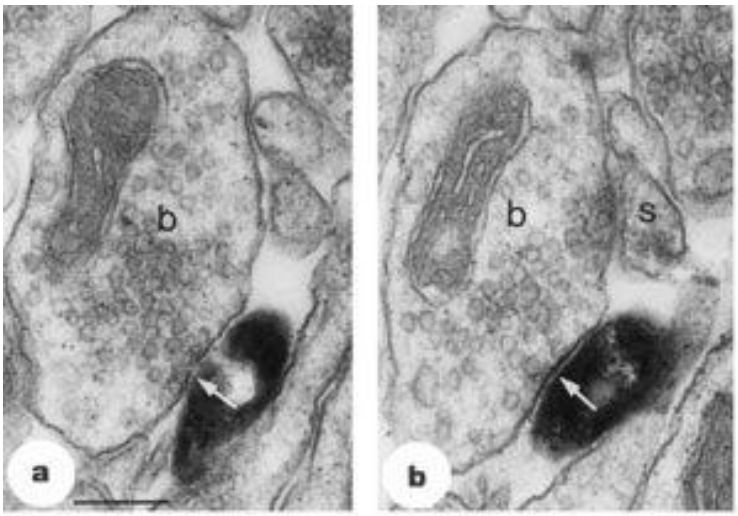


**Figure 1-7. The formation of axon terminals and OPCs.**

(a-b) Two serial sections of images from electron microscope illustrates that the process of OPC labeled with biocytin (black) is apposed to the bouton. (b) forming like a synapse (arrow). From [74], modified.

Studies published later demonstrated that the formation of neuron-OPC synapses also takes place in rodent white matter, i.e. corpus callosum and optic nerve ([75, 76]). First, evoked synaptic currents could be recorded in white matter OPCs upon axonal electrical stimulation [75, 76]. The kinetics of evoked currents was fast: rise time$_{20\text{-}80\%}$: 655±44 μs, and decay time constant $\tau_{decay}$: 1.9±0.2 ms [75], similar to neuronal EPSCs and neuron-OPC EPSCs in the hippocampus [74]. Furthermore, evoked neuron-OPC synaptic currents in white matter were blocked by the antagonists of AMPARs indicating that they are mediated by AMPARs. Evoked responses were abolished by application of 0.5 μM tetrodotoxin (TTX) which blocks voltage-gated $Na^+$ channels and abolishes axonal action potentials, suggesting the glutamate release at neuron-OPC synapses in white matter is activity-dependent. Second, AMPARs-mediated mEPSCs with rapid kinetics (rise time: 330±55 μs; $\tau_{decay}$: 1.1±0.2 ms) could also be recorded in white matter OPCs. Third, anatomical synaptic structures have been described between white matter axons and OPC processes [75, 76]. Electron microscopic analysis demonstrated that axonal and OPC processes membrane are located in a close parallel opposition. Clear vesicles are accumulated in the axon close to the axonal membrane [75]. In addition, immunofluorescent and electron microscopic evidence showed that type 1 vesicular glutamate transporter (VGLUT1) could be found inside white matter axons, close to the axonal membrane opposing the OPC processes [76]. VGLUT1 is one of three VGLUTs expressed by glutamatergic neurons [77]; it is responsible for packing glutamate into synaptic vesicles in the presynaptic terminals [78].

In subsequent studies, glutamatergic synapses between neurons and OPCs were also discovered in different regions of the rodent brain, including cerebral cortex, cerebellum, brain stem, and ventrobasal thalamus [79-82]. In addition, glutamatergic neuron-OPCs synaptic currents were also recorded in human brain [83]. In that study, the authors had access to human hippocampal tissue surgically removed from the patients with pharmacoresistant temporal lobe epilepsy. They recorded OPCs in the fimbria and induced glutamatergic mEPSCs in OPCs using application of 100 μM Ruthenium Red which induces vesicular release of glutamate from the presynaptic sites [83].

*1.7. The changes in the $Ca^{2+}$ permeability of AMPARs in OPCs.*

During development and also in the adult brain many OPCs effectively differentiate into oligodendrocytes. At the same time, many OPCs remain un-differentiated. Surprisingly, neuron-OPC synapses are also observed in mature animals [74, 84] (Fig. 1-8), and glutamatergic synaptic currents can be elicited not only in juvenile (P7) and adolescent (P21), but also in the adult (P66) animals. In each case, the currents are abolished by 5 μM NBQX application indicating that they are mediated by AMPARs [74].

It has been reported that the subunit composition of synaptic AMPARs in OPCs changes with age of the animal [76] and depends on the brain region. For instance, in the corpus callosum of young rodents, I-V relationship of axo-glial currents recorded in OPCs displays linearity (Fig. 1-9 a), suggesting that callosal OPCs express GluA2-containing $Ca^{2+}$-impermeable AMPARs [75, 76]. In contrast to young animals, I-V relationship of EPSCs in callosal OPCs from adult animals (P42-52) shows marked inward rectification (Fig. 1-9 b), indicating that GluA2-lacking $Ca^{2+}$-permeable AMPARs are expressed in callosal OPCs later in development [76].

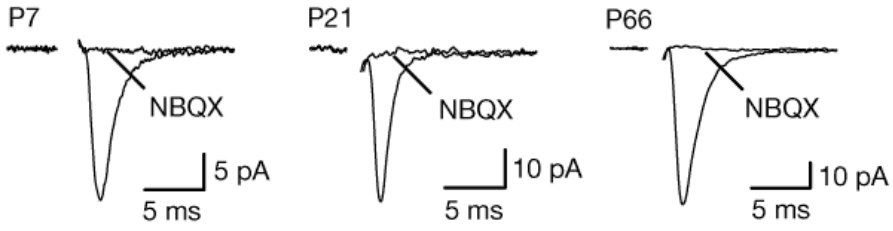


**Figure 1-8. Synaptic responses are evoked in OPCs at P7, P21, and P66.**

OPC from hippocampal slice is whole-cell voltage-clamped at different age of animal. Evoked EPSCs upon axonal stimulation from OPCs are blocked by NBQX. From [74], modified.

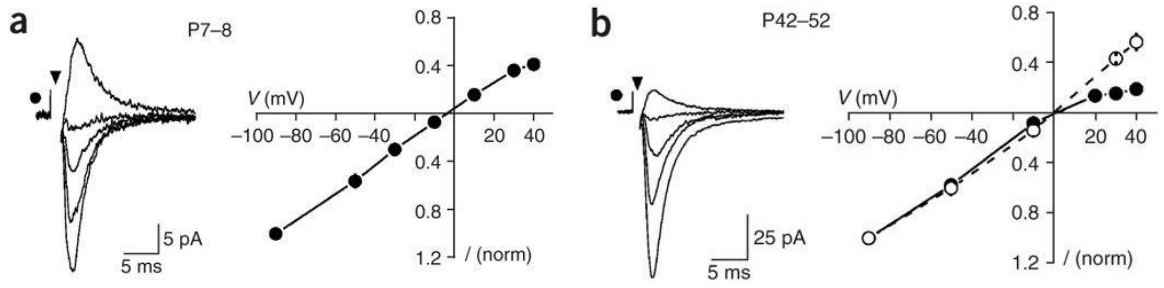


**Figure 1-9. OPCs in adult corpus callosum express GluA2-lacking AMPARs and permeate to $Ca^{2+}$.**

(a) *(Left)* The traces illustrate the evoked EPSCs recorded in a callosal OPC with an internal solution containing spermine at holding potential of -90, -50, -10, and 30 mV. (Right) I-V relationship of evoked axon-OPC EPSCs recorded in OPC from P7-8 animals. (b) Same as in (a) but from P42-52 mature animals. Note that filled and open circles in the I-V relationship represent the present and absent of spermine in the internal solution. From [76].

In hippocampal OPCs, changes in the $Ca^{2+}$ permeability of synaptic AMPARs during development are different from those in callosal OPCs. In the study of Ge et al. [85], the authors examined rectification of evoked EPSCs by calculating the rectification index (as mentioned in part 1.5). The rectification index in this study was the ratio of the current amplitude recorded at a negative potential (e.g. -60 mV) and the current amplitude recorded at a positive potential (e.g. +40 mV). In this case, theoretically, if the I-V relationship is linear, the rectification index will be close to 1.5, meaning that AMPARs are $Ca^{2+}$-impermeable. If the I-V relationship shows inwardly rectification, the rectification index should be larger than 1.5 depending on the currents recorded at +40 mV, meaning that they are $Ca^{2+}$-permeable AMPARs. In young animals at P8-P10, the rectification index was higher than that at P13-15 and P19-21(Fig. 1-10 a). In addition, upon application of 1-naphthyl acetyl-spermine (NAS), an analog of Joro spider toxin which is specific blocker for $Ca^{2+}$-permeable AMPARs [86], the axon-OPC EPSCs elicited by the stimulation of Schaffer collaterals, are inhibited stronger at P7-P10 than P15-P21 (Fig. 1-10 b). This indicates that in the early developmental stage, EPSCs in hippocampal OPCs are mediated by $Ca^{2+}$-permeable AMPARs, but during aging AMPARs become $Ca^{2+}$ impermeable [85]. Taken together, $Ca^{2+}$ permeability of synaptic AMPARs in OPCs gets altered with age but the changes in $Ca^{2+}$ permeability (from $Ca^{2+}$-impermeable to $Ca^{2+}$-permeable and vice versa) of AMPARs depends on the brain region. The reasons for these differences remain unclear so far. It is

possible that AMPAR-mediated signaling in OPCs in different brain regions have different roles, or that $Ca^{2+}$ permeability of synaptic AMPARs depends on the cellular environment, i.e. neuronal bodies in the hippocampus vs. only axons in the corpus callosum.

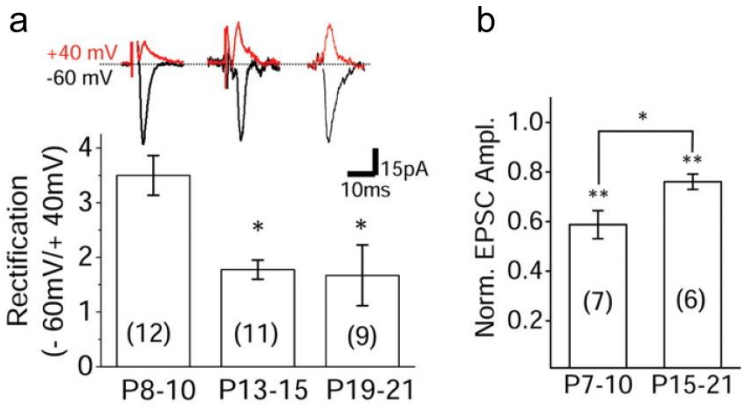


**Figure 1-10. The alteration of $Ca^{2+}$-permeability of AMPARs in developmental hippocampal OPCs.**

(a) Averaged rectification index of evoked EPSCs recorded in hippocampal OPCs. Insets illustrate the example EPSCs recorded at holding potential of -60 mV (black) and +40 mV (red). Asterisks indicate the significant differences as compared to P8-10 group. $p < 0.01$. (b) Averaged EPSCs are normalized by EPSCs in the presence of NAS divided by control EPSCs (before NAS application). Comparison is performed between two experimental groups indicating as one asterisk ($p < 0.05$) or with control group indicating as two asterisks ($p < 0.001$). From [85], modified.

*1.8. Synaptic inputs are lost during the differentiation of OLs lineage.*

As indicated above, OPCs constantly differentiate into OLs. Therefore it was important to find out what happens to the synaptic inputs between axons and OPCs when OPCs differentiate into OLs. In theory, these inputs may disappear or they may persist in all cells of the oligodendrocytes lineage. To address this question, Ruthenium Red, a drug which provokes vesicular release of neurotransmitters from presynaptic terminals and increases the frequency of mEPSCs in hippocampal pyramidal neurons [87] has been tested in the oligodendrocyte lineage cells [31, 65, 76]. Application of 100 µM RR to OPCs in hippocampal slices induced inward currents with fast kinetics (rise time: 0.5±0.07 ms; decay time constant: 2.4±0.19 ms), similar to mEPSCs (Fig. 1-11 a). On the contrary, inward currents could not be detected in mature myelinating OLs recorded under similar conditions (Fig. 1-11 c, d). In pre-myelinating OLs only

very few mEPSCs with similar amplitude and kinetics could be recorded upon Ruthenium Red application (Fig. 1-11 b, d), indicating that they receive much less synaptic input than OPCs [31]. These data show that axons establish synaptic inputs mediated by AMPARs only with OPCs, but not with more mature cells of the OLs lineage.

The reduction in the frequency of mEPSCs in pre-myelinating OLs, and subsequently in mature OLs, reflects the loss of the synaptic signaling upon differentiation of OPCs. A possible reason for this can be the decrease in the expression of functional AMPARs. To address this question, inward currents triggered by uncaging of 500 µM 4-Methoxy-7-nitroindolinyl-caged-L-glutamate (MNI- glutamate) were tested in different stages of OLs lineage [37]. Glutamate-induced currents were detected in OPCs and pre-myelinating OLs, and the induced currents were blocked by the antagonists of AMPARs NBQX and GYKI53655 (Fig. 1-12 a,b). However, the current amplitude in pre-myelinating OLs was remarkably smaller than in OPCs (Fig. 1-12 d). Photolysis of MNI-glutamate also induces detectable inward current in OLs; however, this current was not inhibited by antagonists of AMPARs (5 or 50 µM NBQX and 100 µM GYKI 53655) but was significantly reduced by application of 300 µM DL-threo-β-benzyloxyaspartic acid (TBOA), a potent glutamate transporter blocker, indicating that it is contributed largely by glutamate transporters (Fig. 1-12 c), although AMPARs expression has been reported in OLs [88]. During oligodendrogenesis, the cells become larger [37], therefore to compare the inward currents in OPCs, pre-myelinating OLs, and OLs, the amplitude of AMPARs mediated currents triggered by glutamate un-caging, were normalized on the membrane capacitance. The density of AMPAR-mediated currents in OPCs turned out to be significantly higher than in pre-myelinating OLs and OLs (Fig. 1-12 d), suggesting the surface expression of AMPARs gets reduced when OPCs commence to differentiate.

Taken together, these data indicate that AMPAR-mediated synaptic input is lost and the expression of functional AMPARs is downregulated during maturation of the OL lineage cells [31, 37]. These may imply that synaptic input acts as a modulator for OPCs to undergo differentiation.

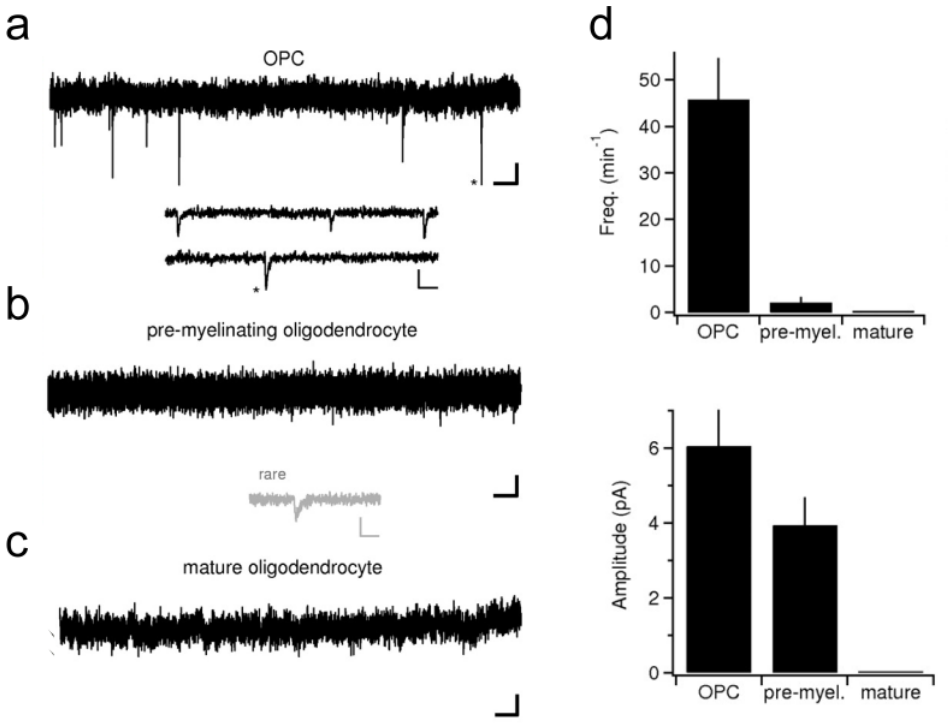


**Figure 1-11. Synaptic currents are vanished during the maturation of OL lineage cells.**

(a) Ruthenium Red induces mEPSCs obtained in OPC from the whole-cell voltage clamp recording. Calibration: 0.2 s, 2 pA. Inset: The expended trace is from the part of the top trace. Calibration: 20 ms, 5 pA. The asterisks from both traces indicate the same events. (b) Same as (a) but obtained from pre-myelinating OL. (c) Same as (a, b) but obtained from pre-myelinating OL. (d) (*Top*) Summary bar graph represents the mean frequencies of mEPSCs recorded from OL lineage cells. (*Bottom*) Summary graph depicts the mean amplitude of mEPSCs recorded from OL lineage cells. From [31], modified.

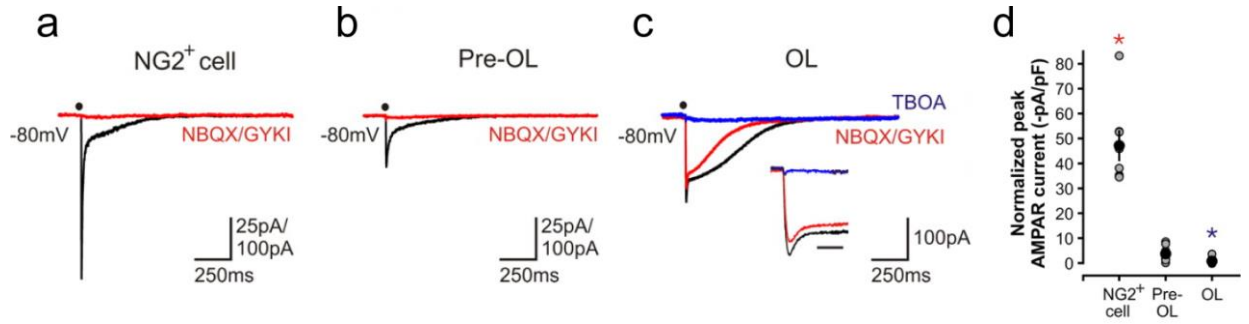


**Figure 1-12. Expression of AMPARs is declined in the oligodendrogenesis.**

(a) Glutamate uncaging (black dot) triggers inward current in OPC ($V_h$=-80 mV). (b) Same as (a) but in pre-myelinating OL. (c) Same as (a, b) but in OL. Inset: expanded trace from the top trace showing initial response at the shorter time scale. Bar: 20 ms. (d) AMPAR current is normalized by the membrane capacitance for OPCs, pre-myelinating OL, and OLs. Red asterisk: OPC vs pre-myelinating OL and OPC vs OL, $p < 0.001$; blue asterisk: pre-myelinating OL vs OL, $p < 0.001$. From [37], modified.

### *1.9. Synaptic currents in proliferating OPCs.*

OPCs receive synaptic inputs from neurons in both young and adult animals [74]. At the same time, OPCs continue proliferation throughout the life [23]. Do OPCs pass through their synaptic connection with neurons to their daughter cells upon cell division? Or do the daughter cells lose synaptic inputs during mitosis and establish synaptic connection with neurons *de novo* after completing the cell division? To answer this question, it was tested whether glutamatergic or gamma-aminobutyregic (GABAergic) synaptic currents can be recorded in OPCs at different stage of the cell cycle. It turned out that during metaphase and telophase of mitosis, mEPSCs mediated by AMPARs and GABARs could be recorded in OPCs suggesting that functional synaptic connections are preserved during cell division [38, 89]. In addition, immunolabeling data showed that punctate glutamic acid decarboxylase 65 (GAD65, localized preferentially in GABAergic terminals [90]) staining was observed close to the processes of mitotic OPCs filled with a fluorescent dye Lucifer yellow [89]. Taken together, OPCs keep functional synaptic connections with neurons during their division, and their daughter cells inherit the glutamatergic and GABAergic synaptic inputs from parent OPCs. This inheritance of synapses may help OPCs to continue being involved in synaptic signaling with neurons immediately after the cell division, and may be a mechanism important for maintaining the OPC populations in the brain.

*1.10. The role of AMPAR-mediated signaling in OPCs during demyelination and remyelination process***.**

In the experimental models of demyelination induced by injection of lysolecithin or ethidium bromide in the rodents, OPCs are recruited to the demyelination lesion and establish AMPARs mediated synaptic connections with axons approximately one week after induction of demyelination [91-93]. The number of newly-born OLs increases in the lesion 10-14 days after demyelination [91, 93]. Interestingly, infusing 250 µM NBQX (antagonist of AMPARs) into the demyelinating lesion via an intrancerebral cannula decreases remyelination [92]. This evidence suggests that synaptic connection between neurons and OPCs via AMPARs may initiate activation of intracellular cascades in OPCs which are required for differentiation of OPCs into OLs and/or for remyelination.

*1.11. Neuronal activity affects differentiation and proliferation of OL lineage cells, as well as myelination.*

It has been shown in different brain regions and in the optic nerve *in vivo*, *ex vivo, or in vitro* that neuronal activity affects differentiation and/or proliferation of OPCs, or myelination [18, 82, 94-98]. Published research on this topic can be grouped in two parts: studies focusing on the effects of inhibition of neuronal activity on OPCs development and studies focusing on the effects of enhanced neuronal activity on OPCs development.

In general, the results of the studies reporting effects of reduced neuronal activity on proliferation and differentiation of OPCs are so far contradictory. Elimination of electrical activity from the axons of retinal ganglion cells by transection of the rat optic nerve, resulted in reduction of proliferative capacity of OPCs [96]. However, an increase in proliferation of OPCs upon inhibition of neuronal activity has also been reported [82, 95]. Sensory deprivation by removing and cauterizing the whisker at birth of a mouse resulted in reduced thalamocortical glutamatergic (mainly AMPARs-mediated) synaptic inputs to OPCs, but increased proliferation of OPCs in the barrel cortex during early mouse development [82]. In addition, another study using similar approach for sensory deprivation by whisker clipping found increase in the apoptosis of dividing OPCs in somatosensory barrel cortex [98]. Blockade of neuronal activity by 1 mM TTX application in cerebellar slice culture increased proliferation of OPCs and the

generation of OL [95]. Moreover, blockade of neuronal activity has also been reported to alter the morphology of OPCs, e.g. induced shortening the processes length and processes branching points [95]. In addition to the effects of reduced/diminished neuronal activity on differentiation and/or proliferation of OPCs, blockade of neuronal activity has also been shown to affect myelination. Thus, application 1 mM TTX in cerebellar slice culture suppressed myelination [95]. In co-culture of neurons and OPCs prepared from cerebral hemispheres, 1 μM TTX treatment decreased the number of myelinated segments [97]. This study further demonstrated that intravitreal injection of 100 μM TTX into P4 mouse optic nerve *in vivo* decreased the total number of myelinating OLs. Interestingly, similar effects was not observed in P5 mouse optic nerve, suggesting that electrical activity in axons affects only the onset of myelination [97].

Augmentation of neuronal activity also has an effect on the OL lineage cells. Enhancement of neuronal activity in co-culture of neurons and OPCs by treatment with highly selective $Na^+$ channel activator alpha-ScTX increased the number of myelinated segments without increasing the number of OLs [97]. Furthermore, increase of neuronal activity via optogenetic stimulation of the premotor cortex in awake and behaving mice *in vivo* led to increase in proliferative capacity of OL lineage cells in several brain regions including premotor cortex and corpus callosum [94]. Optogenetic stimulation also promoted oligodendrogenesis [94] and resulted in thicker myelin which was reflected in the reduction of g-ratio, which is the ratio between the diameter of an axon and the diameter of this axon together with myelin sheath [94]. Remarkably, it appeared that differentiation and proliferation of OPCs is not only affected by neuronal activity itself but also depends on the patterns of activity. Thus, a recent study showed that stimulation of callosal axons at 5 Hz but not at 25 or 300 Hz in freely moving mice *in vivo* promoted differentiation of OPCs into OLs [18]. On the other hand, stimulation at 25 and 300 Hz but not at 5 Hz enhanced proliferation of OPCs. , All frequencies tested in that study (5, 25, and 300 Hz) promoted oligodendrogenesis of newly born OPCs into OLs [18].

Taken together, neuronal activity, indeed, affects the differentiation and proliferation of OPCs and the further myelination of OLs in the different systems. However, the mechanisms mediating the effects of neuronal activity on the OLs lineage are still ambiguous. Further studies addressing this question are necessary.

*1.12. AMPARs in OPCs affect proliferation and differentiation of OPCs, as well as myelination.*

Glutamatergic AMPAR-mediated neuron-OPC signaling may be one of the mechanisms mediating the effects of neuronal activity on the behavior of OPCs. AMPARs have been shown to participate in regulation of the behavior of OPCs in different systems. Application of 200 µM AMPA, an agonist of AMPAR, in rat cerebellar tissue culture decreased the percentage of proliferating OPCs ($NG2^+$ cells), and also decreased the level of 2', 3'-cyclicnucleotide 3'-phosphodiesterase (CNP) mRNA. CNP is expressed selectively in OLs [99] and represents a marker of maturation of OLs. These findings indicated that activation of AMPARs inhibited proliferation of OPCs and suppressed OLs maturation [33]. Application of 30 µM 6,7-dinitroquinoxaline-2,3-dione (DNQX), an antagonist of AMPAR, reversed this effect by increasing the number of proliferating OPCs ($NG2^+$ cells) and the level of CNP mRNA [33]. Similar results were obtained in a study from a different group who demonstrated that blockade of AMPAR function by GYKI (9.74 mM) increased proliferation of oligodendrocyte lineage cells, increased generation of OLs, and suppressed myelination in cerebellar slice culture [95]. Furthermore, blockade of AMPARs reduced the length and the number of branching points of OPCs processes [95]. Although these findings are valuable, the environment in the slice culture is more simplified than *in vivo,* and the blockade of AMPARs in culture systems is not specific to OPCs but is also expected to affect neurons. Therefore, the observed effects on OPCs may (partially) be mediated through other surrounding cells which express AMPARs and probably release several factors onto OPCs. Thus, it was important to study role of AMPARs for OPCs development and function *in vivo*, and this question was addressed in a recent study which aimed to understand the effects of AMPAR-mediated signaling in OPCs and OL lineage cells in general [65]. As GluA1 subunit is low in callosal OPCs, in order to study AMPAR function the authors ablated two (GluA2/3) or three (GluA2/3/4) subunits of AMPARs in OPCs from the onset of mouse development [65]. In both cases, AMPARs-mediated synaptic input to OPCs was reduced or abolished [65]. In both double and triple knockouts, the proliferation of OPCs was not altered but reduced number of OLs was observed [65]. In triple-knockouts, reduction in the number of OLs continued into adulthood [65]. The authors further showed that reduction in the number of OLs was due to the increased death of OL lineage cells [65]. Interestingly, although the number of OLs was affected in double and triple knockouts, the average length, number and thickness of

myelin internodes remained normal [65]. Together, these findings suggest that AMPARs-mediated signaling between callosal axons and OPCs promotes survival of the OL lineage cells [65]. Regulation of differentiation and proliferation in OPCs is complicated and may involve several pathways. AMPARs-mediated signaling may be one of these mechanisms. Ablation of AMPARs in OPCs from the onset of development may prompt compensatory mechanisms which come from others pathways. This compensation may re-adjust the regulation and balance between differentiation and proliferation in OPCs.

Taken together, functional role of AMPAR-mediated synaptic signaling between axons and OPCs is still ambiguous. In order to investigate the effects of this signaling on differentiation and proliferation of OPCs, the present study modified the GluA2 subunit of AMPARs in OPCs *in vivo*. I have chosen to modify the GluA2 subunit for two reasons. First, GluA2 subunit governs the $Ca^{2+}$ permeability of AMPARs, and $Ca^{2+}$ is a well-known secondary messenger which is involved in several pathways in the cells. Second, $Ca^{2+}$ permeability of AMPARs in OPCs changes during animal age, and this correlates with alterations in the rate of proliferation and differentiation of OPCs. In order to modify the GluA2 subunit of AMPARs in callosal OPCs *in vivo*, I used the retroviral approached and carried out the modifications during the second postnatal week when synaptic connections between neuron and OPCs are established.

## 2. Hypothesis, objectives, and experimental strategy.

### 2.1. Hypothesis.

The major hypothesis of my study is that axon-OPC signaling through AMPARs regulates differentiation and proliferation of OPCs *in vivo*.

### 2.2. Objectives:

To test my hypothesis, I followed three objectives:

(1) Establish an approach to modify AMPARs in callosal OPCs *in vivo*;

(2) Investigate changes in synaptic AMPAR-mediated currents in OPCs;

(3) Investigate how modifications of AMPAR properties in callosal OPCs affect differentiation and proliferation of OPCs.

### 2.3. Experimental strategy.

In order to modify the properties of AMPARs in callosal OPCs, I carried out three modifications of the GluA2 subunit (Fig. 2-1).

(1) The first modification, GluA2(R583Q)-GFP, was aimed at increasing the $Ca^{2+}$ permeability of AMPARs by a point mutation, i.e. replacing Arg(R)583 with Gln(Q) [100]; I called this modification "$Ca^{2+}$-permeable".

(2) The second modification, GluA2(R583E)-GFP, was aimed at reducing the conductance of the channel pore by a point mutation, i.e. replacing the Arg(R)583 with Glu(E) in the GluA2 channel pore [101]; I called this modification "pore-dead".

(3) The third modification, expression of cytoplasmic carboxyl-terminal (GluA2(813-862)) of GluA2, was aimed at perturbing the trafficking of GluA2 subunit by affecting the interaction between the GluA2 and the AMPAR-binding proteins [102]; I called this modification "C-tail".

Each construct was tagged with the green fluorescent protein (GFP) to label cells expressing the modified AMPARs.

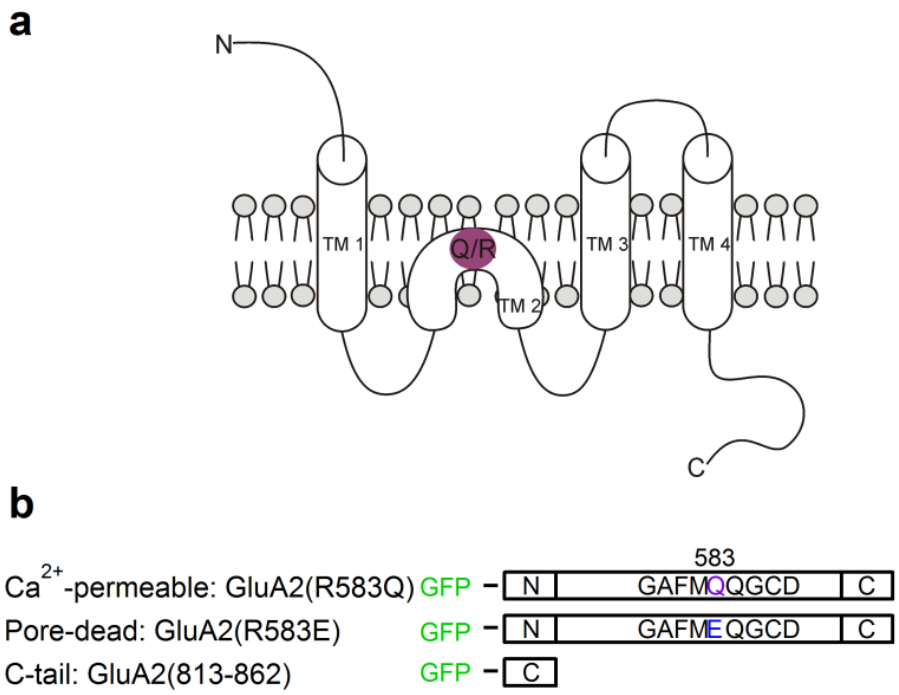


**Figure 2-1. Schematic drawing of GluA2 subunit of AMPARs and the constructs used in the study.**

(a) Schematic drawing of the GluA2 subunit of AMPARs. Magenta dot indicates the Q/R editing site of the GluA2 subunit. Q: glutamine, R: arginine, TM: transmembrane domain, N: N-terminus, C: C-terminus. (b) Scheme illustrating the mutated and truncated GluA2 subunits expressed by the viral vector shown in Figure 4a. The number 583 indicates the amino acid site of the point mutation. N: N-terminus, C: C-terminus.

## 3. Materials and Methods.

### 3.1. Animals.

NG2DsRedBAC transgenic mice [76] and C57BL/6N mice of both sexes were used in all experiments. Breeding pairs of NG2DsRedBAC transgenic mice were originally obtained from The Jackson Laboratory (stock 008241) and C57BL/6N mice were originally obtained from Charles River. Mice were bred in house and kept in 12-12 hours of light-dark cycle; food and water were available *ad libitum*. All experiments were performed in accordance with current European Union guidelines and approved by the local government authorities for Animal Care and Use (Regierungspraesidium Tuebingen, State of Baden-Wuerttemberg, Germany).

### 3.2. Molecular biology.

pCI-EGFPGluA2(R583Q) was a gift from Roberto Malinow (University of California, USA). pEGFPC1-GluA2(813-862) was a gift from Ingrid Ehrlich (University of Tübingen, Germany). The plasmids for viral production (pRetroCAG-GFP, pCMV-gp and pCMV-vsv-g) were the gifts from Fred Gage (The Salk Institute, USA).

#### *3.2.1. Mutagenesis.*

The point mutation of GluA2(R583Q) to GluA2(R583E) was introduced using the Quick Change II XL Site-Directed mutagenesis kit (Stratagene). The primers for the point mutation were (5' to 3'): fwd: CTTGGGTGCCTTTATGGAGCAGGGATGCGATATTTC and rev: GAAATATCGCAT CCCTGCTCCATAAAGGCACCCAAG. For all procedures I followed the instruction manual provided by Stratagene. Briefly, the sample reaction included 5 µl of 10x reaction buffer, 10 ng of double-stranded DNA (dsDNA) template, 125 ng of forward primer, 125 ng of reverse primer, 1 µl of deoxynucleotide triphosphates (dNTP) mix, 3 µl QuikSolution and distilled $H_2O$ ($ddH_2O$) to a final volume of 50 µl. Then 1 µl of *PfuUltra* high-fidelity (HF) DNA polymerase (2.5 U/µl) was added into mixture. 18 cycles were performed (95°C, 1 minute; denaturation at 95°C, 50 seconds; annealing at 60°C, 50 seconds; extension at 68°C, 8.5 minutes; final elongation at 68°C, 7 min). After cycling, 1 µl of the *Dpn* I restriction enzyme (10 U/µl) was added directly to each amplification reaction and incubated at 37°C for 1 hour in order to digest the parental supercoiled dsDNA. DNA was treated with *Dpn* I and was transformed into

XL10-Gold ultracompetent cells. After transformation, XL10-Gold ultracompetent cells was plated onto lysogeny broth (LB: 10 g of tryptone, 5 g of yeast extract, 10 g of NaCl, 15 g of agar and dd$H_2O$ up to 1 liter) agar plates containing ampicillin (100 µg/ml) and incubated at 37°C overnight. The liquid bacteria culture was inoculated in the LB medium by picking single colony. Miniprep and Maxiprep were performed using QIAprep Spin Miniprep Kit (Qiagen) and QIAfilter Plasmid Maxi Kit (Qiagen) respectively. The mutant plasmid was checked by the restriction enzymes HindIII (New England Biolabs) and NdeI (New England Biolabs). The digested plasmid was run on 0.7% agarose gel. The expected fragments were 8.2 kbp for HindIII digestion, and 3 kbp, 2.7 kbp, and 2.4 kbp for NdeI digestion. The 1 kbp-DNA marker (Roth) was used. The gel was visualized by BIOVISION-3020-WL/LC/20M system (Vilber Lourmat) and the software VisioCapt 15.06 (Vilber Lourmat).

*3.2.2. Subcloning.*

The procedure of cloning is shown on Figure 3-1. In general, the restriction enzymes (AgeI and PmeI) for the subcloning were added to the flank of insert by polymerase chain reaction (PCR). At the same time, the vector was digested with the same restriction enzymes which were used for the insert. Both insert and vector were isolated by gel purification and the insert was ligated into the vector. The newly generated retroviral vector was transformed into Stabl3 competent cells (Invitrogen). Finally, the single bacterial colonies were picked and purified and the DNA was checked by several digestions with restriction enzymes. All plasmids were sequenced to ensure the accuracy.

To construct pRetroCAG-EGFPGluA2(R583Q), pRetroCAG-EGFPGluA2(R583E) and pRetroCAG-EGFPGluA2Ctail, I inserted EGFPGluA2(R583Q), EGFPGluA2(R583E) and EGFPGluA2(813-862) by PCR amplication. PCR primers included PmeI and AgeI restriction site for insertion into pRetroCAG-GFP. The primers are listed in Table 3-1.

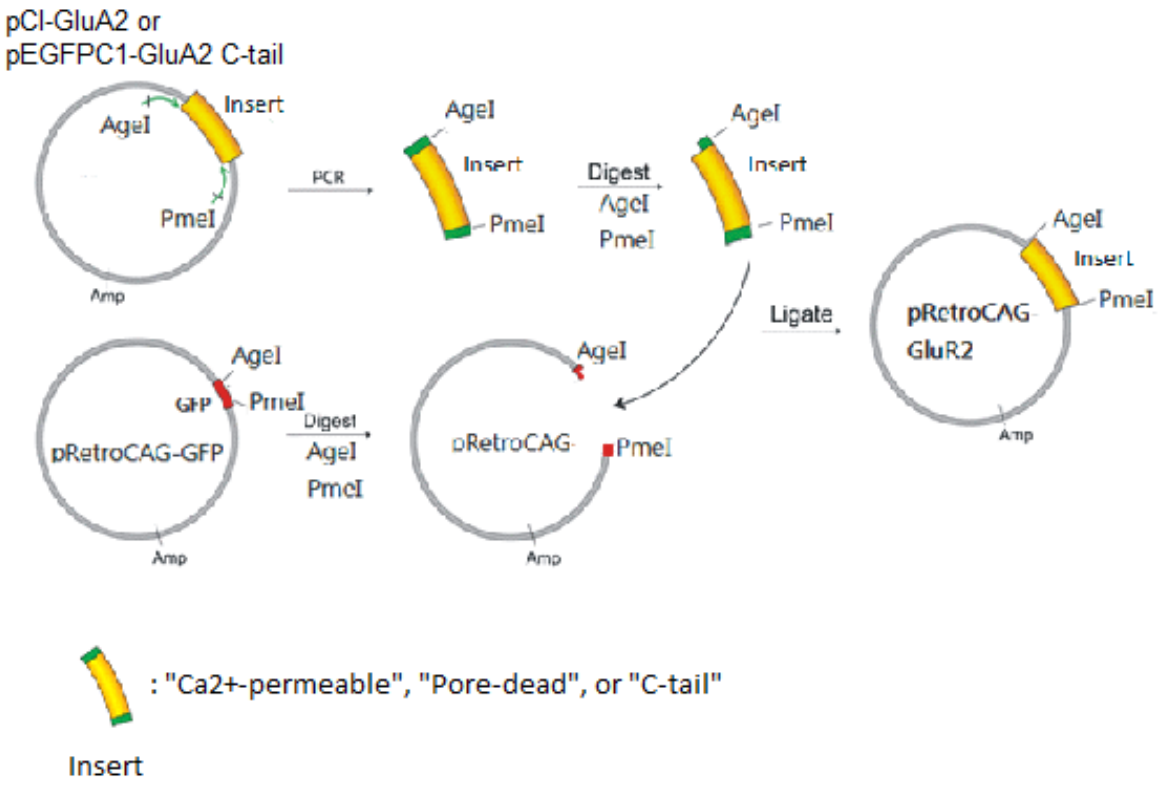


**Figure 3-1. Schematic diagram of the subcloning procedure.**

The insets were digested with the respective digestion enzymes from original plasmids. The digested insets were subcloned into retroviral backbone. From [103], modified.

| Construct | Primers (5' to 3') | Insert size |
|---|---|---|
| EGFPGluA2(R583Q) and EGFPGluA2(R583E) | Forward: TTACCGGTACGACTCACTATAGGCTAGAACTAG AgeI | 3.855 kbp |
| | Reverse: TGTTTAAACCCAAGGCCTGCATGCACTGCTTTG PmeI | |
| EGFPGluA2(813-862) | Forward: TAGCGCTACCGGTCGCCACCATGGTG AgeI | 975 bp |
| | Reverse: TGGTTTAAACACCTCTACAAATGTGGTATGGCTG PmeI | |

**Table 1. The primers used for cloning the inserts into retroviral backbone.**

The nucleic acid sequences underlined with red line indicate the sequences for PmeI or AgeI restriction enzyme.

The master mix included 50 ng template, 10 mM dNTP, 10 µM forward primer, 10 µM reverse primer, 1 units Phusion DNA Polymerase (New England Biolabs) and 1x Phusion HF buffer. The PCR cycle is listed below:

- 98°C 30 sec – Initial Denaturation
- 3-step cycling

1. 98°C 10 sec
2. 70 °C 30 sec
3. 72°C 2 min for EGFPGluA2(R583Q) and EGFPGluA2(R583E); 30 sec for EGFPGluA2(813-862)

30 cycles for 1-3 steps

- 72°C 10 min – Final Extension
- 4°C forever

After PCR cycling, PCR product was loaded onto 0.7 or 1% agarose gel. DNA was extracted from the gel by QIAquick Gel Extraction Kit (QIAGEN).

10 µg of vector and purified insert were digested by AgeI and PmeI at 37°C for 3 hours. Digested insert was purified by the QIAquick PCR Purification Kit (QIAGEN). The digested vector was heat inactivated at 65°C for 20 minutes. Subsequently, 1 µl of calf intestinal alkaline phosphatase (CIP; New England Biolabs) was added and the mixture was incubated at 37°C for 1 hour to avoid the self-ligation. Digested vector was run onto 0.5% agarose gel and extracted DNA from the gel. The expected size of digested vector was 6.8 kbp.

1:3 and 1:5 of ligation ratio were used as a starting point. 300 ng of vector was applied to each ligation. The amount of insert was calculated by the formula shown below:

$$\text{X ng of insert} = \frac{\text{Y ng of vector} * \text{kb size of insert}}{\text{kb size of vector}} * \text{molar ratio of } \frac{\text{insert}}{\text{vector}}$$

The mixture of ligation reaction included vector, insert, 10 µl of 2X Quick Ligation Reaction Buffer and 1 µl of Quick T4 DNA Ligase (Quick Ligation Kit, New England Biolabs). The reaction was incubated at room temperature for 10 minutes. The ligation mixture was transformed into Stbl3 competent cell and cultured single colony in the LB medium. Plasmid was purified as described above. Plasmids were checked by the restriction enzymes and run onto 0.7% agarose gel. The restriction enzymes and fragment size are listed in Table 2.

To check whether GFP, used as a fusion protein, was functionally expressed, HEK 293 cells were transfected with each newly generated retroviral plasmid (Table 2) using lipofection 2000 (Invitrogen) according to the manufacturer's protocol. 48 hours after the transfection, cells were fixed on the glass coverslips with 4% paraformaldehyde at room temperature for 20 minutes and washed with 10 mM phosphate-saline buffer (PBS). For counterstaining of the nuclei I used Diamidino-2-phenylindole dihydrochloride (DAPI, 0.2 µg, Sigma).

| Plasmid | Restrict enzyme | Fragment size | Purpose |
|---|---|---|---|
| pRetroCAG-EGFPGluA2(R583Q) and pRetroCAG-EGFPGluA2(R583E) | PmeI | 10.6 kbp | Linearised |
| | AgeI/PmeI | 6.8 and 3.841 kbp | Backbone and Insert |
| | PvuII/ClaI | 8.278 and 2.35 kbp | Orientation |
| pRetroCAG-EGFPGluA2(813-862) | PmeI | 7.7 kbp | Linearised |
| | AgeI/PmeI | 6.8 and 0.9 kbp | Backbone and Insert |
| | XhoI | 6.935 and 0.779 kbp | Orientation |

**Table 2. Overview of the diagnostic restriction digestion.**

### 3.3. Retrovirus production.

For retroviral production, I used the procedure described previously [104], with few modifications. HEK 293T/17 (ACTT) cells were used for virus preparation. HEK 293T/17 cells were cultured with complete growth medium (Dulbecco's Modified Eagle's Medium containing 4500 mg glucose/L, 110 mg sodium pyruvate/L and L-glutamate (PAA and Sigma), 10% fetal bovine serum (Life technologies), and 1% Penicillin/Streptomycin (PAA)). 0.25% Trypsin-EDTA (Sigma) was used to detach the cells during subculturing. All procedures are described in details shown below:

Day1: Plate $5X10^6$ cells per 10 mm plate for a total of 6 plates.

Day2: Transfection: transfect three plasmids into cells with lipofectamine 2000

(1) Prepare 4 tubes with 2.4 ml OptiMEM (Invitrogen)

(2) Two tubes: add 45 µg plasmid DNA mixture

- 22.5 µg pRetroCAG - with GFP, GluA2(R583Q) or GluA2Ctail
- 15 µl pCMV-gp
- 7.5 µg pCMV-vsv-g

(3) Two tubes: add 150 µl lipofectamine 2000

(4) Mix one tube of plasmid DNA with one tube of lipofectamine 2000

(5) Incubate at room temperature for 20-30 minutes

(6) Transfer 1.6 ml of the DNA/lipofectamine solution onto each plate of HEK293T/17 cells containing 10 ml of OptiMEM

(7) Incubate for 9-16 hours at 37°C, 5% $CO_2$

(8) Replace supernatant with 10 ml complete growth medium

Day4: Concentrate virus – 48 hours after transfection

(1) Collect the supernatant in 50 ml Falcon tube and add 10 ml complete growth medium into each plate

(2) Centrifuge at 1000g for 3 minutes in order to remove cell debris

(3) Pre-wet the 0.45 µm filter (Merck) with complete growth medium

(4) Filter the supernatant through pre-wet 0.45 µm filter in two 36 ml ultracentrifuge tubes (Thermo Scientific)

(5) Add Dulbecco's Phosphate-Buffered Saline (PBS; PAA and Sigma) till ~ 0.5 cm from the top of the tubes

(6) Centrifuge at 65,000g and 4°C with the rotor AH-629 (Thermo Scientific) for 2 hours

(7) Remove the supernatant

(8) Add around 400 µl of PBS in the tubes

(9) Cove the tubes with parafilm and store at 4°C for overnight

Day5: Concentrate virus – 72 hours after transfection

(1) Collect the supernatant in 50 ml Falcon tube

(2) Centrifuge at 1000g for 3 minutes in order to remove cell debris

(3) Pre-wet the 0.45 µm filter with complete growth medium

(4) Filter the supernatant through pre-wet 0.45 µm filter in two 36 ml ultracentrifuge tubes from Day4

(5) Add PBS till ~ 0.5 cm from the top of the tubes

(6) Centrifuge at 65,000g and 4°C with the rotor AH-629 for 2 hours

(7) Remove the supernatant

(8) Resuspend virus with 0.7 ml PBS for each tube (total is 1.4 ml)

(9) Pipette up and down for 20-30 times (avoid any air bubbles during pipetting)

(10) Transfer 1.4 ml into one 4 ml ultracentrifuge tubes (Thermo Scientific)

(11) Wash tubes with 0.7 ml PBS and transfer to 4 ml tube mentioned in step (10)

(12) Fill more PBS till 0.5 cm from the top of the tube

(13) Centrifuge at 65,000g using the rotor TH-660, 4°C for 2 hours

(14) Remove the supernatant as much as possible

(15) Add 40 µl PBS in to the tube and resuspend the final pellet by vortexing for 30 seconds and then by pipetting

(16) Transfer 40 µl virus solution to 0.5 ml tube

(17) Wash 4 ml tube once with 5 µl PBS (optional)

(18) Put 0.5 ml tube on ice and shake for 1-3 hours

(19) Spin o.5 ml tube briefly, aliquot and store at -80°C

To estimate the viral titers, the procedure was followed:

(1) Dilute 2 µl of the viral stock solution into 100 µl medium (1:50) and mix well

(2) Make a series of 10 + 90 µl dilutions:

1. Prepare 6 eppendorf tubes with 90 µl medium in each
2. Add 10 µl of the initial dilution from step (1) into the first tube and mix well (1:500)
3. Add 10 µl of the 1:500 dilution into the second tube and mix well (1:5000)
4. Proceed down to 1: 5 x $10^7$

(3) Adjust HEK293T/17 cells to 1 x $10^6$ cells/ml

(4) Add 100 µl of the cell suspension to each viral dilution and mix well.

The viral dilution factor is now 1:1000, 1:10000 down to 1: $10^8$.

The cell density in all samples is 5 x $10^5$/ml

(5) Add 250 µl medium per well (6 wells in total) in a 48-well plate

(6) Plate each dilution directly into the wells (100 µl each), starting with 1: $10^4$

Mix each sample well before plating

(7) Grow cells for 3 days

(8) In order to have better GFP visualization from the groups of retrovirus carrying point mutation of GluA2 subunit, the GFP staining was performed: fix with 4% PFA at room temperature for 20 minutes, apply chicken anti-GFP antibody at 4°C overnight followed by applying anti-chicken FITC secondary antibody

(9) Count fluorescent clones per sample; count samples containing > 20, but < 200 clones

(10) Calculate titer (unit is presented as per ml) as the formula shown below:

N of clones x 2 (1/2 of 200 µl cell suspension) x $10^x$ (dilution factor which the number of clones counted) x 500 (initial dilution)

The viral titers were tested with HEK293T/17 cell line and were $10^8$-$10^9$/ml.

**3.4. Experimental groups of animals.**

In the majority of experiments the following 4 groups of animals were used: (1) Animals injected with retrovirus-GFP (called "GFP"); (2) Animals injected with retrovirus-GluA2(R583Q)-GPF (called "$Ca^{2+}$-permeable"); (3) Animals injected with retrovirus-GluA2(R583E)-GFP (called "pore-dead"); and (4) Animals injected with retrovirus-GluA2(813-862)-GFP (called "C-tail"). In some expetriments (see text) a fifth group of mice was used which contained intact animals, which were not injected with retrovirus (non-injected). The number of animals (*n*) used in each experiment is indicated in the corresponding figure legends.

**3.5. Retrovirus injection.**

10-12 days-old NG2DsRedBAC transgenic mice were anesthetized with a mixture of isoflurane and oxygen (1-3 % v/v) and fixed in the stereotaxic frame (Stoelting, USA). The depth of the anaesthesia was monitored by testing the reaction of the mouse to a toe pinch. For analgesia metacam (1 mg/kg bodyweight, Boehringer Ingelheim) was injected subcutaneously before the surgery. The skin above the skull was disinfected, a small cut was made, and xylocaine (2%, Astra Zeneca) was applied locally. Bilateral injections of the virus into the corpus callosum were performed using the following coordinates (in mm from Bregma): anteroposterior 0.23, mediolateral ±0.23-0.25, dorsoventral 1.77. For each injection I used a glass micropipette containing ~2.5 µl viral stock solution. The micropipette was connected to the fast pressure application system (PDES-01D-4, NPI Electronic, Germany), and the following parameters were used for injection: pressure 16-20 psi, application duration 60-90 ms. Subsequently, the wound was sutured with silk (Ethicon, USA). After the surgery, mice recovered rapidly from anesthesia and were returned to their home cages with parents.

For electrophysiological experiments I used $DsRed^+$ mice; for immunohistochemistry and cell counting I used $DsRed^-$ littermates in order to have red fluorescent channel available for antibodies labeling.

### 3.6. *In vivo* EdU treatment.

To study cell proliferation, mice were administrated with 5-ethynyl-2'-deoxyuridine (EdU, Thermo Fisher) [105] intraperitoneally at a dose of 25 mg/ kg body weight. EdU was applied three times, i.e. on the third, fourth, and fifth day after the viral injection at an interval of 24 hours.

### 3.7. Slice preparation for electrophysiology.

Three to five days after the viral injection mice were anesthetized with a mixture of isoflurane and oxygen (3% v/v) and decapitated. The brain was dissected in the ice-cold N-methyl-D-glucamine (NMDG)-based solution containing (in mM): 135 NMDG, 1 KCl, 1.2 $KH_2PO_4$, 20 choline bicarbonate, 10 glucose, 1.5 $MgCl_2$, and 0.5 $CaCl_2$ (pH 7.4, 310 mOsm), gassed with carbogen (95% $O_2$, 5% $CO_2$). 270-300 µm thick coronal brain slices were cut in the same solution using Leica VT 1200S vibratome. The slices were transferred to the 32$^oC$ Haas-type interface incubation chamber and perfused with Ringer-solution containing (in mM): 124 NaCl, 3 KCl, 1.25 $NaH_2PO_4*H_2O$, 2 $MgCl_2$, 2 $CaCl_2$, 26 $NaHCO_3$, 10 glucose; 300 mOsm/kg; 7.4 pH; gassed with carbogen. The chamber was gradually cooled down to room temperature.

### 3.8. Patch-clamp recordings.

At least one hour after the preparation, individual slices were transferred to a submerged recording chamber mounted on a stage of an up-right microscope (FN-1, Nikon, Japan) equipped with infrared differential interference contrast (IR-DIC) filters and a fluorescence light source. The slices were kept at room temperature and superfused continuously (~2 ml/min) with carbogenated Ringer solution. OPCs were selected for recordings based on the fluorescence: red fluorescence ($NG2DsRed^+$ cells) for intact mice, or green and red double-fluorescence ($GFP^+NG2DsRed^+$ cells) for mice injected with retrovirus. Patch pipettes were pulled from borosilicate glass capillaries (Science Products, Germany) on a vertical puller (Model PC10, Narishige, Japan). Pipettes had resistance of 4.8-7 MOhms when filled with K-gluconate-based

internal solution containing (in mM): 125 K-gluconate, 2 $Na_2ATP$, 2 $MgCl_2$, 0.5 EGTA, 10 HEPES, 20 KCl, 3 NaCl; 280-290 mOsm/kg; titrated to pH 7.3 with KOH. Cells were voltage-clamped at the holding potential $V_h$ = -80 mV with an EPC-8 amplifier (HEKA, Germany). Liquid junction potential was calculated using the software JPCalc for Windows (Peter H. Barry, Sydney, Australia) and $V_h$ was corrected for a -13 mV liquid junction potential before seal formation. Series resistance was not compensated. After establishing the whole-cell configuration, ten depolarizing voltage steps (increment +10 mV) were applied to each cell from $V_h$=-80 mV, and corresponding current responses were recorded in order to verify that the selected cell was an OPC [106]. Evoked synaptic currents were elicited with isolated pulse stimulator (A-M Systems, Model 2100, Science Products, Germany) using mono-polar glass electrode (resistance 5-6 MΩ) filled with Ringer solution and placed at 50-150 µm from the recorded cell ($V_h$=-80 mV). Paired (40 ms inter-pulse interval) monophasic rectangular pulses of 100-250 µsec duration were applied every 15 sec. Trains of stimuli (20 pulses @ 100 Hz or 20 pulses @ 25 Hz) were applied each 15 sec.

For I-V curve recordings, I used a Cs-based internal solution containing (in mM): 100 $CsCH_3SO_3H$ (CsMeS), 20 tetraethylammonium (TEA) chloride, 20 HEPES, 10 EGTA, 2 $Na_2ATP$, and 0.2 NaGTP; 280-290 mOsm/kg; titrated to pH 7.3 with CsOH, and a Ringer solution containing (in mM): 119 NaCl, 2.5 KCl, 1 $NaH_2PO_4*H_2O$, 1.3 $MgCl_2$, 2.5 $CaCl_2$, 26.2 $NaHCO_3$, 11 glucose; 300 mOsm/kg; 7.4 pH; gassed with carbogen. Spermine (Sigma, 100 µM) was included into the internal solution in all recordings of evoked EPSCs in order to test for the presence of $Ca^{2+}$-permeable AMPARs in OPCs. $V_h$ was corrected for a -7 mV liquid junction potential before seal formation. The cells were held at different potentials (-90, -40, 0, +20, and +40 mV) and 10-15 sweeps were recorded at each potential.

When recording synaptic currents, I applied a voltage step of -5 mV at the beginning of each sweep to monitor series resistance. Whole-cells currents in response to voltage steps were low-pass filtered at 10 kHz and digitized with a sampling frequency of 20 kHz (ITC-18, HEKA Instruments Inc, USA). All recordings of synaptic currents were low-pass filtered at 1 kHz and digitized with a sampling frequency of 10 kHz. Data acquisition was performed using Recording Artist (written by Rick Gerkin, Arizona State University, USA) running under Igor Pro 6.3 (WaveMetrics, Lake Oswego, USA). All recordings of evoked synaptic currents were performed

in the presence of NMDA-receptor antagonist (RS)-3-(2-Carboxypiperazin-4-yl)-propyl-1-phosphonic acid (CPP, 10 µM, Tocris) and $GABA_A$ receptor antagonist (RS)-3-(2-Carboxypiperazin-4-yl)-propyl-1-phosphonic acid (gabazine, 5 µM, Sigma). In some experiments, tetrodotoxin citrate (TTX, 0.5 µM, Abcam) or 6-Cyano-7-nitroquinoxaline-2,3-dione (CNQX, 10µM, Abcam) was applied at the end of the recording. All drugs were dissolved in Ringer solution and applied via the bath. All patch-clamp recordings were performed at room temperature.

### 3.9. Analysis of electrophysiology data.

Only those recordings in which the offset drift by the end of the experiment was smaller than ±5 mV, and the change of the series resistance was < 30% of the original value were considered for the analysis. The series resistance was between 20 and 40 MΩ.

*3.9.1. Analysis of evoked EPSCs, I-V curve, and paired-pulse ratio.*

Analysis of evoked EPSCs was performed using custom-written macros in IgorPro. Stimulus artefacts were removed using the following procedure: sweeps containing failures (absence of postsynaptic response) after the first stimulus, or sweeps recorded in the presence of TTX or CNQX, were averaged and the segment of the averaged sweep from time-point of stimulation to last point before the second stimulus was cut out, duplicated and concatenated. The resulting sweep was subtracted from each recorded sweep.

To measure the EPSC amplitude (after first or second pulse), I used the following procedure: for each recorded sweep the baseline was adjusted to the 100-ms segment immediately preceding the stimulation; the peak-center of each event was determined as the time-point at which the first derivative of the sweep crossed zero; the amplitude values of the current in the peak-center and in 4 points around it (2 points to the right and 2 points to the left) were averaged, and the resulting value was taken as current amplitude. The threshold for event detection was determined individually for each recorded sweep and was equal to three times the standard deviation of the noise. In case several EPSCs occurred after a given stimulus, care was taken to measure the amplitude of the first event.

Although I used paired-pulse stimulation in all experiments, in order to generate the I-V curve I considered only the EPSCs occurring after the first pulse. 10-15 sweeps were recorded at each holding potential (-90, -40, 0, +20, +40 mV, and back to -90 mV), the current amplitude in each sweep was measured as described above, and all amplitude values at a given holding potential were averaged. The resulting averages were used to generate the I-V curve in each cell. To calculate the rectification index, the average value of the EPSC amplitude at +40 mV was divided by the average value of the EPSC amplitude at -90 mV.

To determine the paired-pulse ratio, the average amplitude value of the EPSC occurring after the second pulse was divided by the average amplitude value of the EPSC occurring after the first pulse at a holding potential of -90 mV.

*3.9.2. Analysis of the delayed EPSCs*.

To study the quantal amplitude of synaptic currents in OPCs, I analyzed the delayed EPSCs occurring in OPCs after the train stimulation of callosal axons with 20 pulses at 25 or 100 Hz. The delayed EPSCs were defined as those with an onset of >10 ms after the last stimulus of the train. In each recorded cell I collected the delayed EPSCs in 20-160 sweeps of 1.73-2.3 s length each. The EPSCs were detected using a deconvolution-based algorithm [107] in FBrain, a customized program running under IgorPro 6 (WaveMetrics, Lake Oswego, USA). FBrain was kindly provided by Peter Jonas Lab (IST, Klosterneuburg, Austria). Additional digital high-pass (10 Hz) and Notch (50 Hz) filtering was applied to the recorded sweeps in FBrain before the analysis. The deconvolution trace was passed through a digital band-pass filter at 0.001 to 200 Hz. The event detection template had a rise-time of 0.5 ms, a decay time constant of 4 ms, and amplitude of -3 pA. The event detection threshold ($\theta$) was set to 4.2 times the standard deviation of a Gaussian function fitted to the all-point histogram of the deconvolved trace [107]. All events detected by the algorithm were inspected visually, and those events which clearly did not show kinetics of typical excitatory postsynaptic currents (i.e. fast rise and exponential decay) were manually removed from the subsequent analysis. The subsequent analysis was performed using custom-written macros in IgorPro.

*3.9.3. Cumulative probability histogram of the amplitude of the delayed EPSCs.*

The following procedure was used: (1) The amplitude of all delayed EPSCs was measured in each cell as described above; (2) 67 delayed EPSCs were randomly selected from each cell using the StatsSample procedure in IgorPro and their amplitude was measured; (3) The amplitude distribution of randomly selected events was compared to the amplitude distribution of all events within a given cell using the Kolmogorov-Smirnov test in IgorPro to ensure that the two distributions were similar, and the pool of randomly selected events was representative of the whole population of events. In case the two distributions were found to be different, the random selection was automatically repeated by the software in a loop until no difference was found between the distributions; (4) In each cell the steps (2)-(3) were repeated 100 times; (5) For each of the 100 trials, the randomly selected events from all cells within a given experimental group were pooled together to generate an EPSCs amplitude distribution per experimental group; (6) For each of the 100 trials this new amplitude distribution of the events in a group of animals expressing one of the GluA2-subunit modifying constructs was compared to the GFP group using the Kolmogorov-Smirnov test in IgorPro. In selected trials the comparison was repeated using SPSS.

For the data presentation in Figure 4-11 e and Supplementary Figure 4-14 c, I selected one representative example for each experimental group out of the 100 trials. The bin size for each cumulative probability histogram was 0.5 pA, and each histogram was normalized onto the probability density using build-in function in IgorPro.

**3.10. Immunohistochemistry.**

For MBP staining, C57BL/6N mice were sacrificed at P9, P10, P11, P12, P15, and P18. For all other stainings, mice were sacrificed 5 days after the retroviral injection. The brain was removed, and 350-400 µm thick coronal slices were cut using the Leica VT 1200S vibratome in the solution of the following composition (in mM): 87 NaCl, 2.5 KCl, 1.25 $NaH_2PO_4*H_2O$, 7 $MgCl_2$, 0.5 $CaCl_2$, 25 $NaHCO_3$, 25 glucose, 75 sucrose. The slices were fixed overnight at $4^oC$ in 4% paraformaldehyde, dissolved in 10 mM PBS. Then the 350-400 µm thick slices were washed, embedded into Agar and re-sectioned in PBS to 30 µm thick slices using a Microtome (HM 650V, Thermo Scientific). All 30 µm thick slices were inspected visually for quality and for the

GFP-expressing (green) cells using an epi-fluorescence microscope (Axio Imager Z1m, Zeiss, Germany). Slices which did not contain green cells or appeared damaged were discarded. From the remaining pool, 4-12 slices per mouse were selected and used for immunohistochemistry and cell counting. All stainings were performed on 30 µm free floating slices placed into multi-well plates. For antigen retrieval, I incubated the slices in 10 mM citric acid (pH=6.0) at 37$^{o}$C. After washing I applied blocking solution containing: 0.1 M Tris-buffer saline (TBS), 3-5 % Albumin Fraction V (Roth), and 0.2-0.5% Triton-X (Roth), at 37$^{o}$C for 1 hour. Slices were incubated with primary antibody overnight in blocking solution. The following primary antibodies were used: rabbit or guinea pig anti-NG2 (1:500, gift from Bill Stallcup, Burnham Institute, La Jolla, USA), mouse anti-APC (1:250, Ab-7, CC-Calbiochem), rabbit anti-Cleaved-Caspase-3 (1:500, Cell Signalling Technology), chicken anti-GFP (1:500, Abcam), rat anti-MBP (1:125, Abcam). Detection was performed using the following secondary antibodies: goat anti-rabbit Alexa Fluor 568 (1:500, Invitrogen), goat anti-rabbit Cy5 (1:500, Dianova), goat anti-guinea pig Alexa Fluor 633 (1:500, Invitrogen), goat anti-mouse Alexa Fluor 555 (1:500, Invitrogen), donkey anti-chicken FITC (1:1000, Dianova) or goat anti-rat biotin-SP (1:200, Dianova) following by streptavidin-Cy3 (1:200, Dianova). Secondary antibody was applied for 3 hours at 37$^{o}$C. For EdU visualization I followed the protocol recommended by Thermo Fisher Scientific. For counterstaining of the nuclei I used Diamidino-2-phenylindole dihydrochloride (DAPI, 0.2 µg, Sigma).

### 3.11. Image acquisition.

A confocal LSM 710 system (Zeiss, Germany) was used for image acquisition. Images containing corpus callosum were acquired and saved as z-stacks with 16 bit pixel depth. Each z-stack was 6-18 µm thick and consisted of 6-18 z-slices; and the z-step was 1 µm. Each layer of a z-stack was acquired as a tile-scan (vertical x horizontal: 3 x 7 or 2 x 7 images), where each tile was 512 x 512 pixels of size. Pixel size was 0.415 x 0.415 µm. Each tile-scan represented a triple-channel fluorescence image, where channels were acquired sequentially in ZEN software using 40x oil-immersion objective (NA=1.3). The following excitation laser lines and emission detection ranges were used: for DAPI excitation 405 nm, emission 414-490 nm; for FITC excitation 488 nm, emission 497-556 nm; for Alexa-555, Alexa-568 or Cy3 excitation 561 nm, emission 569-633 nm; for Alexa-633 or Alexa-647 excitation 633 nm, emission 650-740 nm.

The beam splitters for each dye matched the excitation laser lines. The pinhole was set to 1.07-1.42 airy units and adjusted such that the optical section for each channel was 1.2 µm. Laser power, detector gain and offset were adjusted such that in the final scan (averaging or average of 2 frames) I had good signal to background noise ratio. For visualization purpose, few images presented in the figures were adjusted for brightness/contrast in ImageJ (NIH, USA), as follows: Fig. 4-8 e, brightness for GFP staining; Fig. 4-8 h, brightness and contrast for NG2 and CC1 staining; Fig 4-8 i, brightness and contrast for CC1 staining; Fig. 4-16 e, brightness for GFP and NG2 staining; Fig. 4-16 f, brightness for GFP and NG2 staining; Fig. 4-16 g, brightness and contrast in CC1staining; Fig 4-17 b, brightness and contrast for NG2 ; Fig 4-17 c, brightness and contrast for CC1; Fig. 4-17 e, brightness for NG2 staining; Fig. 4-17 f, brightness for NG2 staining; Fig. 4-17 g, contrast for CC1 staining; Fig. 4-22 a, brightness of EdU staining.

### 3.12. Cell counting.

I counted GFP-labeled infected cells in z-stack images using ImageJ Cell Counter plugin (NIH, USA). No contrast or brightness adjustment was made in any of the images, but the background subtraction was applied to the green channel before counting. For this the background fluorescence was measured using linear 'plot profile' function in ImageJ and the resulting value was subtracted from each pixel of the original image. The ventral and dorsal borders of corpus callosum were identified based on the CC1 or NG2 and DAPI staining. To define the lateral borders of the region of interest (ROI) used for counting, in each coronal slice I determined the midline of the brain and outlined the area of the corpus callosum approximately 500-700 µm to each side from the midline. Thus, the ROI spanned 1-1.4 mm along the mediolateral axis of the corpus callosum and avoided the cells in the vicinity of lateral ventricles. For the cells located at this predefined border of the ROI, only those cells were included in the analysis whose nucleus was ≥50% within the border. Cells were counted in 4-12 slices from each mouse and the counts within one animal were summed, resulting in 29-486 $GFP^+$ cells per animal. OPCs were identified as $GFP^+NG2^+CC1^-$ cells, pre-myelinating oligodendrocytes as $GFP^+NG2^+CC1^+$ cells, and myelinating oligodendrocytes as $GFP^+NG2^-CC^+$ cells. To avoid individual bias, in randomly selected experiments the counting was repeated by one or two additional investigators blind with respect to the experimental group of animals. The resulting differences in counts were minor and did not affect the final results.

### 3.13. Statistics.

All data acquisition was randomized (animals for viral injections, cells during patch-clamp experiments). Throughout the study I made all efforts to avoid pseudoreplications, both when performing experiments in slices and *in vivo*. For patch-clamp recordings I used in total 59 mice of the age P12-17. The exact number of cells and animals used in each experiment are given in the figure legends.

Statistical analysis was performed using SPSS, including tests for homoscedasticity and normal distribution. If the datasets had normal distributions and equal variances, one-way ANOVA with post-hoc Bonferroni test was used. If the datasets had normal distributions but unequal variances, one-way ANOVA with post-hoc Games-Howell test was used. If the datasets were not normally distributed, Kruskal-Wallis with post-hoc Dunn's test was used. To compare values of rectification index and paired-pulse ratio between cells in non-injected and the GFP expressing animals, I tested the data sets for normal distribution and used the 2-tailed t-test. To compare cumulative probability histogram of the amplitude of the delayed EPSCs between control (GFP) and each experimental group ("$Ca^{2+}$-permeable", "pore-dead", or "C-tail"), 100 trials of random selections were performed and compared in IgorPro as described above. Comparison of the GFP and "$Ca^{2+}$-permeable" groups showed that the two distributions were different in all 100 trials (D value > critical value); therefore, I considered the difference between these two distributions statistically significant. Comparison of the GFP and "pore-dead" groups showed that the two distributions were different in 98 out of 100 trials (D value > critical value); therefore, I considered the difference between these two distributions statistically significant. Comparison of the GFP and "C-tail" groups showed that the two distributions were different in only 46 out of 100 trials (D value > critical value); therefore, I considered the difference between these two distributions was not statistically significant. To report the corresponding *p* values in the figure, I used the Kolmogorov-Smirnov test in the SPSS. Significance level was set at $p<0.05$. Statistically significant differences are indicated by *p* values in the figure legends. For graphs, each point represents an individual data point and the diamond represents the mean ± SEM. Data in the text is also represented as mean ± SEM.

## 4. Results.

### 4.1. Construct the recombinant plasmids containing modified GluA2 subunit of AMPARs and establish a retroviral delivery approach *in vivo* for modifying AMPAR function in callosal OPCs.

To target the GluA2 subunit of AMPARs specifically in callosal OPCs *in vivo*, I employed retroviral gene delivery approach, which has been successfully used previously to label progenitor cells of OL lineage cells derived from the subventricular zone [93, 108]. Before generating the retrovirus carrying the modified GluA2 subunit, it was necessary to construct the recombinant retroviral plasmids containing the desired modifications.

*4.1.1. Plasmids used in the study.*

As indicated above, in the present study I used three ways to modify the GluA2-containing AMPARs: $Ca^{2+}$-permeable, pore-dead, and C-tail. The constructs of pCI-EGFPGluA2(R583Q) ("$Ca^{2+}$-permeable") and pEGFPC1-GluA2Ctail ("C-tail") were the gifts from Roberto Malinow (University of California, USA) and from Ingrid Ehrlich (University of Tübingen, Germany), respectively. But I had to make the "pore-dead" construct myself. For this, I used mutagenesis and made the point mutation from the plasmid of pCI-EGFPGluA2(R583Q) with PCR. After the mutagenesis from pCI-EGFPGluA2(R583Q) to pCI-EGFPGluA2(R583E) by PCR, I transformed the pCI-EGFPGluA2(R583E) into XL 10-Gold Ultracompetent cells (provided from the kit), picked up three different colonies next day, and isolated the plasmid of pCI-EGFPGluA2(R583E) from bacteria. After that, I diagnosed the plasmid by using restriction enzymes and analyzed the digested fragments by electrophoresis. The purpose was to check whether the plasmid was at the desired size. First, I checked the size of entire plasmid by selecting the restriction enzyme which cuts the plasmid once (unique cutting site) to linearize the construct. For this purpose the enzyme HindIII was chosen. The expected size of pCI-EGFPGluA2(R583E) was 8.218 kbp and the size of the fragment on the agarose gel after digestion was above 8 kpb of DNA marker. Second, I selected another restriction enzyme which cut the plasmid at multiple sites and yielded multiple fragments. For this purpose, I selected the enzyme NdeI which is expected to cut at the sites of 388, 3398, and 6140 of the sequences of pCI-EGFPGluA2(R583E). Three fragments were expected to appear on the agarose gel: 3.01, 2.742, and 2.466 kpb respectively. As a positive

control for digestion, I used the pCI-EGFPGluA2(R583Q) plasmid. It served for the comparison to make sure that the pattern of fragments after mutagenesis was similar to the input plasmid. The negative control for the digestion was the pCI-EGFPGluA2(R583Q) plasmid without restriction enzymes. Uncut plasmid is a supercoiled DNA and it appears as three bands at different band size on the gel because of different conformation. It is useful to check the background of the plasmid on the agarose gel and avoid the false positive result from the digested fragments.

The results from the digestion with Hind III and NdeI are shown in (Fig. 4-1 a). The band size of the entire linearized pCI-EGFPGluA2(R583E) plasmid after Hind III digestion (Fig. 4-1 a, lane 1-3) was between 8-10 kbp of DNA marker and comparable to positive control (Fig. 4-1 a, lane P). The bands from pCI-EGFPGluA2(R583E) after the NdeI digestion were of the expected sizes and comparable to the positive control (Fig. 4-1 b, lanes 1-3 and P). The bands from the negative control, supercoiled uncut pCI-EGFPGluA2(R583Q), were above 5 kbp and thus were far away from the sizes of the digested fragments of pCI-EGFPGluA2(R583E) (Fig. 4-1b, lanes 1-3 and N).

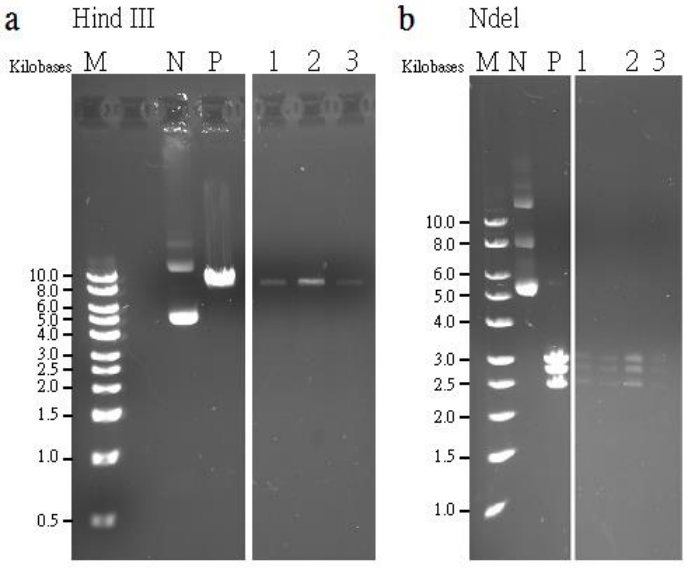


**Figure 4-1. Analysis of digested plasmid (pCI-EGFPGluA2(R583E) by restriction enzyme using agarose gel electrophoresis.**

(a) The plasmid of pCI-EGFPGluA2(R583E) was digested by the enzyme of Hind III. The digested fragment was expected at 8.218 kpb. (b) The same as (a) but digested by NedI. The size of three fragments was 3.01, 2.742, and 2.466 kpb respectively. The gels were truncated for clarify. M: 1kb DNA marker; N: negative control; P: positive control; 1, 2, 3 denote three different colonies.

*4.1.2. Subcloning the recombinant retroviral vector carrying modified GluA2 subunit.*

I used retroviral approach to deliver modified GluA2 subunit to the callosal OPCs. The retroviral vector is based on the Moloney murine leukemia virus (MoMLV). The cytomegalovirus (CMV) promoter was used to drive the transcription of the viral genome. In addition, chicken-beta actin (CAG) promoter was used to drive the expression of GFP or a gene of interest (Fig. 4-2) [104]. My next goal was to subclone the inserts ("$Ca^{2+}$-permeable", "pore-dead", and "C-tail") from the original vectors (pCI and pEGFPC1) into the retroviral vector based on the cloning site of AgeI and PmeI (the schematic procedure was shown in Fig. 3-1 in 3.2.2) and to generate new plasmids: pRetroCAG-EGFPGluA2(R583Q), pRetroCAG-EGFPGluA2(R583E), and pRetroCAG-EGFPGluA2(813-862). I also had to verify that (1) the new retroviral plasmids were of the correct size, (2) the new retroviral plasmids really contained the insert ("$Ca^{2+}$-permeable", "pore-dead", or "C-tail"), and (3) the inserts in the new plasmids (pRetroCAG-EGFPGluA2(R583Q), pRetroCAG-EGFPGluA2(R583E), and pRetroCAG-EGFPGluA2(813-862)) were inserted in the correct orientation (the sequence of insert from 5' to 3' to the retroviral vector) after subcloning. I used the following restriction enzymes: PmeI in order to linearize each of the plasmids; AgeI and PmeI to check the size of the vector and of the insert in each of the three plasmids; PvuII and ClaI to verify the correct orientation of the EGFPGluA2(R583Q) and EGFPGluA2(R583E) inserts (Fig. 4-3 a); and XhoI to check for the correct orientation of the EGFPGluA2(813-862) insert (Fig. 4-3 b) (Detailed information about the corresponding band sizes after digestion are shown in Table 2 within part 3.2.2). Selection of the restriction enzymes for testing the orientation of the inserts was based on the following criteria: (a) The enzyme should cut the insert at around one third of the total length of insert; (b) The enzyme should avoid digesting in the center of the insert and yield two identical fragments in length; (c) The enzyme(s) should make one cut in the insert and another cut in the backbone which is close to one side of the insert. Taken together, the ideal enzymes for verification of the insert orientation should generate two fragments which are different in length.


**Figure 4-2. Scheme of the recombinant retroviral vector.** The vector uses cytomegalovirus (CMV) promoter (P-CMV) to direct transcription of the viral genome and the chicken-beta actin (CAG) promoter to drive the expression of green fluorescent protein (GFP). LTR: long terminal repeat; Ψ: viral packing signal; WPRE: Woodchuck hepatitis virus post-transcriptional regulatory element.

The schematic drawing shown in (Fig. 4-3) explains the digestion sites in the inset and in the backbone and indicates the expected size of the fragments. The total length of pRetroCAG-EGFPGluA2(R583Q) or pRetroCAG-EGFPGluA2(R583E) is 10.6 kbp (Fig. 4-3 a-c). The enzyme PvuII cuts at the position around one third in the insert and yields two fragments: 1.77 kbp and 2.07 kbp (Fig. 4-3 c). In addition, ClaI cuts at the 3' of WPRE which is located in the retroviral backbone (Fig. 4-3 c). The length of WPRE is 0.596 kbp. Therefore, one fragment after double enzymatic digestion is expected to be of 8.278 kbp (i.e. length of the retroviral backbone minus length of WPRE plus length of the insert which is cut by PvuII) (Fig. 4-3 c). Another fragment is expected to be 2.35 kbp (i.e. length of WPRE plus length of the insert cut by PvuII) (Fig. 4-3 c). If the insert orientation is wrong (i.e. opposite direction), the expected size of the band is 7.977 kbp and 2.67 kbp. To verify the orientation of pRetroCAG-EGFPGluA2(813-862) insert, the enzyme XhoI was selected because there are two digestion sites for XhoI in the pRetroCAG-EGFPGluA2(813-862) (Fig. 4-3 d-f). One digestion site is within the insert EGFPGluA2(813-862) and another is at 3' of WPRE in the retroviral backbone (Fig. 4-3 d-f). Thus, two digested fragments of pRetro-EGFPGluA2(813-862) after XhoI treatment were expected: one of 6.935 kbp (i.e. length of the retroviral backbone without the length of WPRE plus length of insert which is cut by XhoI), and another of 0.779 kbp (i.e. length of WPRE plus length of the insert cut by PvuII) (Fig. 4-3 f). If the insert orientation is wrong (i.e. opposite direction), the expected size of the bands is 6.386 kbp and 1.327 kbp.

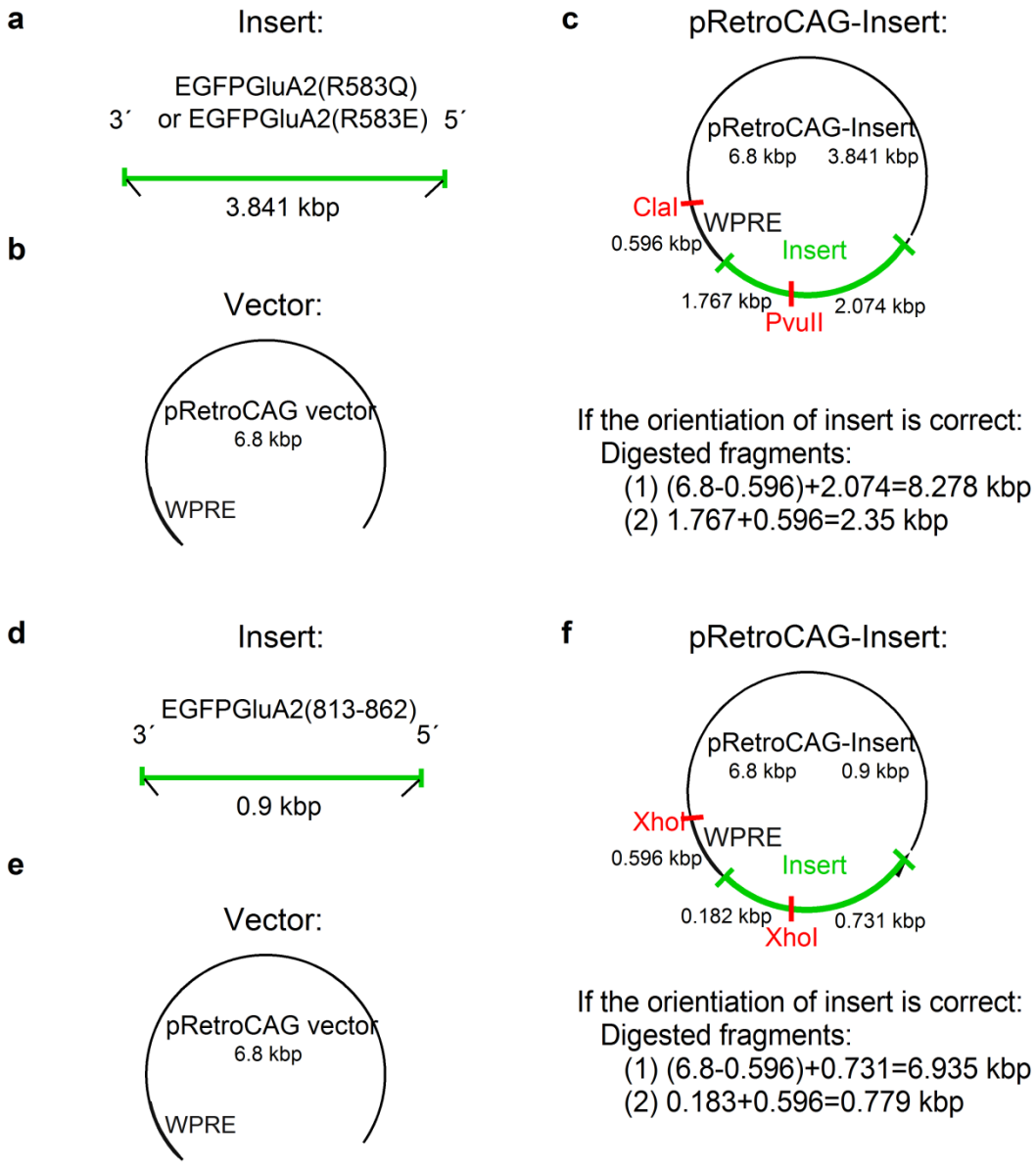


**Figure 4-3. Schematic drawing for verifying the insert orientation in the new generated retroviral plasmids.**

(a-c) Description of correct orientation of inserts in pRetroCAG-EGFPGluA2(R583Q) and pRetroCAG-EGFPGluA2(R583E). (a) The length of the insets was indicated. 5´and 3´: direction of nucleic acids. (b) The length of the vector-retroviral backbone. (c) Newly generated retroviral plasmid with the indication of the enzyme digestion site to examine the orientation of insert. (d-f) Description of correct orientation of insert in pRetroCAG-EGFPGluA2(813-862). (d) As in (a). (e) As in (b). (f) As in (c).

The results of the enzymatic digestion are shown in (Fig. 4-4). The entire size of pRetroCAG-EGFPGluA2(R583Q) and pRetroCAG-EGFPGluA2(R583E) after linearizing the plasmids with PmeI was expected to be 10.64 kbp. Indeed, one band appeared on the agarose gel; it was located close to 10 kbp of DNA marker (Fig. 4-4 a, b; lane: PmeI). Upon digestion with PmeI and AgeI, there were two bands located at 6.8 kbp and 3.841 kbp on the gel Fig. 4-4a, b; lane: PmeI+AgeI). These two bands represented retroviral backbone and insets (EGFPGluA2(R583Q) and EGFPGluA2(R583E) in these cases) (Fig. 4-4 a, b; lane: PmeI+AgeI). In the experiments designed to verify the insert orientation, and using the enzymes PvuII and ClaI, two bands appeared on the gel: close to 8 kbp and 2.5 kbp of DNA marker. These bands corresponded to the expected band sizes, i.e. 8.278 kbp and 2.35kbp. It is important to note that the lower band was below 2.5 kbp of DNA marker (Fig. 4-4 a, b; lane: PvuII+ClaI). These results indicate that the insert orientation in my experiments was correct.

The entire size of pRetroCAG-EGFPGluA2(813-862) was 7.7 kbp after linearizing the plasmids with PmeI (Fig. 4-4 c; lane: PmeI) and the band was appeared close to 8 kbp of DNA marker. In the experiments investigating the backbone and the pRetroCAG-EGFPGluA2(813-862) insert, two bands were detected on the gel after co-digestion of PmeI and AgeI for examination: one of 6.8 kbp and another of 0.9 kbp (Fig. 4-4 c; lane: PmeI and AgeI). To test for the insert orientation, the plasmid of pRetroCAG-EGFPGluA2(813-862) was digested with XhoI. This generated two bands: one was between 6 and 8 kbp of DNA marker and another was close to 1 kbp of DNA marker (Fig. 4-4 c; lane: XhoI). These bands agree well with the expected band sizes of 6.8 kbp and 0.9 kbp, and indicate that the insert orientation in my experiments was correct.

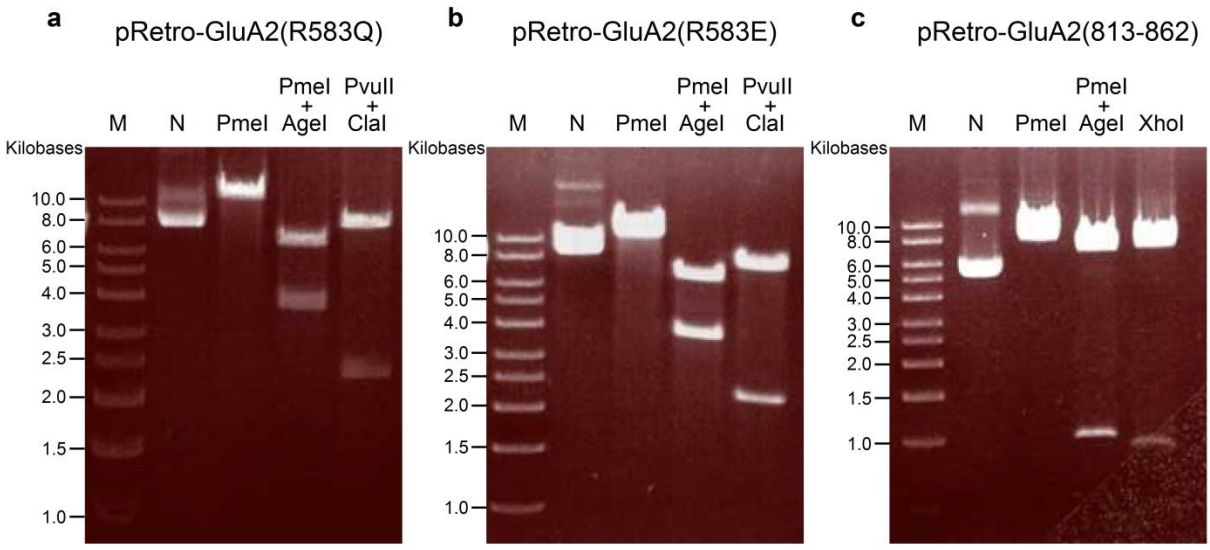


**Figure 4-4. Detection of digested newly generate plasmid (pRetro backbone with insert) by restriction enzyme using agarose gel electrophoresis.**

(a) The plasmid of pRetro-GluA2(R583Q) was digested by the enzyme of PmeI, PmeI/AgeI, and PvuII/ClaI. The digestion aimed to check the properties of cloned plasmid. (b) The same as (a) but for pReto-GluA2(R583E). (c) The plasmid of pRetro-GluA2(813-862) was digested by the enzyme of PmeI, PmeI/AgeI, and XhoI. M: 1 kbp DNA marker, N: negative control, input plasmid.

*4.1.3. GFP expression in HEK 293 cells after transient transfection of retroviral plasmid.*

In each of the constructs containing the modified GluA2 subunit or the GluA2 C-tail the sequence of GFP was also present (Fig. 2-1 in the section 2.3) Therefore, my next goal was to test whether GFP expression can be detected when each of the plasmids was transiently transfected into the HEK 293 cells. In cells transfected with pRetroCAG-EGFPGluA2(R583Q) or pRetroCAG-EGFPGluA2(R583E), GFP appeared in the cytoplasm and close to the cell membrane but did not overlap with the nucleus (Fig. 4-5 b, c). In contrast, the pattern of GFP expression in cells transfected with pRetroCAG-GFP or pRetroCAG-EGFPGluA2(813-862) was different: GFP was visible in the cell cytoplasm and also in the nucleus (Fig. 4-5 a, d). These differences of GFP expression pattern may be due to the protein size. The protein size of pRetroCAG-GFP and pRetroCAG-EGFPGluA2(813-862) is relatively small, i.e. about 25 and 34 kDa, respectively. The protein size of pRetroCAG-EGFPGluA2(R583Q) and pRetroCAG-EGFPGluA2(R583E) is much larger, i.e. about 140 kDa (using DNA sequences calculated by the website of http://www.molbiol.ru/eng/scripts/01_06.html, [109]). It has been suggested that proteins smaller than 90-110 kDa can passively diffuse through the nuclear pore complex [110]. This may explain why in cells transfected with pRetroCAG-GFP and pRetroCAG-EGFPGluA2(813-862), the GFP expression was detected in the whole cell including in the nucleus, while in cells transfected with pRetroCAG-EGFPGluA2(R583Q) and pRetroCAG-EGFPGluA2(R583E), GFP was found mainly in the cytoplasm (Fig. 4-5).

**Summary of part 4.1.**

Taken together, subcloning of EGFPGluA2(R583Q), EGFPGluA2(R583E), and EFGPGluA2(813-862) from original plasmid into retroviral vector was successful and the expression of GFP was detected in the HEK 293 cells transfected with each of the new retroviral plasmids. I then used the retroviral plasmids for the further production of retrovirus carrying each modifying construct. To simplify the name of each constructs, I named pRetroCAG-GFP, pRetroCAG-EGFPGluA2(R583Q), pRetroCAG-EGFPGluA2(R583E), and pRetroCAG-EGFPGluA2(813-862) hereafter as GFP (control group), "$Ca^{2+}$-permeable", "pore-dead", and "C-tail", respectively.

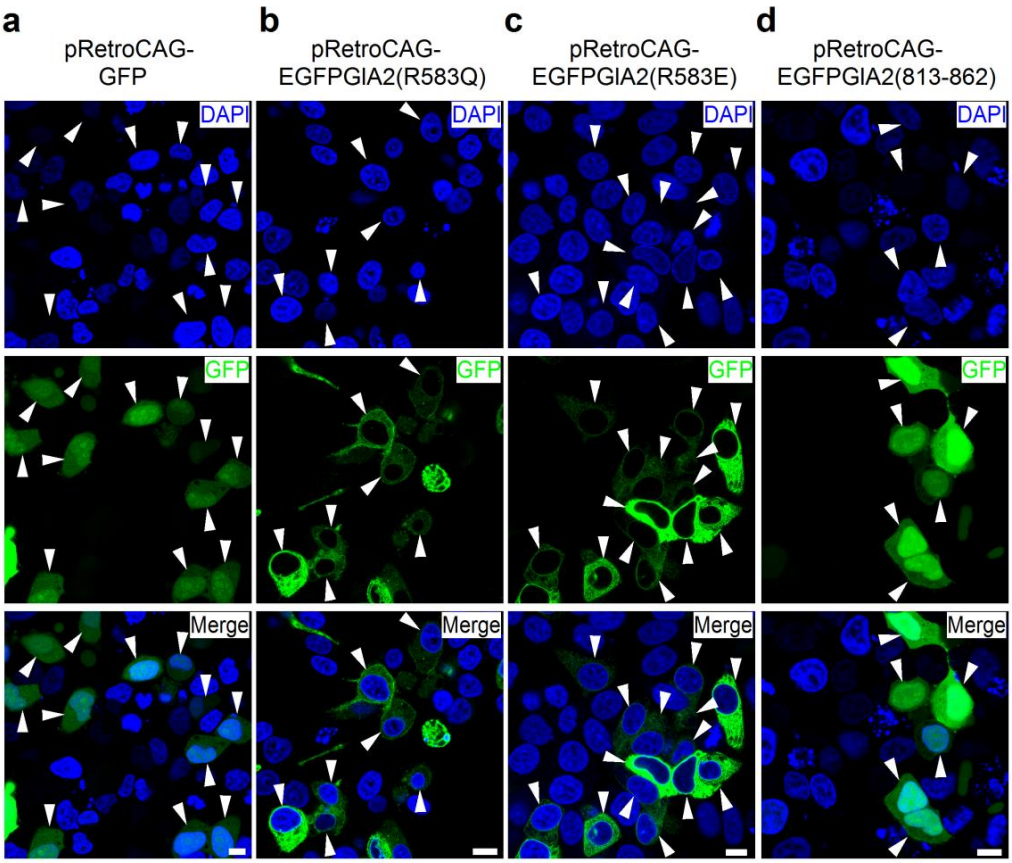


**Figure 4-5. The transfection of the retroviral plasmid containing modified GluA2 subunit into HEK 293 cells and GFP expression was monitored 48 hours after transfection.**

(a) Examples of single plane of confocal images from HEK 293 cells transfected with construct of pRetroCAG-GFP showing DAPI, GFP, and merge for two channels. (b) As in (a) but from pRetroCAG-EGFPGluA2(R583Q). (c) As in (a) but from pRetroCAG-EGFPGluA2(R583E). (d) As in (a) but from pRetroCAG-EGFPGluA2(813-862). White arrowheads point to the soma of the transfected cells. Scale bar: 10 μm.

## 4.2. Changes in synaptic AMPAR-mediated currents in OPCs.

My next goal was to test whether retrovirus carrying GFP (as a control group) targeted OPCs specifically. Next, I expressed three GluA2 subunit modifications, "$Ca^{2+}$-permeable", "pore-dead", and "C-tail", in callosal OPCs *in vivo* using retroviral approach and aimed to investigate whether three GluA2 subunit modifications altered the $Ca^{2+}$-permeability and quantal amplitude of AMPARs in callosal OPCs due to the changes in the subunits compositions or the replacements of AMPARs. For doing that, I applied whole cell voltage clamp technique to record the evoked AMPARs mediated current in OPCs upon axonal electrical stimulation (detail information is mentioned below) and quantal amplitude by axonal train stimulation.

*4.2.1. Expression of myelin basic protein (MBP) increases gradually in the mouse corpus callosum during the second and third postnatal weeks.*

To investigate the importance of AMPAR-mediated signaling for differentiation and proliferation of OPCs, the developmental time-window for introducing the modified GluA2 subunit should be selected such that the rate of OPCs differentiation and proliferation is high. There are two reasons for that. First, retrovirus infects proliferating cells. Therefore, in order to infect many OPCs, the retrovirus should be injected into the corpus callosum at the time-point when many proliferating OPCs are present. Secondly, if I interfere with AMPAR-mediated signaling in OPCs during the time-window when differentiation and proliferation rate of OPCs is high, it is easier to observe the differences in the experimental groups and the control group. During the first 2-3 postnatal weeks, the differentiation and proliferation rate of OPCs is high [9, 14, 111], and therefore this time-window is suitable for the study. To determine the optimal time-window more precisely, I performed immunolabeling for MBP in brain slices from mice of P9, P10, P11, P12, P15 and P18. MBP is a major myelin protein and is mainly expressed in the processes of OLs. Expression of MBP in OLs acts as an indicator of the differentiation of OPCs into OLs.

I found that expression of MBP in the mouse corpus callosum increases gradually between P9 and P18 indicating that OPCs differentiate into myelinating OLs during this time-window of development (Fig.4-6). Therefore, I thought that the age of mice between P10 and P18 would be

the most suitable for modifying AMPAR-mediated on neuron-OPC signaling, and studying the effects of modifications on proliferation and differentiation of OPCs.

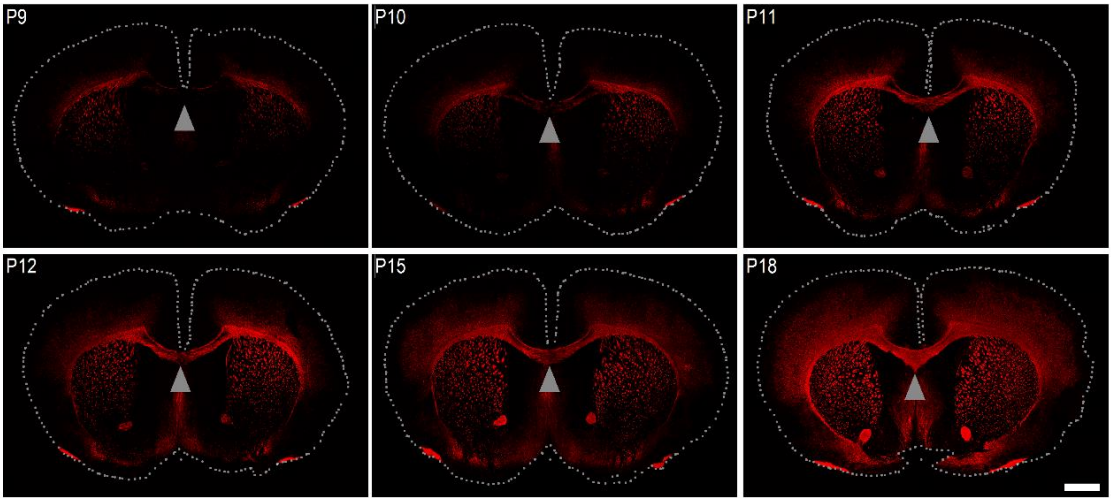


**Figure 4-6. Expression of myelin basic protein in the mouse corpus callosum increases between P9 and P18.**

Representative overview images of coronal brain slices stained for myelin basic protein (MBP, red). Images were taken with a confocal laser scanning microscope using a 10x objective and an optical section thickness of 12.3 µm. Slices were prepared from mice of different ages: P9, P10, P11, P12, P15 and P18, as indicated on the panels. Dashed lines indicate the borders of each slice. Arrowheads point to the midline of the corpus callosum. Scale bar: 1mm. MBP expression is increasing gradually in the corpus callosum between P11-P18. Stainings were replicated in three mice of each age-group.

*4.2.2. GluA2 subunit of AMPARs is present in callosal OPCs in P12-P17.*

It has been reported that callosal OPCs express GluA2-containing $Ca^{2+}$-impermeable AMPARs in P7-P8 mice [76] and P8-P16 rats [75]. I wanted to verify these findings in my study and to make sure that edited GluA2 subunit of AMPARs is expressed in callosal OPCs during the developmental time-window of my interest (P12-P17). For this, I performed whole cell voltage clamp recordings from callosal OPCs in $NG2DsRed^{+}$ mice (called "non-injected" hereafter and in the figures) and studied evoked AMPARs-mediated currents at several holding potentials (-90 mV, -40 mV, 0 mV, +20 mV, and +40 mV). After the recording, I built the I-V curve by plotting the amplitude of evoked currents vs. holding potential (Fig. 4-7 a), and calculated the rectification index as a ratio of current amplitude at $V_h$ of +40 mV and at $V_h$ of -90 mV. If GluA2-lacking AMPARs are present in OPCs, it is expected that there are less outward currents passing through the receptors when positive holding potentials are applied and polyamine spermine (100 μM) is present in the internal solution. In this case, the I-V relationship is inwardly rectifying. If AMPARs in OPCs contain GluA2 subunit, I-V curve displays linearity because ions flow through the receptors equally good when cells are clamped negative or positive potentials. Theoretically if the rectification index is close to 0.44, it is considered that AMPARs contains GluA2 subunit; if the rectification index is near 0, it is considered that GluA2-lacking AMPARs are present.

As mentioned above, callosal OPCs in mice express GluA2-containing $Ca^{2+}$-impermeable AMPARs during the developmental window of my interest. Therefore, I expected to record linear I-V curve and to obtain rectification index close to 0.44. In all experiments polyamine spermine was included into the intracellular solution in order to preserve inward rectification of I-V relationship. I found that I-V relationship of AMPARs in callosal OPCs showed only slight inward rectification, and the averaged rectification index was 0.33±0.058 (Fig. 4-7 b) which was close to the index of linear I-V relationship. This data demonstrated that GluA2-containing $Ca^{2+}$-impermeable AMPARs are indeed present in callosal OPCs in P12-P17 mice.

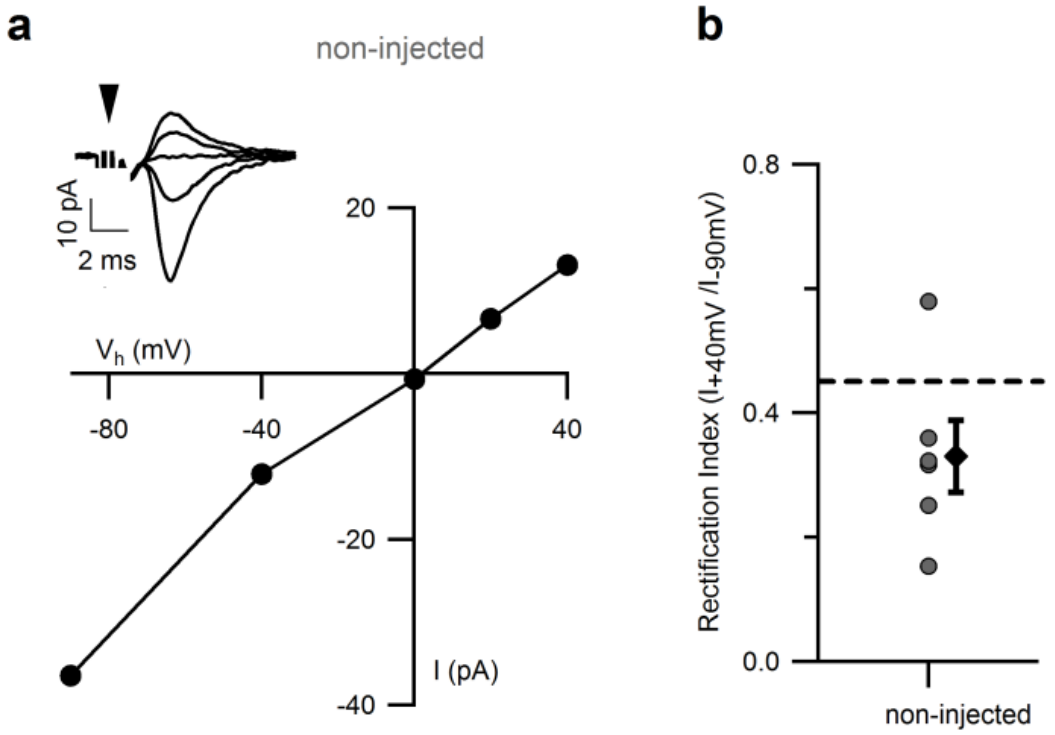


**Figure 4-7. Callosal OPCs in P12-17 mice express GluA2-containing AMPARs.**

(a) I-V relationship of evoked axon-glia EPSCs recorded in an OPC from a non-injected mouse. Each graph represents one example cell. Each black dot represents the amplitude measurement performed from the average of 10 sweeps recorded at a given holding potential ($V_h$). Corresponding examples of the averaged sweeps are shown above each graph. The arrowhead indicates the time of stimulation. The stimulation artifacts are blanked for clarity. (b) The summary graph showing rectification index for evoked EPSCs recorded in the OPCs from the non-injected (n=6 cells from 5 mice) animals. Each dot represents one cell. The black diamonds represent mean ± SEM for each group. The dashed line indicates the theoretical rectification index of the linear I-V relationship (no rectification).

*4.2.3. Retrovirus-GFP targeted oligodendroglia lineage cells specifically.*

Retrovirus infects dividing cells and OPCs are the major cycling cells in the brain [112]. However, during second-third postnatal weeks, some other types of proliferating cells may be also present in the mouse corpus callosum, in addition to OPCs. In order to test the specificity of retrovirus for OPCs, I wanted to find out whether retrovirus infected proliferating cells other than OPCs and what the percentage of those cells was. I stereotaxically injected retrovirus-carrying GFP (Fig. 4-2) into the corpus callosum of P10-P12 mice (Fig. 4-8 a), sacrificed the injected mice 5 days later (Fig. 4-8 b) and performed immunofluorescent labeling for GFP, NG2 and CC1 to label all infected cells, OPCs and OLs, respectively (Fig. 4-8 f-h). $GFP^+$ cells were found in the corpus callosum (Fig. 4-8 d) and spread both in medial-lateral and rostro-caudal direction from the injection site (Fig. 4-8 c). Remarkably, 94% of the $GFP^+$ cells were oligodendrocyte lineage cells: 33.3% were OPCs ($NG2^+$ $GFP^+$) and 43.2% were mature OLs ($CC1^+GFP^+$); the remaining 17.4% of cells were weakly positive for both, NG2 and CC1, and I considered them to be pre-myelinating oligodendrocytes, i.e. intermediate between OPCs and mature OLs (Fig. 4-8 f-h). These findings suggested that retrovirus itself infected oligodendrocyte lineage cells specifically and infected only few cells of other types.

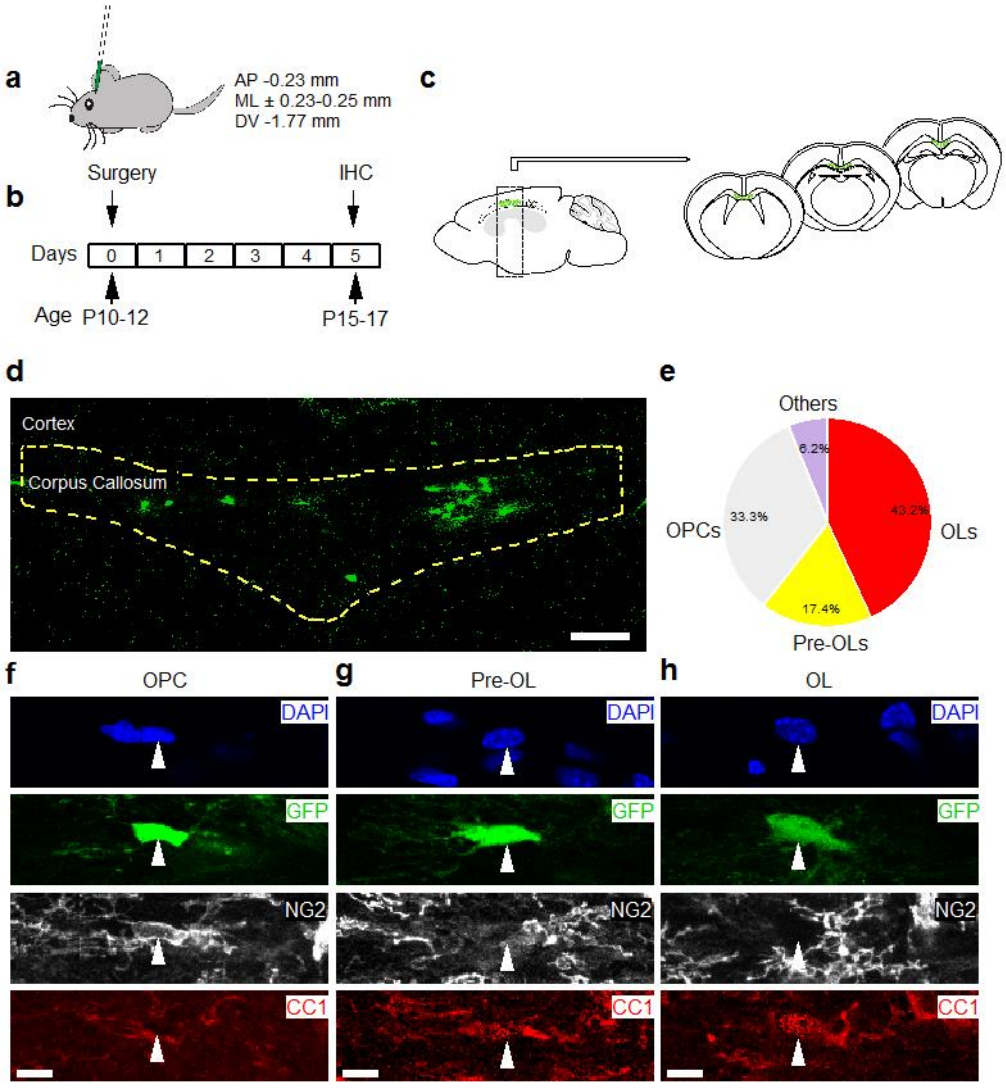


**Figure 4-8. Retrovirus targets oligodendroglia lineage cells specifically**.

(a) Stereotaxic coordinates used for bilateral virus injection into the corpus callosum. AP, anteroposterior; ML, mediolateral; DV, dorsoventral. (b) Experimental time-frame and animal age. IHC: Immunohistochemistry. (c) Scheme showing the distribution of cells targeted with retrovirus (green dots) in the corpus callosum. Virally-transduced cells were found in several 300-µm-thick coronal slices along the rostro-caudal axis. Cells were counted in 4-12 slices of 30 µm in thickness from each mouse. (d) Maximum intensity projection from 6 successive confocal planes showing cells infected with retrovirus and expressing GFP in the corpus callosum. Yellow dashed line indicates the area used for counting. Scale bar: 100 µm. (e) Diagram showing that the majority of cells targeted with retrovirus ($GFP^+$) belonged to the oligodendrocyte lineage (n=8 animals). OPCs, oligodendrocyte precursor cells; pre-OLs, pre-myelinating oligodendrocytes; OLs, oligodendrocytes. (f) Maximum intensity projection from 3 successive confocal planes showing quadruple labeling for DAPI, GFP, NG2, and CC1. The arrowhead points to an OPC ($GFP^+NG2^+CC1^-$). Scale bar: 10 µm. (g) Same as in g but the arrowhead points to a pre-OL ($GFP^+NG2^+CC1^+$). (h) Same as in g but the arrowhead points to an OL ($GFP^+NG2^-CC1^+$).

*4.2.4. Retrovirus infection does not affect AMPAR properties or presynaptic release probability at axon-OPC synapses.*

The processes of retroviral infection and GFP expression in OPCs may alter the composition of AMPARs and affect their $Ca^{2+}$ permeability. Therefore, I verified the $Ca^{2+}$ permeability of AMPARs in callosal OPCs by recording I-V relationship of evoked axon-OPC EPSCs. I stereotaxically injected retrovirus carrying GFP into the corpus callosum of P10-P12 NG2DsRed$^{+}$ mice, sacrificed the animals 3-5 days later (Fig. 4-9), and performed I-V recordings as described above in part 4.2.2.

I found that current-voltage relationship of AMPARs recorded from GFP$^{+}$ OPCs showed only slight inward rectification (Fig. 4-10 a), and the averaged rectification index was 0.35±0.049 which is comparable to non-injected group (RI=0.33±0.058) (Fig. 4-10 b) (non-injected vs. GFP: 2-tailed t-test; t(16)=-0.222, p=0.827). This data suggested that GluA2-containing $Ca^{2+}$-impermeable AMPARs were present in callosal OPCs expressing GFP, and retrovirus infection or GFP expression did not alter $Ca^{2+}$-permeability of AMPARs at axon-OPC synapses.

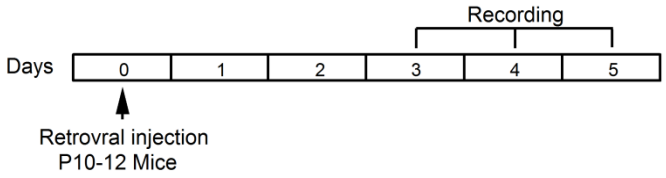


**Figure 4-9. Experimental time-frame and animal age used for electrophysiological experiments.**

Retrovirus carrying modifications was injected into mouse corpus callosum at P10-12. The electrophysiological recordings were performed on the third to fifth days after retroviral injection.

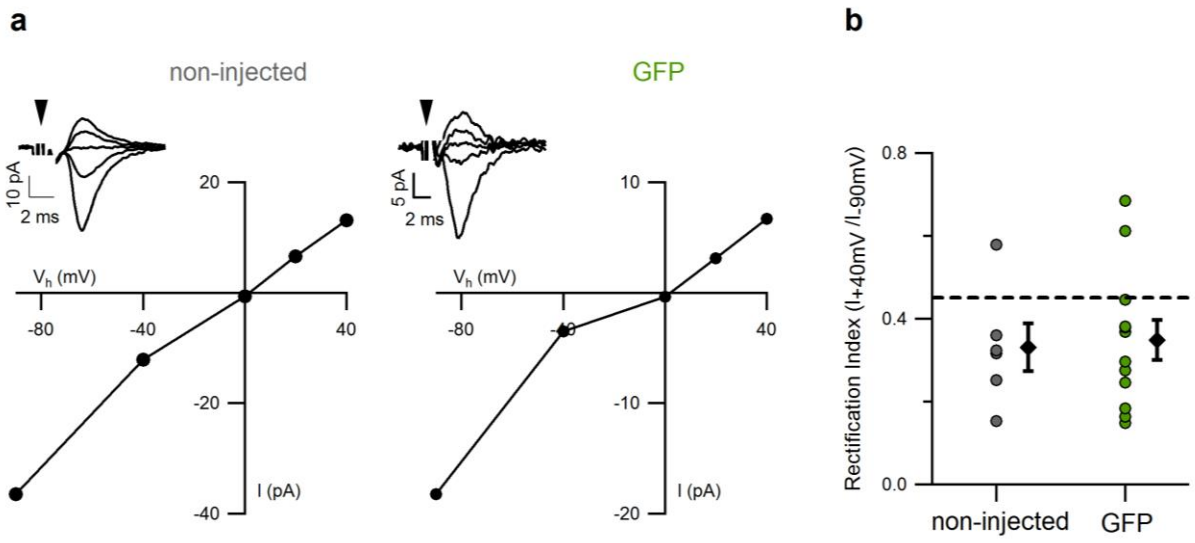


**Figure 4-10. Retrovirus infection does not affect $Ca^{2+}$-permeability of AMPAR at axon-OPC synapses.**

(a) I-V relationship of evoked axon-glia EPSCs recorded in an OPC from a non-injected (*left*) or a GFP-injected (*right*) mouse. Each graph represents one example cell. Each black dot represents the amplitude measurement performed from the average of 10 sweeps recorded at a given holding potential ($V_h$). Corresponding examples of the averaged sweeps are shown above each graph. The arrowhead indicates the time of stimulation. The stimulation artifacts are blanked for clarity. The I-V curve for the non-injected group is the same as shown in Figure 4-7. (b) The summary graph showing rectification index for evoked EPSCs recorded in the OPCs from the non-injected (n=6 cells from 5 mice) or the GFP-injected (n=12 cells from 9 mice) animals. Each dot represents one cell. The black diamonds represent mean ± SEM for each group. The dashed line indicates the theoretical rectification index (RI=0.44) of the linear I-V relationship (no rectification). The dataset for the non-injected group is the same as in the Figure 4-7.

The processes of retroviral infection and GFP expression in OPCs may suppress or enhance AMPARs trafficking to the postsynaptic membrane in OPCs and to affect the number and/or conductance of AMPARs. This would be reflected in the alteration of the amplitude of quantal excitatory postsynaptic currents (EPSCs). To address this issue, I studied the amplitude of quantal AMPAR-mediated EPSCs in callosal OPCs of non-injected and GFP-injected NG2DsRed$^{+}$ mice. I recorded quantal EPSCs ($V_h$ = -80 mV) as delayed currents appearing after the train of 20 electrical stimuli applied to callosal axons at 25 or 100 Hz. (Fig. 4-11 a). Delayed EPSCs are considered as quantal events in neuronal synapses because those delayed EPSCs have amplitude and kinetics similar to miniature EPSCs [113, 114]. Delayed EPSCs after the train of electrical stimuli are also considered as quantal events at axon-OPC synapses due to similarities of amplitude and kinetics between mEPSCs and delayed EPSCs [18]. After recording, I selected 67 delayed events randomly from each cells, pooled the selected events from all OPCs within the GFP-group or within the group of non-injected mice, and built the cumulative probability histograms (the procedure is described in details in part 3.9.3). These histograms were not significantly different between non-injected and GFP-injected mice (Kolmogorov-Smirnov test; p=0.470) (Fig. 4-11 b-c). This finding suggested that retrovirus injection and/or GFP expression in OPCs did not alter the quantal EPSCs mediated by activation of postsynaptic AMPARs (postsynaptic responsiveness to the neurotransmitters) upon release of single glutamatergic vesicles from callosal axons.

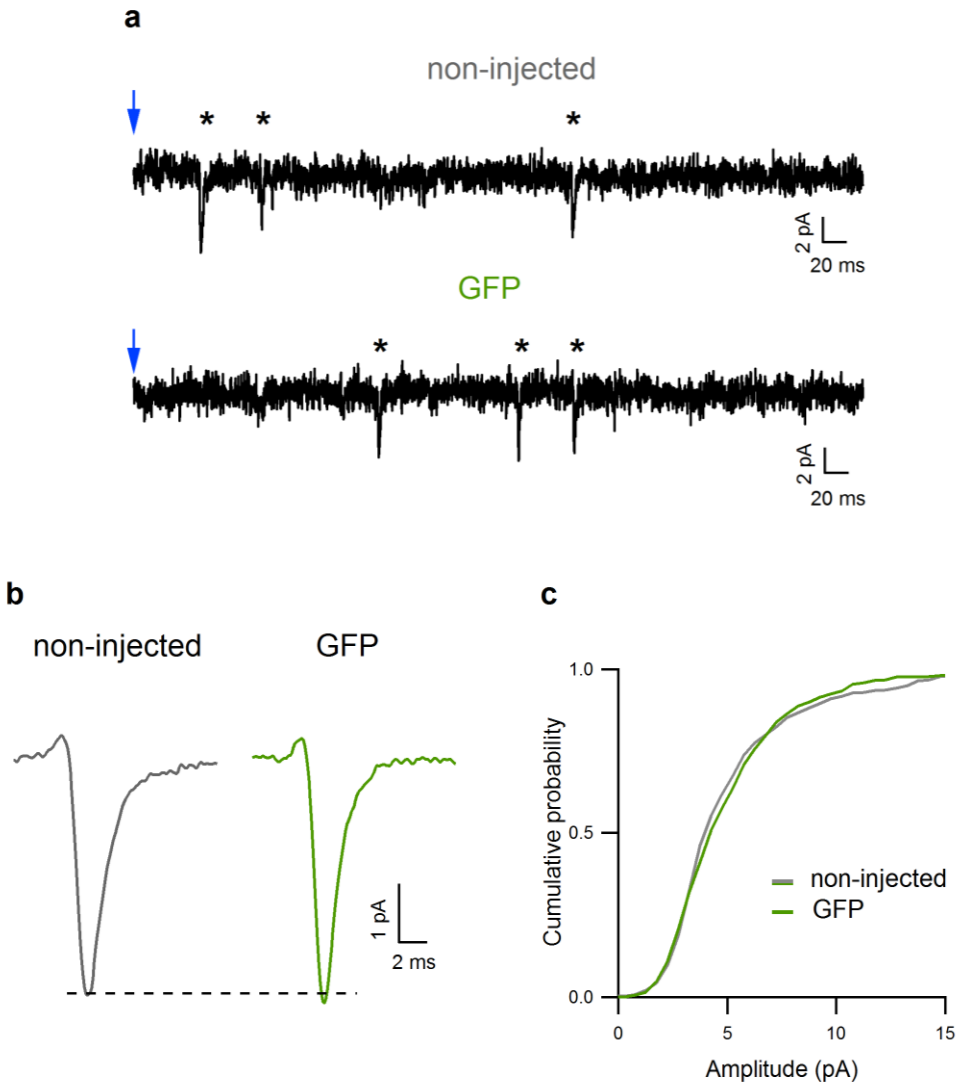


**Figure 4-11. Retrovirus does not affect number of AMPAR in OPCs activated upon release of single glutamatergic vesicles.**

(a) *Top*, Representative example trace recorded from an OPC in a non-injected mouse ($V_h$=-80 mV) after cessation of the train stimulation of callosal axons. Stars indicate delayed events. The arrow indicates the end of the train stimulation. *Bottom*, same as the top panel but for an OPC in the GFP group. (b) Averaged delayed events from 6 cells (non-infected, *left*), 7 cells (GFP, *right*). In each cell, 67 events were randomly selected and averaged. Subsequently, the averages from all cells within each experimental group were put together to generate the average EPSC for each group. (c) Cumulative probability distribution histograms of the amplitude of delayed axon-glia EPSCs. 67 events were randomly selected from each cell, and the events from all cells within each experimental group were pooled: non-infected: 402 events from 6 cells in 4 mice; GFP: 469 events from 7 cells in 6 mice.

Next, I wanted to test whether retroviral infection and/or GFP expression affected presynaptic part of axon-OPC synapses. To do so, I analyzed paired-pulse ratio (PPR) of evoked axon-glia EPSCs. PPR is a measurement of short-term forms of presynaptic plasticity and is widely used to estimate the release probability in neuronal field [115, 116]. I recorded the evoked AMPARs-mediated EPSCs by applying pairs of stimuli at 25 Hz and measured the amplitudes of each response in a pair. I then calculated the PPR by dividing the amplitude of the second response by the amplitude of the first response, and compared PPR in non-infected and GFP-injected mice (Fig. 11a-b). PPR was 1.67±0.19 in non-injected mice and 1.65±0.11in GFP animals, indicating that EPSCs in both groups displayed paired-pulse facilitation. There was no statistically significant difference between two groups (2-tailed t-test; $t(16)=0.126$, $p=0.901$) indicating that retroviral infection or GFP expression did not affect axonal release probability.

Taken together, these findings demonstrate that retrovirus infection itself or GFP expression in OPCs did not modify the presynaptic release probability, the quantal amplitude, or $Ca^{2+}$ permeability of the postsynaptic AMPARs in OPCs. Therefore, in subsequent experiments I used the animals which received injections of retrovirus expressing GFP alone, as a control group. I compared this group to the animals injected with one of GluA2-subunit modifying constructs.

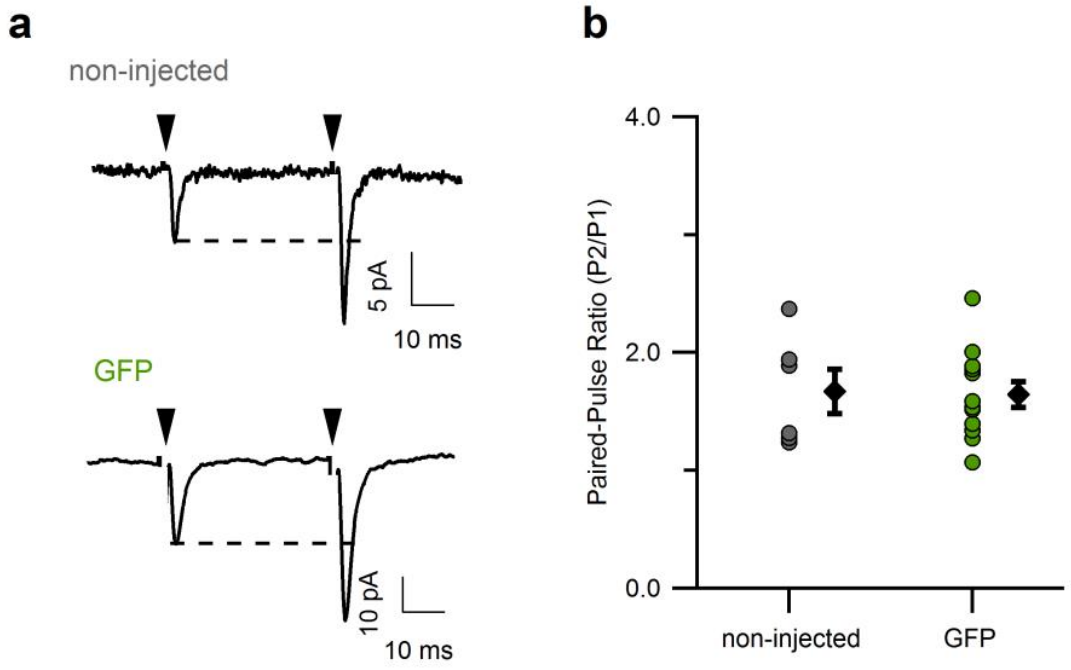


**Figure 4-12. Retrovirus infection does not affect presynaptic release probability at axon-OPC synapses.**

(a) Representative example traces showing evoked axon-glia EPSCs recorded in an OPC ($V_h$ = -90 mV) from a non-injected mouse (*top*) and from a GFP-injected mouse (*bottom*). Each trace represents the average of 30-35 sweeps. The black arrowheads indicate the time-point of stimulation. The stimulation artifacts are blanked for clarity. The dashed lines indicate the peak of EPSC elicited by the first stimulus. (b) Summary graph showing the paired pulse ratio of the evoked EPSCs recorded in the OPCs. Each dot represents one cell. The black diamonds represent mean ± SEM for each group. Non-infected: n=6 cells from 5 mice; GFP: n=12 cells from 9 mice.

*4.2.5. Modifications of the GluA2 subunit of AMPARs in OPCs change rectification and amplitude of axon-glia EPSCs.*

To check whether modified GluA2 subunits incorporated into the functional AMPARs in the OPCs membrane, I examined the properties of AMPARs in callosal OPCs expressing GluA2-modifying constructs (Fig. 2-1 b). First, I investigated $Ca^{2+}$-permeability of AMPARs in OPCs by recording I-V relationship of AMPAR-mediated EPSCs in OPCs 3-5 days after retroviral injection (Fig. 4-9). The I-V relationship of AMPARs-mediated EPSCs from OPCs expressing "$Ca^{2+}$-permeable" construct, displayed noticeable inward rectification (RI=0.093±0.018; Fig. 4-13 a-b) as expected for $Ca^{2+}$-permeable AMPARs [54]. Inward rectification was significantly larger than in GFP group (One-way ANOVA with Games-Howell test; F(3, 30)=11.800, p=0.000028; GFP vs. $Ca^{2+}$-permeable: p=0.001 ). The result indicated that exogenous $Ca^{2+}$-permeable GluA2 subunit formed functional receptors with or without endogenous subunits and integrated into the axon-OPC synapses. Similarly, evoked EPSCs in OPCs expressing "pore-dead" GluA2 showed marked inward rectification (RI=0.078±0.034; Fig. 4-13 a-b) , indicating that $Ca^{2+}$-permeability of AMPARs was significantly larger than in GFP group (One-way ANOVA with Games-Howell test; F(3, 30)=11.800, p=0.000028; GFP vs. pore-dead: p=0.002). These findings suggested that exogenous subunit replaced the $Ca^{2+}$-impermeable AMPARs, the delivery of GluA2-containging AMPARs to the synapses was blocked, and/or additional GluA2-lacking AMPARs were inserted at the postsynaptic sites in OPCs. Interestingly, nearly linear I-V relationship of evoked EPSCs (RI=0.38±0.054; Fig. 4-13 a-b) was obtained from OPCs expressing GluA2 "C-tail", and it was not different from GFP group (One-way ANOVA with Games-Howell test; F(3, 30)=11.800, p=0.000028; GFP vs. C-tail: p=0.969). These experiments suggested that pore mutations of the GluA2 subunits ("$Ca^{2+}$-permeable" and "pore-dead") changed the $Ca^{2+}$ permeability of AMPARs resulting from adding more GluA2-lacking AMPARs to the postsynaptic site in OPCs. On the contrary, expression of GluA2 "C-tail" did not result in changes of $Ca^{2+}$ permeability of AMPARs in OPCs.

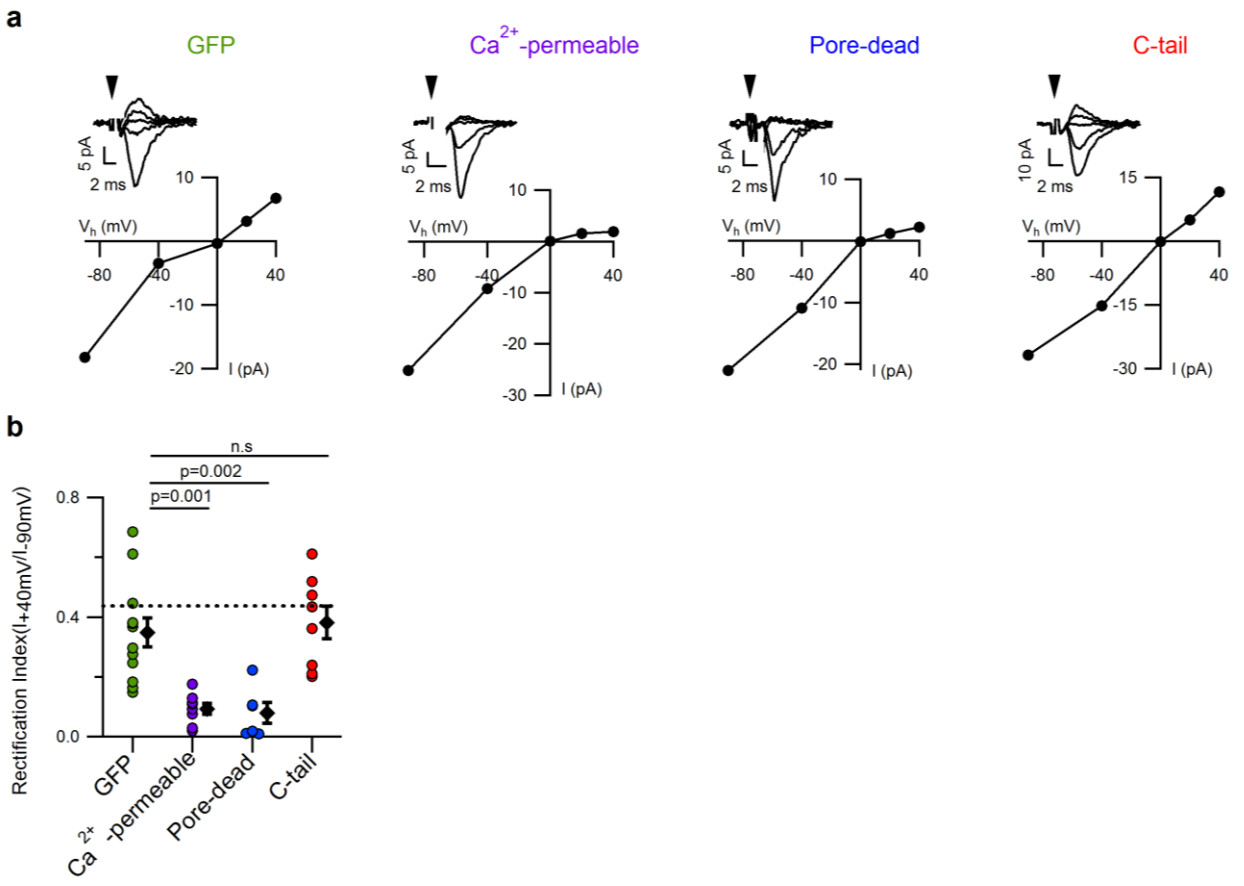


**Figure 4-13. Modifications of the GluA2 subunit of AMPARs in OPCs change rectification of axon-glia EPSCs.**

(a) Current-voltage (I-V) relationship of evoked axon-glia EPSCs in OPCs infected with a virus carrying GFP or one of the AMPAR-modifying constructs. Each graph represents one example cell. Each black dot represents an amplitude measurement performed from an average of 10 sweeps recorded at a given holding potential ($V_h$). Corresponding averaged sweeps are shown above each graph. Arrowheads indicate time of stimulation. Stimulation artifacts are blanked for clarity. The dataset of GFP is the same as in the Figure 4-11. (b) Summary graph showing the rectification index for evoked EPSCs recorded in OPCs infected with retrovirus which expresses GFP (n=12 cells from 9 mice), "$Ca^{2+}$-permeable" GluA2 (n=8 cells from 7 mice), "pore-dead" GluA (n=6 cells from 6 mice), or "C-tail" of GluA2 (n=8 cells from 6 mice). Each dot represents one cell. Black diamonds represent mean ± SEM for each group. The dashed line indicates the theoretical rectification index (RI=0.44) of the linear I-V relationship (no rectification).

Changes in $Ca^{2+}$ permeability of AMPARs in OPCs (Fig. 4-13) represented the differences in the combinations of AMPARs after introduced the modified GluA2 subunit in OPCs. These may affect the number of AMPARs due to the insertion and/or removal and the conductance of the receptors. Therefore, I analyzed the amplitude of the quantal EPSCs occurring after a train of 20 stimuli at 25 or 100 Hz applied to callosal axons (Fig. 4-14 a), as described above (see part 4.2.4). I found that cumulative amplitude distribution histogram of events recorded in OPCs expressing "$Ca^{2+}$-permeable" construct shifted towards the larger amplitudes compared to GFP (Kolmogorov-Smirnov test: GFP vs. $Ca^{2+}$-permeable: p=0.00000013492) ( Fig. 4-14 c). These data, together with the findings that EPSCs in this group of animals showed strong inward rectification (I-V relationship), suggests that increase in the quantal EPSCs amplitude was due to a higher conductance of postsynaptic AMPARs composed mainly of $Ca^{2+}$-permeable subunits (un-edited GluA2, GluA3, and GluA4, and possibly also GluA1) [117].

Comparing the cumulative amplitude distribution histogram between OPCs expressing GFP and "pore-dead", I found that cumulative amplitude distribution histogram was shifted towards the larger amplitude in the "pore-dead" group (Kolmogorov-Smirnov test: GFP vs. pore-dead: p=0.000006) (Fig. 4-14 b-c), similar to animals expressing "$Ca^{2+}$-permeable" construct (Fig. 4-14 b-c). The inwardly rectifying I-V relationship and the larger amplitude in the OPCs with GluA2 "pore-dead" expression suggested that additional GluA2-lacking AMPARs were inserted to the postsynaptic sites in OPCs (see below in the discussion part for detailed explanations).

The expression of the GluA2 "C-tail" in OPCs did not affect the quantal EPSC amplitude when compared to the GFP group (Kolmogorov-Smirnov test: GFP vs. C-tail: p=0.101) (Fig. 4-14 b-c). The findings of un-changed quantal EPSC amplitude and un-changed I-V relationship of the evoked EPSCs (Fig. 4-14 a-b), suggest that expression of the GluA2 "C-tail" did not affect the ionotropic function or number of AMPARs at individual neuron-OPC synapses. However, I cannot exclude the possibility that the GluA2 "C-tail" interfered with intracellular signaling via intracellular binding partners as has been proposed for neuronal synapses [102].

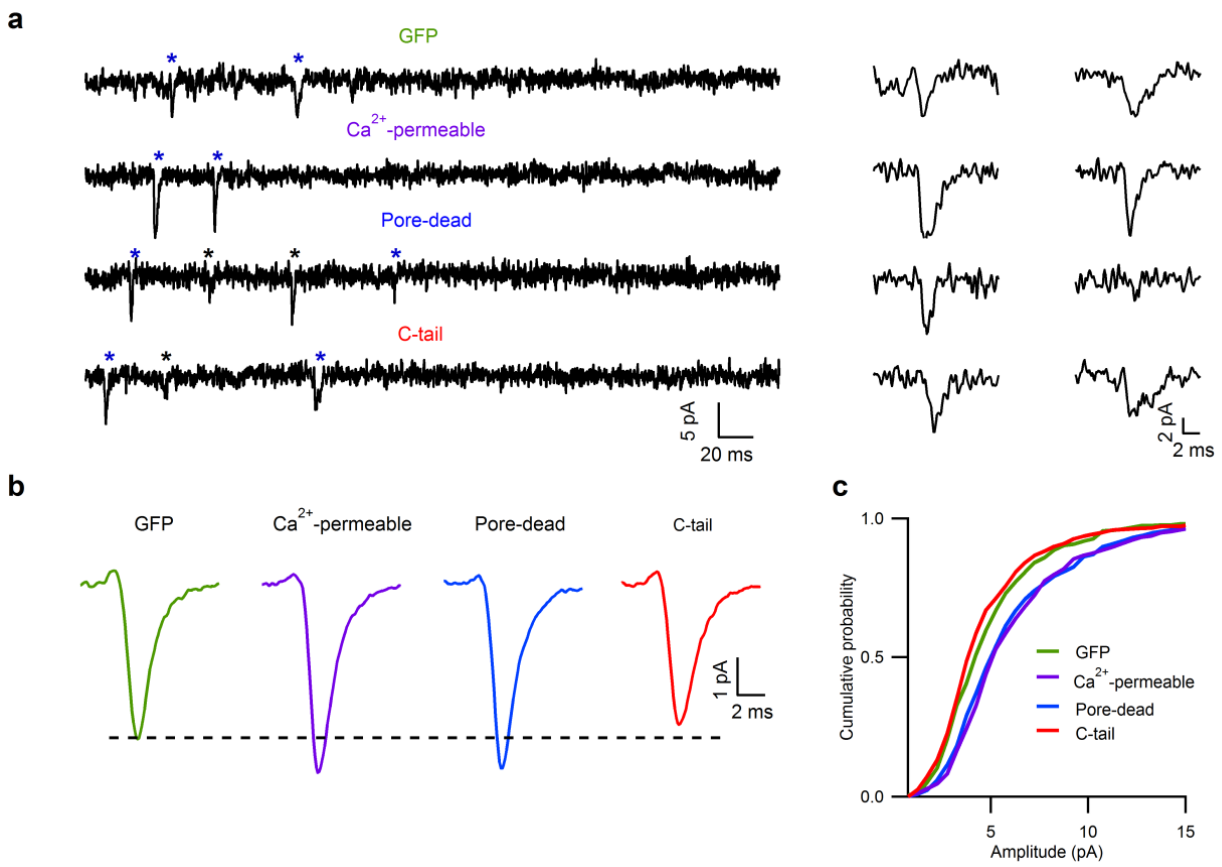


**Figure 4-14. Modifications of the GluA2 subunit of AMPARs in OPCs change amplitude of axon-glia EPSCs.**

(a) *Left*, Representative example traces of EPSCs recorded in OPCs targeted with retrovirus carrying GFP or one of the AMPAR-modifying constructs ($V_{hold}$=-80 mV). The segments of the sweeps recorded immediately after the cessation of train stimulation of callosal axons with 20 pulses at ≥25 Hz are shown. Stars indicate delayed events; blue stars indicate events shown on the right. (b) Averaged delayed EPSCs from 7 cells (GFP), 7 cells ("$Ca^{2+}$-permeable"), 8 cells ("pore-dead"), and 8 cells ("C-tail"). In each cell, 67 events were randomly selected and averaged. Subsequently, the averages from all cells within each experimental group were put together to generate the average EPSC for each group. (c) Cumulative probability distribution of EPSC amplitudes obtained by pooling 67 randomly selected events from each cell within each experimental group. GFP: 469 events (n=7 cells from 6 mice), "$Ca^{2+}$-permeable": 469 events (n=7 cells from 6 mice), "pore-dead": 536 events (n=8 cells from 6 mice), and "C-tail": 536 events (n=8 cells from 6 mice). The dataset from GFP is the same as in the Figure 4-11.

*4.2.6. Modifications of the GluA2 subunit of AMPARs in OPCs did not affect paired-pulses ratio of EPSCs.*

To test whether modified GluA2 subunits influenced the presynaptic part of axon-OPC synapses, I studied PPR, an indicator of the release probability of the presynaptic axons. I found that PPR was 1.64±0.11 in GFP group, 1.54±0.156 in "$Ca^{2+}$-permeable" group, 1.91±0.235 in "pore-dead" group, and 2.15±0.23 in "C-tail" group (Fig. 14a-b). There was no statistically significant difference between GFP animals and any of the mice expressing GluA2-modifying constructs (One-way ANOVA, $F(3,30)=2.484$, $p=0.080$) suggesting that the axonal release probability was not changed.

**Summary of part 4.2.**

Altogether, AMPARs carrying "$Ca^{2+}$-permeable" and "pore-dead" modifications of the GluA2 subunit in callosal OPCs, inserted to the cell membrane, and this was reflected in the change of $Ca^{2+}$-permeability of AMPARs. On the contrary, the expression of GluA2 "C-tail" affected neither the ionotropic function of AMPARs, not the quantal amplitude.

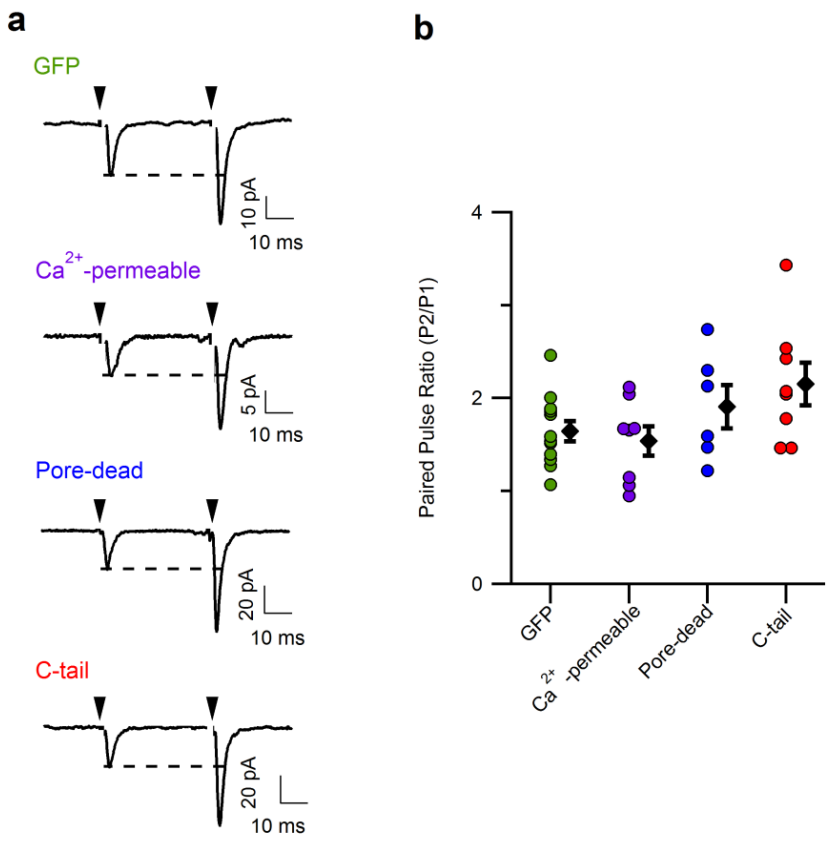


**Figure 4-15. Modifications of the GluA2 subunit of AMPARs in OPCs do not alter the probability of the glutamate release from callosal axons.**

(a) Representative example traces showing evoked axon-glia EPSCs ($V_h$ = -90 mV) recorded in OPCs expressing GFP or one of the GluA2 subunit modifying constructs. Each trace represents an average of 10-52 sweeps. Black arrowheads indicate times of stimulation. The stimulation artifacts are blanked for clarity. The dashed lines indicate the peak of EPSC elicited by the first stimulus. (b) Summary graph showing the paired pulse ratio of the evoked EPSCs recorded in the OPCs. Each dot represents one cell. The black diamonds represent mean ± SEM from each group. GFP: n=12 cells from 9 mice; "$Ca^{2+}$-permeable": n=8 cells from 7 mice; "pore-dead": n=6 cells from 6 mice; and "C-tail": n=8 cells from 6 mice. The dataset from GFP is the same as shown in Figure 4-12.

## 4.3. Investigation of the effects of modified GluA2 subunit of AMPARs for differentiation and proliferation of callosal OPCs.

*4.3.1. Modifications of the GluA2 subunit of AMPARs decrease OPC differentiation.*

After verifying changes in $Ca^{2+}$ permeability of AMPARs and quantal amplitude of AMPAR-mediated current in OPCs, I studied the influence of GluA2 subunit modifications on differentiation and proliferation of OPCs. I stereotaxically injected retrovirus carrying one of the GluA2-subunit-modifying constructs into the corpus callosum of P10-P12 mice and examined the stages of oligodendrocyte lineage cells 5 days after the viral injection (Fig. 4-8 a-b) using labelling for GFP, NG2, and CC1 (Fig. 4-16, 4-17), as described in 4.2.3 above. I then counted the proportion of OPCs, pre-myelinating OLs, and OLs within the total population of cells targeted with retrovirus ($GFP^+$ cells). I found that the percentage of OPCs ($GFP^+NG2^+CC1^-$ cells) within the population of $GFP^+$ cells was remarkably higher in the groups with GluA2 modifications than in the control group: GFP: 33.25±3.27%; "$Ca^{2+}$-permeable": 59.83±1.69%; "pore-dead": 54.50±3.75%; "C-tail": 53.86±2.56% (One-way ANOVA with post-hoc Bonferroni test; F(3, 28)=15.175, p=0.000005; GFP vs. $Ca^{2+}$-permeable: p=0.000008, GFP vs. pore-dead: p=0.000143, GFP vs. C-tail: p=0.000146) (Fig. 4-18 a-b). Contrary to the rise in the proportion of $GFP^+$OPCs, the proportion of OLs ($GFP^+NG2^-CC1^+$ cells) was lower in animals with modified AMPARs: GFP: 43.18±4.16%; "$Ca^{2+}$-permeable": 16.71±2.25%; "pore-dead": 21.62±3.21%; "C-tail": 23.83±1.33% (One-way ANOVA with post-hoc Bonferroni test; F(3, 28)=15.557, p=0.000004; GFP vs. $Ca^{2+}$-permeable: p=0.000006, GFP vs. pore-dead: p=0.000085, GFP vs. C-tail: p=0.000253) (Fig. 4-18 a, d). No difference was observed in the percentage of the pre-myelinating OLs ($GFP^+NG2^+CC1^+$ cells) between control group and animals expressing one of the GluA2-subunit-modifying constructs: GFP: 17.40±3.59%; "$Ca^{2+}$-permeable": 17.69±2.52%; "pore-dead": 16.82±2.48%; "C-tail": 15.93±2.48% (One-way ANOVA; F(3, 28)=0.077, p=0.972) (Fig. 4-18 a, c). It is possible that when OPCs with modified AMPARs start to differentiate, they remain at the stage of pre-myelinating OLs longer than the OPCs in the control group of animals. These findings suggest that OPCs expressing AMPAR-modifying constructs are less likely to differentiate into OLs than OPCs expressing only GFP.

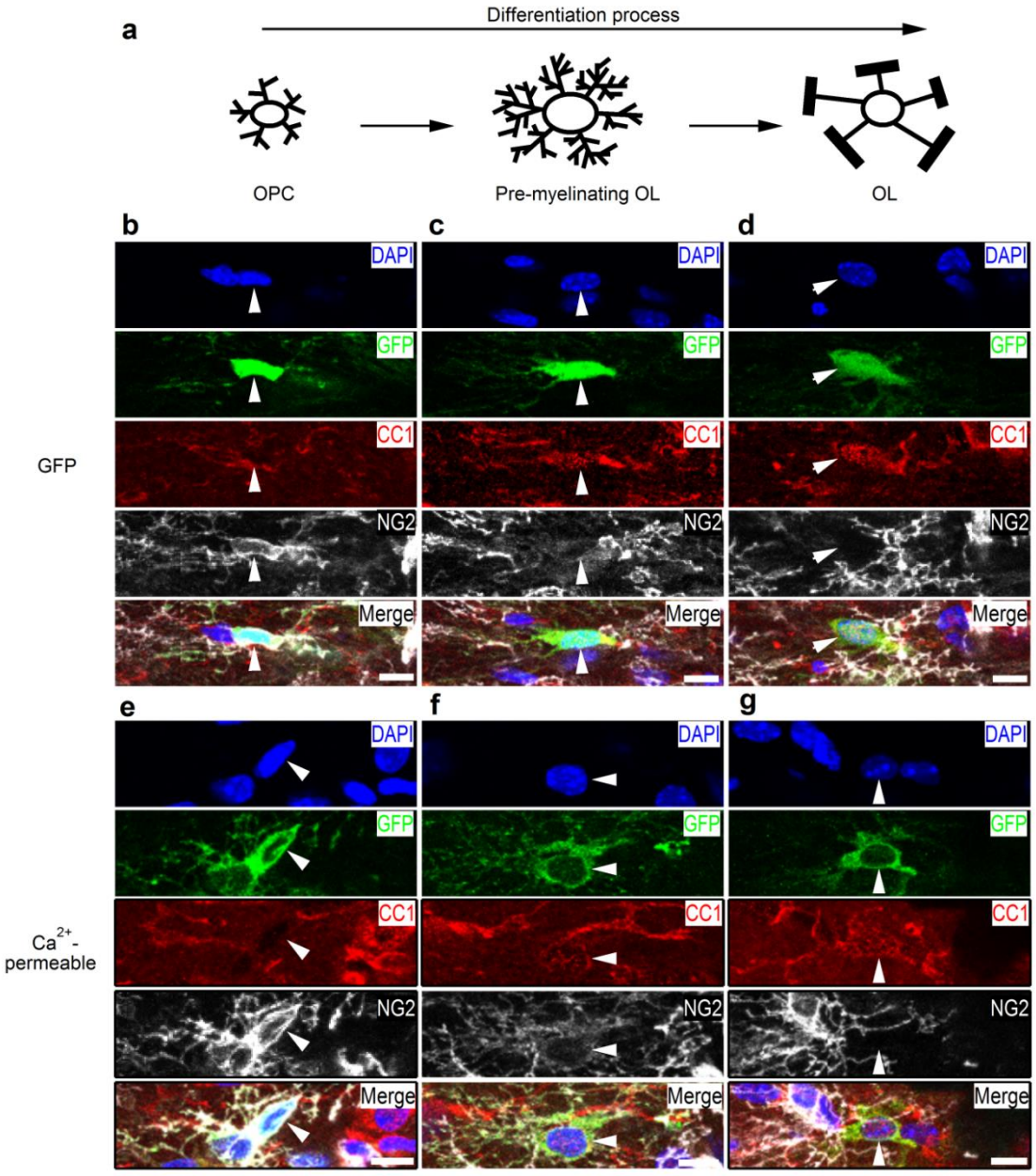


**Figure 4-16. Oligodendrocyte lineage cells targeted with retrovirus carrying GFP and GluA2 "$Ca^{2+}$-permeable" construct.**

(a) Scheme of the differentiation process. (b-d) Examples of the oligodendrocyte lineage cells expressing the GFP. Each panel (b-d) represents maximum intensity projection image from 3 successive confocal planes showing quadruple labeling for DAPI (blue), GFP (green), CC1 (red), NG2 (white), and merge of four channels. OPCs are $GFP^{+}NG2^{+}CC1^{-}$ (b); pre-myelinating oligodendrocytes are $GFP^{+}NG2^{+}CC1^{+}$ (c); mature oligodendrocytes are $GFP^{+}NG2^{-}CC1^{+}$ (d). White arrowheads point to the soma of the infected cells. Scale bar: 10 μm. (e-g) As in (b-d) but for the oligodendrocyte lineage cells expressing the "$Ca^{2+}$-permeable" construct.

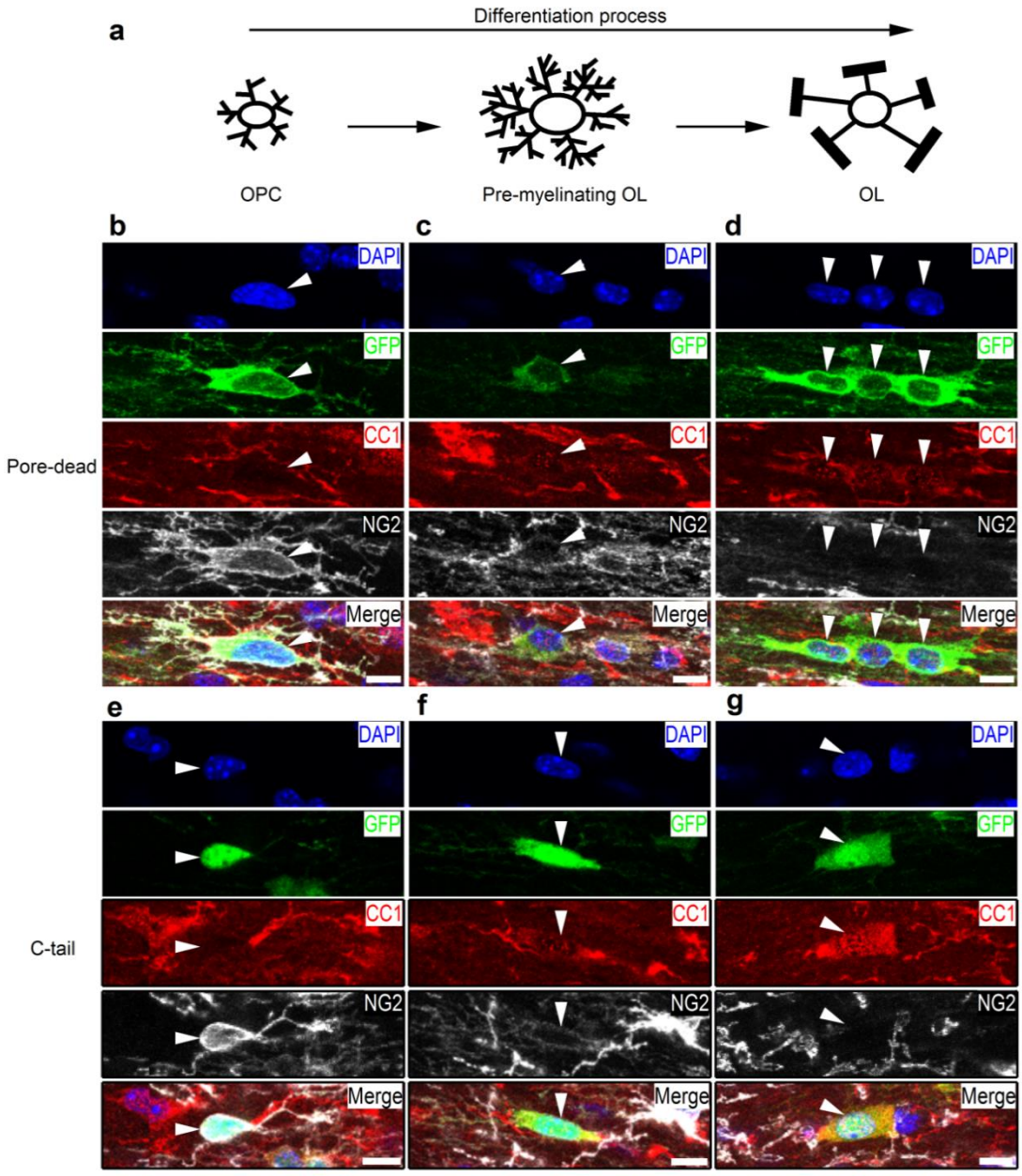


**Figure 4-17. Oligodendrocyte lineage cells targeted with retrovirus carrying GluA2 "pore-dead" and "C-tail" construct.**

(a) Scheme of the differentiation process. (b-d) As in Figure 4-16 b-d but for the oligodendrocyte lineage cells expressing the "pore-dead" construct. Scale bar: 10 μm. (e-g) As in Figure 4-16 b-d but for the oligodendrocyte lineage cells expressing the "C-tail" construct.

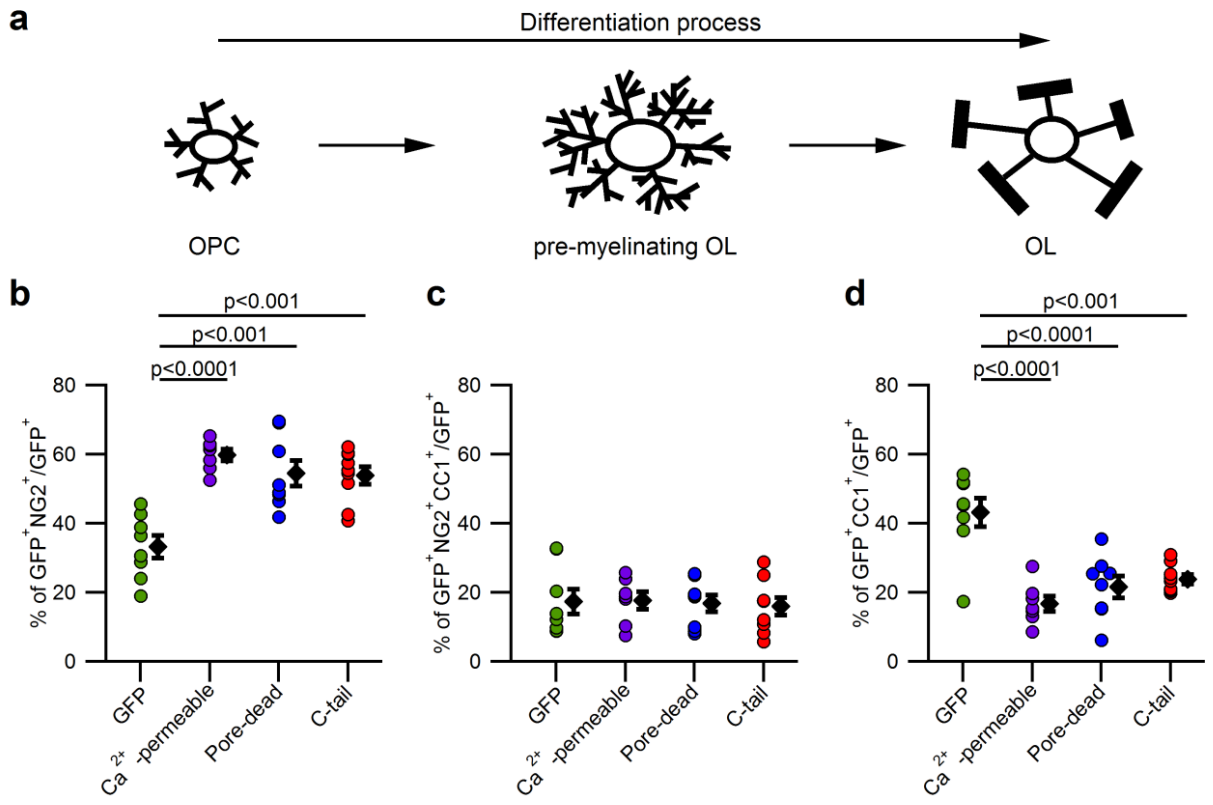


**Figure 4-18. Modifications of the GluA2 subunit of AMPARs decrease OPC differentiation.**

(a) Scheme of the differentiation process. (b) Summary graph showing the percentage of OPCs ($GFP^+$ $NG2^+CC1^-$) within the total population of cells targeted with retrovirus carrying GFP (n=8), "$Ca^{2+}$-permeable" (n=7), "pore-dead" (n=8), and "C-tail" (n=9) constructs. Each dot represents one animal. Black diamonds represent mean ± SEM for each group. (c) As in (b) but for pre-myelinating oligodendrocytes ($GFP^+NG2^+CC1^+$). (d) As in (b, c) but for mature oligodendrocytes ($GFP^+NG2^-CC1^+$). For (b-d), data from GFP group is the same as in Figure 4-8 e.

The lower ratio of $GFP^+$OLs in the groups with modified GluA2 subunit was not the consequence of differentiation of OPCs into other cell types because the proportion of oligodendrocyte lineage cells was similar in all groups: GFP: 93.83±0.95%; "$Ca^{2+}$-permeable": 94.24±1.37%; "pore-dead": 92.95±0.41%; "C-tail": 93.63±1.60% ; One-way ANOVA, $F(3,28)=0.193$, $p=0.90$; Fig. 4-19). It was also not due to the apoptotic cell death through activation of caspase3 pathway because the percentage of $caspase3^+GFP^+$ cells in animals with modified GluA2 subunit was very low and comparable to GFP control group: GFP: 0.5±0.28%; "$Ca^{2+}$-permeable": 0.58±0.58%; "pore-dead": 0%; "C-tail": 0.23±0.23% (Kruskal-Wallis test; $H(3)=2.305$, $p=0.512$; Fig. 4-20).

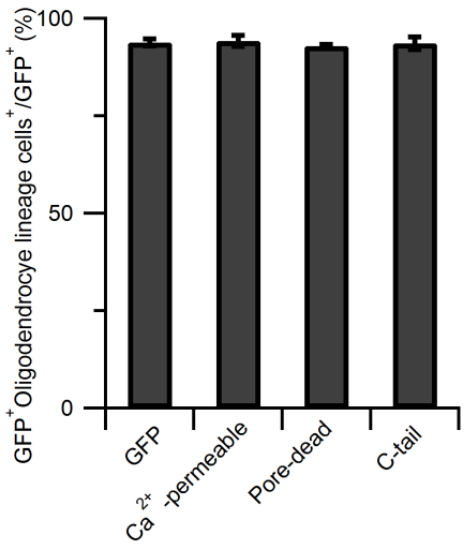


**Figure 4-19. The differentiation of OPCs expressing GFP or constructs modifying the GluA2 subunit of AMPARs was restricted in their fate.**

Summary graph showing the proportion of oligodendrocyte lineage cells within the total population of cells expressing GFP (n=8 mice), "$Ca^{2+}$-permeable" (n=7 mice), "pore-dead" (n=8 mice), and "C-tail" (n=9 mice) constructs. For this graph, counts of OPCs, pre-OLs, and OLs were pooled from datasets shown in Fig. 4-18 b-d.

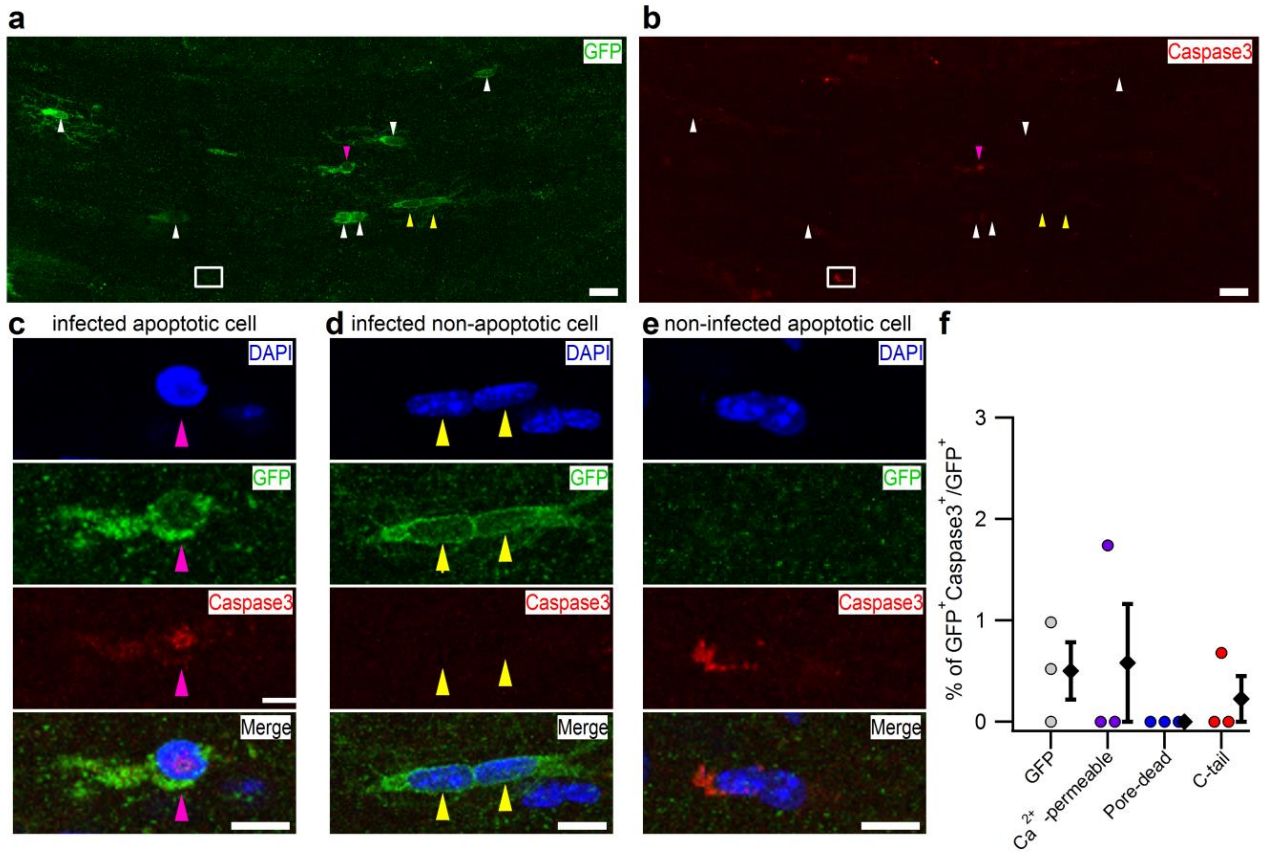


**Figure 4-20. Expression of GFP or constructs modifying the GluA2 subunit of AMPARs in OPCs does not result in cell death within the corpus callosum.**

(a) Maximum intensity projection from 5 successive confocal planes showing cells expressing "$Ca^{2+}$-permeable" construct in the corpus callosum. Arrowheads point to virally-transduced cells. Magenta arrowhead points to an infected apoptotic cell ($GFP^+Caspase3^+$), magnified in (c). Yellow arrowheads point to infected non-apoptotic cells ($GFP^+Caspase3^-$), magnified in (d). White rectangle indicates a non-infected apoptotic cell ($GFP^-Caspase3^+$), magnified in (e). Scale bar: 20 µm. (b) The same as in (a), but the red channel used for Caspase3 labeling is shown. (c) Higher magnification of the $GFP^+Caspase3^+$ cell marked with the magenta arrowhead in (a). Scale bar: 10 µm. (d) Higher magnification of ($GFP^+Caspase3^-$) cells marked with the yellow arrowheads in (a). Panels show triple labeling as in (c).Scale bar: 10 µm. (e) Higher magnification of the $GFP^-Caspase3^+$ cell marked the white rectangle in (a). For (c-e), panels show triple labeling for DAPI (blue), GFP (green), Caspase3 (red), and merge. Scale bar: 10 µm. (f) Summary graph showing the proportion of $GFP^+$ cells labeled for caspase3 within the total population of cells expressing GFP (n=3 mice), "$Ca^{2+}$-permeable" (n=3 mice), "pore-dead" (n=3 mice), and "C-tail" (n=3 mice) constructs. Each dot represents one animal. The black diamonds represent mean ± SEM for each group.

*4.3.2. Pore mutations of GluA2 subunit of AMPARs increase OPCs proliferation.*

The increase in the percentage of OPCs within the population of infected $GFP^+$ cells in animals expressing AMPAR-modifying constructs may be the result of higher proliferation of OPCs, or may have occurred because more OPCs left the cycle and entered the resting phase (G0). To distinguish between these possibilities, I investigated the proliferation of OPCs expressing GluA2-subunit modifying constructs. To label proliferating cells, I used 5-ethynyl-2'-deoxyuridine (EdU), which is an alternative for 5-bromo-2-deoxyuridine (BrdU), and similar to BrdU incorporates into the DNA during the S-phase of the cell cycle [118]. I injected the mice intraperitoneally with EdU on the third, fourth, and fifth days after retroviral injection (Fig. 4-21 a). The interval between EdU injections was 24 hours. I sacrificed the mice on the fifth day, i.e. 6-7 hours after the third EdU injection, performed immunolabeling for GFP, NG2, and EdU, (Fig. 4-22) and counted GFP-expressing cells positive for EdU or NG2EdU (Fig. 4-23 a, c).

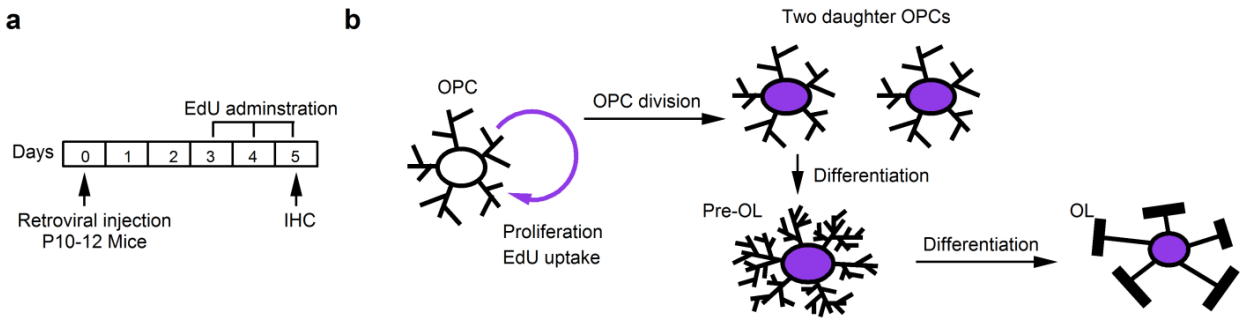


**Figure 4-21. Schematic drawing of experimental time frame of EdU administration and the explanation of OPCs and their progeny carrying EdU.**

(a) Experimental design and timeline for proliferation assay. IHC: Immunohistochemistry. (b) Scheme showing a proliferating OPC. Within the oligodendrocyte lineage, EdU incorporates into the DNA of proliferating OPCs, and is maintained in their progeny including daughter cells and pre-myelinating OLs as well as OLs differentiated from proliferating OPCs.

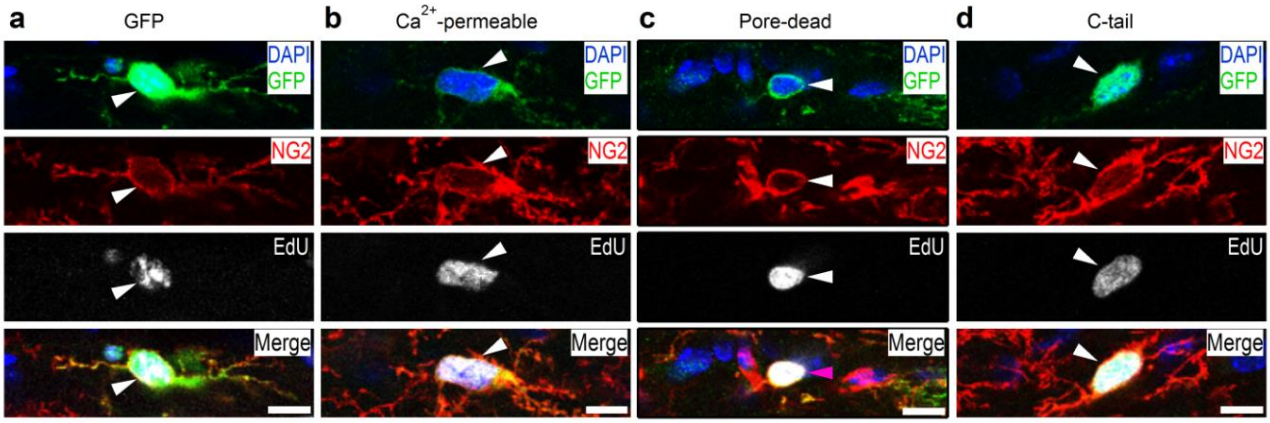


**Figure 4-22. EdU$^+$ OPCs in animals injected with retrovirus carrying GluA2-modifying constructs.**

(a) Example of an EdU$^+$ OPC in animal injected with retrovirus carrying GFP. The panel represents a maximum intensity projection image from 2 successive confocal planes showing quadruple labeling for DAPI (blue), GFP (green), EdU (white), NG2 (red), and merge. The arrowhead points to an infected EdU$^+$ OPC (GFP$^+$NG2$^+$EdU$^+$). Scale bar: 10 μm. (b) As in (a) but for the animal injected with retrovirus carrying "$Ca^{2+}$-permeable" construct. (c) As in (a-b) but for the animal injected with retrovirus carrying "pore-dead" construct. (d) As in (a-c) but for the animal injected with retrovirus carrying "C-tail" construct.

I found that point mutations of GluA2 subunit ("$Ca^{2+}$-permeable" and "pore-dead") which allowed $Ca^{2+}$ to permeate through AMPARs, caused a significant increase in the proportion of $GFP^{+}EdU^{+}$ within the total population of cells targeted with retrovirus (GFP: 26.81±1.51%; "$Ca^{2+}$-permeable": 39.94±3.37%; "pore-dead": 45.31±2.05%; One-way ANOVA with post-hoc Bonferroni test; F(3, 27)=14.234, p=0.000009; GFP vs. $Ca^{2+}$-permeable: p=0.001, GFP vs. pore-dead: p=0.000007; Fig. 4-23 a). Expression of GluA2 "C-tail" did not result in a similar effect ("C-tail": 33.68±1.47%; One-way ANOVA with post-hoc Bonferroni test; F(3, 27)=14.234, p=0.000009; GFP vs. C-tail: p=0.174; Fig. 4-23 a). Consistent with the increase in the proportion of $GFP^{+}EdU^{+}$ within the total population of infected cells (Fig. 4-23 a), I also found the higher proportion of $NG2^{+}EdU^{+}$ cells within the total population of $GFP^{+}$ cells in mice expressing "$Ca^{2+}$-permeable" and "pore-dead" GluA2, compared to GFP control group (GFP: 20.80±1.02%; "$Ca^{2+}$-permeable": 33.15±1.70%; "pore-dead": 37.74±2.22%; Kruskal-Wallis with Dunn's test; H(3)=21.277, p=0.000092; GFP vs. $Ca^{2+}$-permeable: p=0.009, GFP vs. pore-dead: p=0.000084; Fig. 4-23 c). Notably, although originally EdU integrates only into the cycling OPCs, it will also be carried by the progeny of these OPCs, i.e. daughter cells from proliferating OPCs, as well as pre-myelinating OPCs and OLs generated from the newly-born OPCs (Figure 4-21 b). Therefore, I could examine whether cycling $GFP^{+}$ cells ($GFP^{+}EdU^{+}$) expressing modified GluA2 subunits differentiated into pre-myelinating OLs and/or OLs, remained OPCs, or both. I found out that the majority of $GFP^{+}EdU^{+}$ cells were positive for NG2 in all experimental groups and there was no difference from the GFP control group (GFP: 78.34±3.61%; "$Ca^{2+}$-permeable": 84.88±4.76%; "pore-dead": 82.93±2.25%; "C-tail": 79.2±2.15%; Kruskal-Wallis test; H(3)=3.502, p=0.320; Fig. 4-23 b). These data suggest that within the timeframe of my experiments, the majority of newly-born OPCs remained OPCs (and perhaps some were pre-myelinating OLs), and none of the GluA2 modifications specifically promoted the differentiation of newly-born OPCs.

Retrovirus infected OPCs which were undergoing proliferation. Furthermore, some of the $GFP^{+}$OPCs labeled with EdU at the third, fourth, and fifth day after retroviral infection, indicating that those $EdU^{+}$OPCs were still proliferating. This means that infected $EdU^{+}$OPCs entered the cell cycle again and underwent cell division for the second time. Hence, increased number of $EdU^{+}$ cells in animals with "$Ca^{2+}$-permeable" and "pored-dead" modifications indicates that these modifications triggered OPC to undergo another cell division. If increased

$Ca^{2+}$ permeability of AMPARs triggers another cell division, but does not increase the proportion of newly-born pre-myelinating OLs and/or OLs, then the population of $GFP^{+}NG2^{+}$ cells in animals with these modifications should contain more cycling cells and/or cells that have recently completed the cell cycle, i.e. $EdU^{+}$ cells, than in the "C-tail" or GFP groups. However, I found this to be the case only for the "pore-dead", but not the "$Ca^{2+}$-permeable" mutation (GFP: 41.11±1.69%; "$Ca^{2+}$-permeable": 43.54±2.95%; "pore-dead": 52.51±2.76%; "C-tail": 39.72±2.42%; One-way ANOVA with post-hoc Bonferroni test; F(3, 27)=5.569, p=0.004; GFP vs. $Ca^{2+}$-permeable: p=1, GFP vs. pore-dead: p=0.016, GFP vs. C-tail: p=1, pore-dead vs. C-tail: p=0.006**;** Fig. 4-23 d). This suggests that expression of "pore-dead", but not "$Ca^{2+}$-permeable", GluA2-containing AMPARs expedited the OPC cell cycle time and probably prompted OPCs to start another cell division (i.e. the third time). Although "$Ca^{2+}$-permeable" and "pore-dead" modifications resulted in very similar electrophysiological changes at axon-OPC synapses (Fig. 4-13, 4-14), it is possible that the signaling cascades downstream of the AMPARs differ in these two situations resulting in a dissimilar effects of the two modifications on the number of cycling cells within the $NG2^{+}GFP^{+}$ population (Fig. 4-23 d).

**Summary part of 4.3.**

Taken together, all three modifications of GluA2 subunit resulted in the decrease of differentiation of OPCs. The increase in the proportion of proliferating cells was observed only in animals with point mutations of GluA2 subunit which enhanced the permeability of AMPARs for $Ca^{2+}$. Interestingly, "pore-dead" modification had stronger effect on proliferation of OPCs than "$Ca^{2+}$-permeable" modification, had a dissimilar effect on the proliferation.

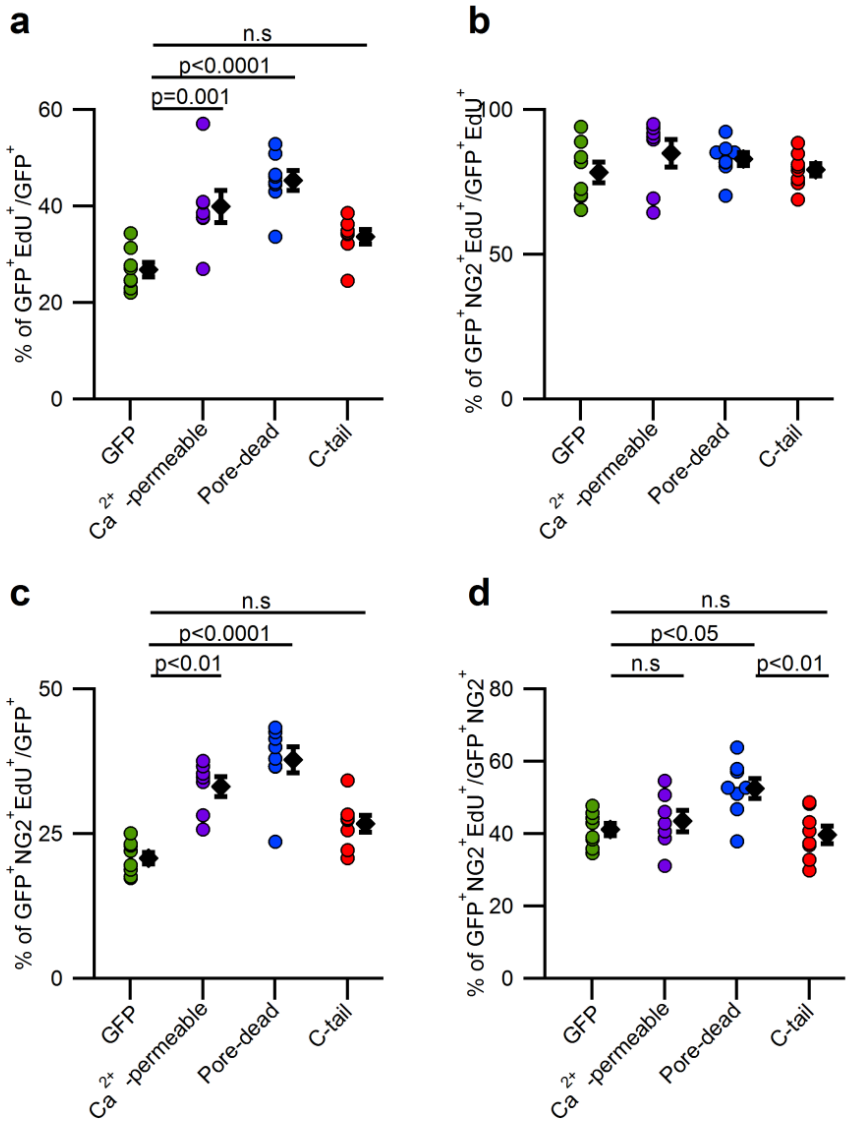


**Figure 4-23. Modifications of the GluA2 subunit of AMPARs increase OPCs proliferation.**

(a) Summary graph showing the proportion of $GFP^+EdU^+$ cells within the total population of cells targeted with retrovirus ($GFP^+$) expressing GFP (n=8), "$Ca^{2+}$-permeable" (n=7), "pore-dead" (n=8), and "C-tail" (n=8) AMPAR-modifying constructs. Each dot represents one animal. Black diamonds represent mean ± SEM for each group. (b) As in (a) but for the proportion of $GFP^+NG2^+EdU^+$ cells within the population of $GFP^+EdU^+$ cells. (c) As in (a-b) but for the proportion of $NG2^+EdU^+$cells within the population of $GFP^+$ cells. (d) As in (a-c) but for the proportion of $GFP^+NG2^+EdU^+$ cells within the population of $GFP^+NG2^+$ cells.

## 5. Discussion.

The major findings of the present study are: (1) Introduced point mutations of GluA2 subunit ("$Ca^{2+}$-permeable" and "pore-dead") altered $Ca^{2+}$ permeability of AMPARs in OPCs; (2) Alteration of $Ca^{2+}$ permeability of AMPARs in OPCs reduced their differentiation into OLs but promoted their self-renewal by proliferation; (3) Expression of GluA2 "C-tail" in OPCs did not change $Ca^{2+}$ permeability and quantal amplitude of AMPARs, however, the differentiation of OPCs was suppressed.

Below I discuss possible trafficking pathways of AMPARs in OPCs and potential reasons for the change in the differentiation and proliferation in OPCs upon modifications of AMPAR properties.

### *5.1. Possible subunit composition and trafficking of AMPARs containing the modified GluA2 subunit in OPCs.*

Based on the published evidences regarding expression of different AMPARs subunits in OPCs and trafficking of AMPARs in neurons, it is interesting to speculate how the modified subunits assembled into homo- or hetero-tertamers to form AMPARs in OPCs in my experiments.

#### *5.1.1 GluA2(R583Q) mutation ("$Ca^{2+}$-permeable").*

In my study I observed that during the second-third postnatal week, evoked axon-glia AMPARs-mediated EPSCs recorded from callosal OPCs displayed nearly linear I-V relationship (Fig. 4-7) suggesting that OPCs contained little/no $Ca^{2+}$-permeable AMPARs. Introducing $Ca^{2+}$-permeable GluA2 subunit with point mutation (GluA2(R583Q)) at the channel pore to the OPCs resulted in strongly inwardly rectifying I-V relationship of evoked axon-glia EPSCs (Fig.4-13) and increased amplitude of quantal axon-glial EPSCs (Fig. 4-14). Evidence from the literature shows that when $Ca^{2+}$ permeable unedited GluA2 subunit is introduced to neurons by viral approach, I-V relationship of EPSCs recorded from the infected neurons display stronger inward rectification than in non-infected neurons [119-121]. This corresponds well to the findings of my study. Furthermore, several studies have shown that $Ca^{2+}$-permeable AMPARs have higher single-channel conductance than $Ca^{2+}$-impermeable AMPARs containing edited GluA2. For example, this has been observed in HEK 293 cells, when single-channel conductance was compared in cells expressing recombinant GluA2/GluA4 vs. unedited GluA2/GluA4 receptors, as well as in

cortical layer 2/3 pyramidal cells [117, 122]. Therefore increase in the quantal amplitude of EPSCs, which I observed in OPCs expressing GluA2(R583Q) subunit, may reflect to the fact that $Ca^{2+}$-permeable AMPARs have higher single-channel conductance.

What can be the subunit composition of AMPARs containing GluA2 subunit with GluA2(R583Q) point mutation in my experiments? Several earlier studies using in situ hybridization, Northern blot, Southern blot, RT-PCR, RNA-Sequencing transcriptome, Western blot, and immunolabeling indicate that mRNAs and protein for GluA1, GluA2, GluA3, and GluA4 subunits of AMPARs are present in the purified O-2A progenitor cells, CG-4 progenitor cell line, and/or in OPCs from several brain regions of the developing rodents, although the expression of GluA1 subunit was reported to be very low [20, 61-72, 123]. It is also known that AMPARs subunits preferentially assemble as receptors containing either two GluA2 or no GluA2 subunits [50]. Keeping in mind that AMPARs are tetramers and assuming that OPCs lack GluA1 subunit, the possible combinations of AMPARs subunits in OPCs during physiological conditions can be: GluA2/3, GluA2/4, or GluA3/4 (Fig. 5-1). If recombinant GluA2 subunits with pore mutation are introduced to the callosal OPCs, the mutated subunits may form homo-tetramers and/or hetero-tetramers with endogenous subunits. Probable resulting subunit combinations of AMPARs are shown in (Fig. 5-2). Subunits with GluA2(R583Q) point mutation can form $Ca^{2+}$ permeable AMPARs, but can also assemble into $Ca^{2+}$-impermeable tetrameric AMPARs if GluA2(R583Q) subunits combine with endogenous GluA2 (Fig. 5-2 *Left*). Nevertheless, the number of possible combinations of $Ca^{2+}$-permeable AMPARs is higher (4 possible combinations; Fig. 5-2 *Right*) than the number of combinations of $Ca^{2+}$-impermeable AMPARs (3 possible combinations; Fig. 5-2 *Left*).

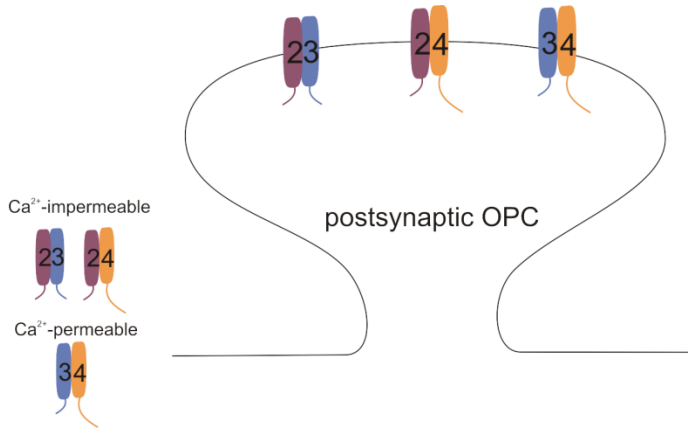


**Figure 5-1. Possible combinations of AMPARs present in OPCs.**

2, 3, and 4 designate GluA2, GluA3, and GluA4 respectively.

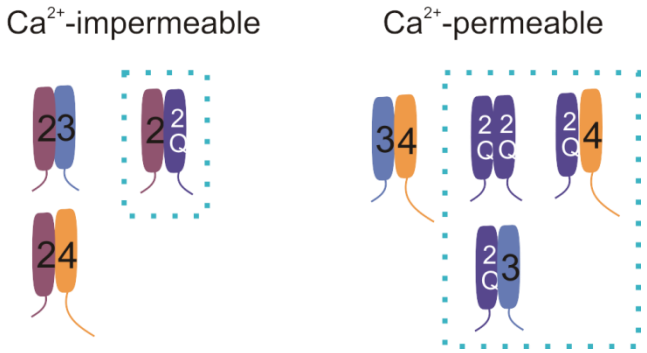


**Figure. 5-2 Possible combinations of AMPARs after GluA2(R583Q) is introduced to OPCs.**

*(Left)* Combinations of $Ca^{2+}$-impermeable AMPARs. *(Right)* Combinations of $Ca^{2+}$-permeable AMPARs. 2, 3, 4, and 2Q designate GluA2, GluA3, GluA4, and GluA2(R583Q) respectively. Blue dash rectangles indicate the possible homo- and hetero-tetrameric AMPARs containing GluA2(R583Q) subunit.

How did AMPARs containing GluA2 subunit with GluA2(R583Q) point mutation traffic to the synaptic sites of axon-OPC synapses? In neurons, AMPARs are assembled as hetero-tetramers of GluA1/2 or GluA2/3 subunits and traffic to synapses in a subunit-specific way depending on the intracellular C-terminal domain of the subunits. GluA1 and GluA4 subunits contain long C-terminal domain and GluA3 contains short C-terminal domain, while GluA2 subunit can contain either short or long C-terminal domain [124]. AMPARs containing subunits with long C-terminal domain are delivered to synapses exclusively in activity-dependent way [125-127], while AMPARs containing subunits with short C-terminal domain continuously incorporate into synapses and replace the existing AMPARs [119]. For hetero-tetrameric AMPARs, the type of trafficking (continuous or activity-dependent) is determined by the subunit with long C-terminal domain [119]. Do AMPARs in OPCs traffic to the synapses in the similar fashion as in neurons? It is possible that trafficking of homo- or/and hetero-tetrameric AMPARs in OPCs follows the rules discovered in neurons [119, 125-127], and AMPARs containing GluA2(R583Q) were continuously delivered to axon-OPC synapses and substituted the existing GluA2-containing AMPARs. As a result, the amount of edited GluA2-containing receptors was reduced and the amount of $Ca^{2+}$-permeable AMPARs, which have higher single-channel conductance [117], was increased. This insertion and replacement of receptors resulted in the inwardly rectifying I-V relationship and in the larger amplitude of quantal EPSCs (Fig. 4-13, 4-14). However, based on my data I cannot fully rule out the possibility that the existing GluA2-containing AMPARs were not removed. Hence, the second possibility is that newly-assembled AMPARs containing GluA2(R583Q), were simply added to the postsynaptic sites of axon-OPC synapses without removal of the existing GluA2-containing AMPARs. In this scenario, the increased total number of the postsynaptic AMPARs may have contributed to the larger quantal amplitude (in addition to the increased single-channel conductance of $Ca^{2+}$-permeable AMPARs). Furthermore, as added receptors containing GluA2(R583Q) subunit, three out of four are permeable for $Ca^{2+}$ (indicated as blue dash rectangles) (Fig. 5-2). Thus, additional receptors containing GluA2(R583Q) subunit enhanced the permeation of $Ca^{2+}$ and resulted in the inwardly rectifying I-V relationship (Fig. 4-13). Along this line, it has been observed that in the CA1 region of the P5-7 rat hippocampus, neurons have $Ca^{2+}$-permeable AMPARs, but larger quantal EPSCs (compared to P8-18 rats) is due to the higher number of activated receptors rather than to the higher single-channel conductance [128].

*5.1.2. GluA2(R583E) mutation ("pore-dead").*

In my study I found that expression of GluA2(R583E) construct ("pore-dead") resulted in increased $Ca^{2+}$ permeability of AMPARs and increased amplitude of quantal EPSCs. This result was not fully predicted because presence of AMPARs containing pore-dead subunits (which have low/no conductance) at synapses is intuitively expected to reduce the amplitude of AMPAR-mediated EPSCs. Indeed, it has been reported that expression of recombinant GluA3(Q613E) subunit of AMPARs, carrying pore-dead mutation at the Q/R site, in oocytes resulted in non-conducting AMPARs [101]. Moreover, co-expressing recombinant pore-dead GluA3(Q612E) subunit together with conducting GluA1 subunit in oocytes caused attenuation of the current response evoked by application of 300 μM kainate, when compared with the expression of GluA1 together with GluA3 subunit [101]. This study indicated that reduced response amplitude may result from the activity of homomeric GluA1 receptors, or from the heteromeric receptors of GluA3(Q612E) with GluA1. Furthermore, expression of the pore-dead mutant GluA2(R586E) in hippocampal pyramidal neuron reduced the amplitude of AMPARs-mediated EPSCs compared to pyramidal neurons without expression of the pore-dead construct of GluA2 subunit [119].

In my study, when recombinant pore mutation of GluA2(R583E) subunits was introduced into OPCs, the modified subunits may have formed homo-tetramers and/or hetero-tetramers with endogenous AMPAR subunits. The resulting possible combinations of AMPARs are shown in (Fig. 5-3). Three groups of receptors could be formed: $Ca^{2+}$-impermeable (Fig. 5-3 *Left*), $Ca^{2+}$-permeable (Fig. 5-3 *Middle)*, and non-conducting (Fig. 5-3 *Right*). Remarkably, heteromeric receptors composed by conducting GluA2 and pore-dead GluA2(R583E) (Fig. 5-3 *Left*) are likely to have very small single-channel conductance because single-channel conductance of edited GluA2 receptors is ~ 300 fS [117]. Taking together, I expected that in my study AMPARs in OPCs expressing pore-dead GluA2(R583E) subunit would be permeable to ions but would allow only reduced flow of ions. However, the results of my electrophysiological experiments appeared more complicated because they showed increase rather than decrease of EPSC amplitude in OPCs with GluA2(R583E) mutation, and also change in I-V rectification (Fig. 4-13, Fig. 4-14).

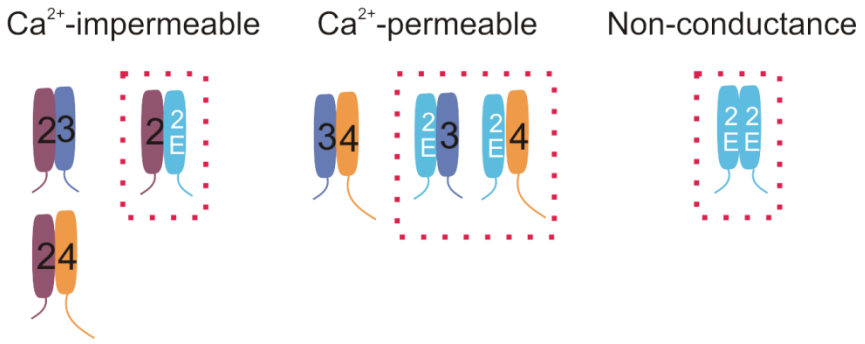


**Figure. 5-3 Possible combinations of AMPARs after GluA2(R583E) is introduced to OPCs.**

*(Left)* Combinations of $Ca^{2+}$-impermeable AMPARs. *(Middle)* Combinations of $Ca^{2+}$-permeable AMPARs. *(Left)* Non-conducted of AMPARs. 2, 3, 4, and 2E designate GluA2, GluA3, GluA4, and GluA2(R583E) respectively. Red dash rectangles indicate the possible homo- and hetero-tetrameric AMPARs containing GluA2(R583E) subunit.

Below I discuss several possibilities regarding the trafficking of GluA2(R583E)-containing AMPARs in OPCs, try to speculate whether GluA2(R583E)-containing AMPARs were delivered to the postsynaptic sites of axon-OPC synapses, and whether they substituted the existing AMPARs, or they were simply added to the postsynaptic sites. I then try to interpret the results of my electrophysiological findings based on these ideas.

First possibility is that trafficking of homo- or/and hetero-tetrameric AMPARs in OPCs follows the rules discovered in neurons [119, 125-127]. In this scenario, AMPARs containing GluA2(R583E) subunit would be delivered to axon-OPC synapses and substitute the existing AMPARs (Fig. 5-4 *top*). As in (Fig. 5-4 *top*), for instance, two GluA2-containing AMPARs (Fig. 5-4 *top left*) could be replaced by two GluA2(R583E)-containing AMPARs, derived from four possible combinations (Fig. 5-4 *top right*, indicated as red dash rectangle). However, as those two GluA2(R583E)-containing AMPARs have low/no conductance, the cell may compensate for this fast by inserting the endogenous AMPARs with higher conductance, e.g. GluA3/4. As a result, the amount of edited GluA2-containing receptors would be reduced, and the amount of $Ca^{2+}$-permeable AMPARs, which have higher single-channel conductance [117], would be

increased. These insertion and replacement of receptors resulted in the inwardly rectifying I-V relationship and larger amplitude of quantal EPSCs.

Second possibility is that GluA2(R583E)-containing AMPARs were not inserted to synapses but expression of GluA2(R583E) pore-dead subunits triggered the substitution of endogenous GluA2-containing AMPARs by GluA2-lacking AMPARs, e.g. receptors comprised of GluA3/4 subunits (Fig. 5-4 *middle*). In this case, inwardly rectifying I-V relationship of axon-OPC EPSCs (Fig. 4-13) would be explained by the absence of GluA2 subunits, and the larger quantal amplitude (Fig. 4-14) would be explained by higher single-channel conductance of GluA2-lacking receptors and/or by higher numbers of GluA2-lacking receptors.

Third possibility is that GluA2(R583E)-containing AMPARs were delivered and incorporated into the synapses but the existing AMPARs were not removed (Fig. 5-4 *Bottom*). In this scenario, inwardly rectifying I-V relationship may be due to the fact that the amount of $Ca^{2+}$-permeable AMPARs was higher than $Ca^{2+}$-impermeable AMPARs (3 out of 5 functional channels) (Fig. 5-3). In addition, the increased number of AMPARs (possible combinations are indicated in Fig. 5-3) may have led to the larger quantal amplitude.

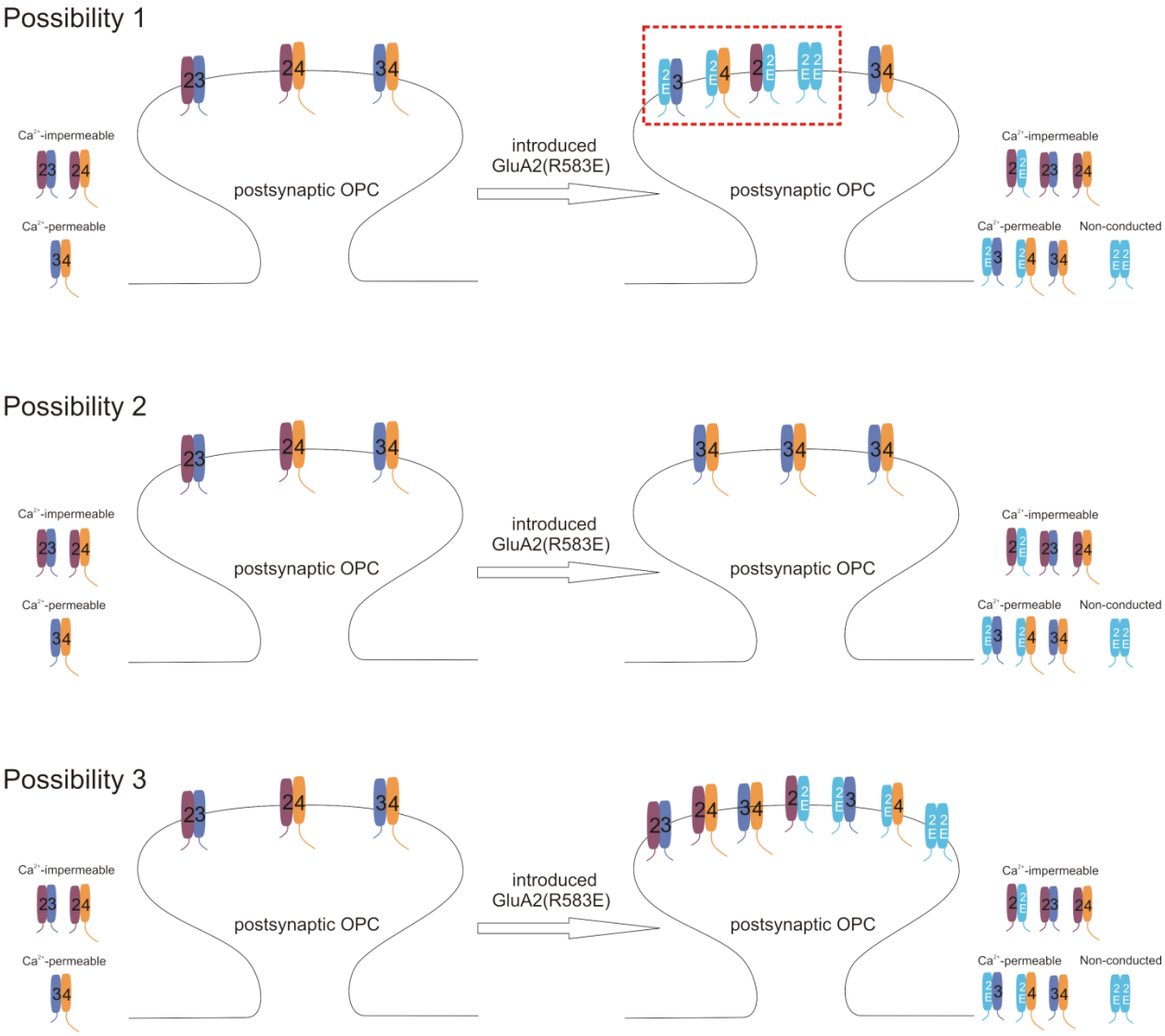


**Figure. 5-4 Three possibilities of subunits compositions of AMPARs after introducing GluA2(R583E) to OPCs.**

(*Top*) Schematic drawing showing that existing AMPARs may be replaced by the AMPARs with new combinations of subunits (red dash rectangle) after introducing GluA2(R583E) in OPCs. (*Middle*) Schematic drawing showing that existing GluA2-containing AMPARs may be removed; this may be accompanied by insertion of endogenous GluA3/4 subunits (in the right). (*Bottom*) Schematic drawing showing that pore-dead GluA2(R583E)-containing AMPARs may be inserted into the postsynaptic site of axon-OPC synapses (in the right) while the endogenous subunits do not get removed.

*5.1.3. GluA2(813-862 ) (“C-tail”) modification of the GluA2 subunit.*

The expression of GluA2 “C-tail” affected neither $Ca^{2+}$ permeability of AMPARs nor the amplitude of quantal axon-glia EPSCs (Fig. 4-13, 4-14). These results were different from the hippocampal pyramidal neurons, where expression of the GluA2 “C-tail” resulted in a decrease of the amplitude of synaptic AMPAR-mediated currents [119]. There may be several explanations why no electrophysiological changes were observed at synapses between axons and OPCs expressing GluA2 C-tail in my study:

(1) As indicated above, AMPARs traffic to synapses in a subunit-specific way depending on the intracellular C-terminal domain of the subunits. In general, if an AMPAR is composed of subunits with long and short intracellular C-terminal domain, trafficking is determined by the subunits with long intracellular C-terminal [119]. For example, for heteromeric GluA1/2 AMPARs trafficking is determined by GluA1 subunit which contains long C-terminal domain, and therefore these receptors traffic to synapses in an activity-dependent way [125-127]. If heteromeric GluA2/3 AMPARs are assembled, both GluA2 and GluA3 contain short C-terminal domain, therefore these receptors can continuously incorporate into synapses and replace the existing AMPARs [119]. Expression of GluA2 “C-tail”, i.e. the short C-terminus, in my experiments may have prevented the continuous synaptic delivery of endogenous AMPARs to the synapse, and in particular the delivery of hetero-tetrameric GluA2/3 receptors could have been affected. As a consequence, no new AMPARs were inserted into the postsynaptic sites, and therefore no existing AMPARs were removed from the synapse.

(2) Expression of GluA2 “C-tail” in OPCs prevented the synaptic delivery of endogenous AMPARs to the synapse, but the “missing” receptors were rapidly replenished from the pool of extrasynaptic AMPARs by lateral diffusion.

(3) It is currently not known whether OPCs express GluA2 subunit with short ($GluA2_{short}$) or with long ($GluA2_{long}$) C-terminus. If they contain only $GluA2_{long}$, the trafficking of AMPARs with this subunit may be activity-dependent, in analogy to neurons [127]. As I expressed short “C-tail” of the GluA2 subunit, this could have no effect on the delivery of the endogenous $GluA2_{long}$-containing AMPARs to axon-OPC synapses.

(4) The trafficking of GluA2-containing AMPARs in OPCs, mainly those with GluA2/3 subunits, did not depend on the interaction between the GluA2 C-terminus and AMPAR-binding proteins. Along this line, it has been demonstrated that in hippocampal neurons the recombinant GluA2 subunit without C-tail is able to traffic to synapse, thus suggesting that GluA2 C-tail may not necessarily be required for the trafficking of GluA2-containing AMPARs [129].

It is important to note that electrophysiological parameters which I have studied, aimed to investigate changes in the ionotropic function of postsynaptic AMPARs. Absence of those changes in OPCs expressing GluA2 "C-tail" does not mean that GluA2(813-862) construct has not modified physiology of the cells. For example, as indicated in the "Results" section, it is possible that GluA2 "C-tail" interfered with intracellular signaling via intracellular binding partners as has been proposed for neuronal synapses [102].

Taking together, up to now the trafficking mechanisms of AMPARs in OPCs are poorly understood, and my results provide some new insights regarding AMPARs trafficking in OPCs. My data suggest that expression of recombinant GluA2 subunits carrying point-mutations in the channel pore resulted in delivery and incorporation of these subunits into the postsynaptic sites of axon-OPC synapses in the corpus callosum. This may, or may not, have been accompanied by the removal of the existing AMPARs. As a result, I have observed changes in the inward rectification of the I-V relationship of axon-OPC EPSCs and a shift of the cumulative histogram of quantal amplitude to larger values. Expression of GluA2 "C-tail", the GluA2(813-862), in OPCs did not result in changes of I-V rectification or quantal amplitude, and different reasons can explain this finding. Importantly, the combinations of AMPARs subunits in OPCs are most likely not similar to neurons: the majority of AMPARs in neurons are composed of GluA1/A2 and/or GluA2/A3 subunits [48], but the expression of GluA1 subunit in OPCs is low [65]. Therefore, AMPARs in OPCs are likely composed of GluA2/A3, GluA2/A4, and GluA3/4 subunits. The composition of AMPARs also determine the ways of their trafficking [130], and therefore trafficking of AMPARs in OPCs is likely different from neurons.

AMPARs mediate most synaptic excitation, participate in synaptic plasticity, and play a role in epilepsy and many other diseases. In particular, it has been shown that AMPARs are among the important molecular targets in the therapy of epilepsy [131]. As AMPARs mediate synaptic

currents between neurons and OPCs, the signaling pathways which they initiate may be essential for remyelination [91-93]. Therefore, it is important to carry out further research aimed at understanding the subunit composition of AMPARs and their trafficking pathways in OPCs. These knowledges can help the development of the new therapeutic strategies for treatment of myelin-related diseases.

*5.2. Differentiation and proliferation of OPCs are influenced by AMPARs.*

*5.2.1. Role of $Ca^{2+}$ for proliferation of OPCs.*

Several studies indicated that AMPARs are involved in regulation of the differentiation and proliferation of OPCs in cell culture [33, 69, 95, 132]. However, it is so far not clear whether synaptic currents mediated by AMPARs in OPCs regulate their maturation or cell division. The findings of the present study demonstrate that introducing point mutation GluA2(R583Q) or GluA2(R583E) in the channel pore of the GluA2 subunit of AMPARs in callosal OPCs *in vivo* during the peak of myelination in the corpus callosum (i.e. second-third postnatal weeks), enhances $Ca^{2+}$ permeability of AMPARs (Fig. 4-13). This, in turn, leads to increased proliferation of OPCs and reduces their differentiation into OLs. $Ca^{2+}$ is known as secondary messenger and is involved in cell cycle regulation, migration, and differentiation of neural cells and oligodendrocyte lineage cells [133, 134]. Increase of cytoplasmic $Ca^{2+}$ level ($[Ca^{2+}]_i$) in OPCs can occur through several pathways, and activation of $Ca^{2+}$-permeable AMPARs is one of them (Fig. 5-5). Elevation of $[Ca^{2+}]_i$ is known to affect the activity of cyclin-dependent kinase activating kinases (CAKs) or cyclin-dependent kinases inhibitors (CKIs); the cell cycle progression, or cell cycle exit followed by differentiation, depends on the balance between these two mechanisms [134]. Therefore, too high or too low $Ca^{2+}$ entry through AMPARs during physiological and/or pathological conditions may affect self-renewal of OPCs and/or their differentiation in OLs, and may also cause imbalance between differentiation and proliferation.

Interestingly, I found that “pore-dead” mutation of GluA2 subunit expedited the cell cycle time of OPCs more than “$Ca^{2+}$-permeable” mutation (Fig. 4-23 d), although both modifications resulted in very similar electrophysiological changes at neuron-OPC synapses (Fig. 4-13, 4-14). The difference may result from the subunit compositions or the location of AMPARs.

Alternatively, or additionally, these two modifications may trigger distinct signaling cascades downstream of the AMPARs.

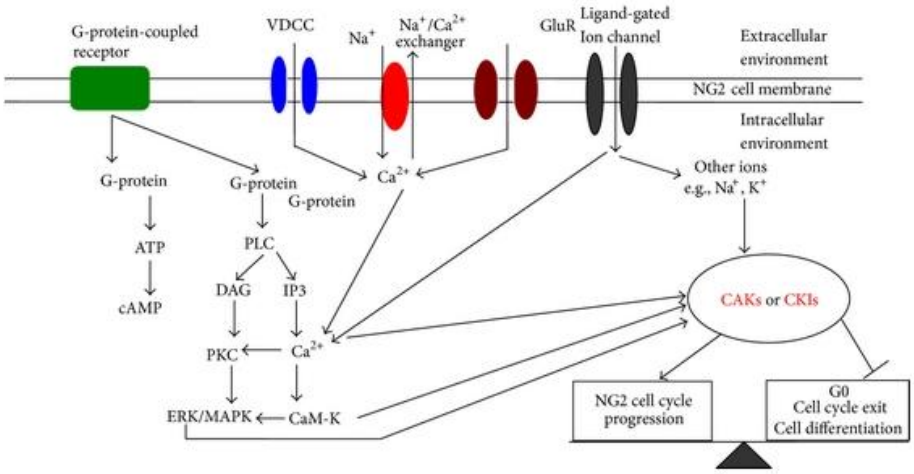


**Figure 5-5. Scheme showing possible signaling pathways of $Ca^{2+}$ entry to activate the cell cycle progression.**

AC: adenylate cyclase; CAKs: cyclin-dependent kinase activating kinases; CaM-K: calmodulin kinase; CKIs: cyclin-dependent kinases inhibitors; DAG: diacylglycerol; ERK/MAPK: extracellular signal-regulated kinase/mitogen-activated protein kinase; PKC: protein kinase C; PLC: phospholipase C. From [134].

### *5.2.2. Possible role of non-ionotropic function of AMPARs for differentiation of OPCs.*

The findings of the present study point to the fact that ionotropic function of AMPARs is not the only mechanism regulating OPC differentiation, because expression of GluA2 "C-tail" most likely altered differentiation of OPCs via a distinct mechanism. It has been reported that expressing β3 integrin in CG-4 cells line or in OPCs isolated from neonatal rat brain, inhibits differentiation of OPCs to MBP-positive cells [135]. Furthermore, the expression of integrin was regulated developmentally during differentiation of OPCs, i.e. $\alpha_v\beta1$ integrin was downregulated during differentiation [136]. GluA2 subunit of AMPARs forms a complex with myelin proteolipid protein (PLP)-integrin in OPCs [70]. Moreover, it has been reported that β3 integrin interacts with GluA2 subunit directly with their cytoplasmic domain and regulates the expression of cell-surface AMPARs in hippocampal neurons [137]. It is possible that "$Ca^{2+}$-permeable" or "pore-dead" GluA2 subunits, or the GluA2(813-826) "C-tail", in OPCs bound to integrin and

affected the ability of integrin to regulate OPCs differentiation by yet un-identified mechanism. This possible protein-protein interaction may explain how the GluA2(813-826) "C-tail", which did not alter ionotropic function of AMPARs in OPCs, reduced their differentiation in the present study. In the future, it would be interesting to investigate interaction between AMPARs and integrins, and to find out whether these interactions represent a mechanism modulating the development of OPCs.

*5.2.3. Energy consumption may contribute to reduced differentiation in OPCs expressing modified GluA2 subunits of AMPARs.*

According to general concept of energy use in the brain, the majority of energy is consumed for synaptic transmission (synaptic signaling), and "housekeeping" (non-signaling) processes, i.e. protein synthesis and/or protein turnover [138, 139]. Expression of exogenous subunits of AMPARs in OPCs may have resulted in additional energy consumption, i.e. for synthesis and turnover (insertion and removal from the synapse) of the added receptors. This may have contributed to the suppression of differentiation of OPCs. However, it is possible that observed reduction in differentiation of OCPs was short-term, and once the balance of energy consumption in OPCs has been re-adjusted, the process of differentiation of OPCs into mature OLs can be re-started and catches up with the loss of mature OLs. In the present study, I monitored the change in differentiation of OPCs 5 days after retroviral injection. As a next step, it would be interesting to check whether the decrease in differentiation of OPCs was short-term, or whether the changes persist at later time-points, i.e. 10 or 15 days after retroviral injection.

*5.2.4. Effects of acute modification versus chronic deletion of AMPARs in OPCs.*

Up to now several studies in cell culture, *in vitro*, and *in vivo* indicated that signal transmission through AMPARs in OPCs may affect differentiation and proliferation of OPCs [33, 82, 95, 99]. However, a recent study in mice *in vivo* has shown that double knock-out of *Gria2/3*, the genes encoding for GluA2 and GluA3 subunits of AMPARs respectively, reduced AMPARs-mediated signaling in OPCs, and the triple knock-out of *Gria2/3/4* abolished this signaling but neither of these modifications caused changes in proliferation of OPCs [65]. Yet, double and triple knock-out of AMPARs subunits in OPCs resulted in the reduced numbers of myelinating OLs, indicating that AMPAR-mediated signaling is important for survival of oligodendrocyte lineage

cells [65]. Knock-out of either *Gria2* or *Gria3* alone did not influence differentiation and proliferation of OPCs [65]. The findings of my study differ from the results of Kougioumtzidou et al. [65]. There may be several reasons for these differences. First, in the study of Kougioumtzidou et al. [65], ablation of single or multiple AMPAR subunits from the onset of mouse development may have initiated the compensatory pathways in the glutamatergic signaling, or in the regulation of proliferation and lineage progression of OPCs. On the contrary, I perturbed the AMPAR-mediated signaling after the neuron-OPC synaptic connections have been already established. This experimental approach may allow less time for compensatory effects to be switched on. Second, using our approach I did not delete the gene regulating expression of the endogenous GluA2 subunit. Therefore, the endogenous GluA2 subunit may have played a role in preventing the excitotoxic death in OPC [140-144]. Third, OPCs investigated in my study may represent a sub-population of OPCs investigated in the study of Kougioumtzidou et al. [65]. I used retroviral gene delivery approach to alter AMPAR-mediated signaling in OPCs. Retrovirus is known to target cells which are dividing at the time of infection; therefore the results observed in my study were from the OPCs which were proliferating at the time-point of viral infection. Those proliferating OPCs differentiated and/or underwent the second cell division within 5 days. In the study of Kougioumtzidou et al. [65], ablation of AMPARs genes was performed in all OPCs regardless of their proliferation status. The populations of OPCs may cause the differences. In the future, it would be interesting to investigate whether several cell divisions are necessary before an OPC starts differentiation and maturation process, and whether a defined time-interval is required between the end of proliferation and beginning of differentiation of OPCs.

Taken together, $Ca^{2+}$ permeability of AMPARs may be one of the mechanisms regulating proliferation of OPCs because $Ca^{2+}$-permeable GluA2 constructs ("$Ca^{2+}$-permeable" and "pore-dead") but not C-terminus of GluA2 led to the increase in proliferation. However, $Ca^{2+}$ permeability of AMPARs is not the only mechanism regulating differentiation of OPCs because expressing constructs of "$Ca^{2+}$-permeable", "pore-dead", or "C-tail" in OPCs resulted in the decrease in their differentiation to OLs.

Differentiation and proliferation are tightly regulated in OPCs because OPCs have to response to the cues for differentiation or proliferation at the right timing. It has been reported that OPCs

purified from optic nerve have an “intrinsic clock” to stop the cell division and start the differentiation [145]. It is possible that those two processes in OPCs are already programmed when OPCs are born. Understanding the mechanisms of differentiation and proliferation in OPCs are important because it may help for “re-program” the differentiation and/or proliferation of OPCs in the pathological conditions.

## 6. Conclusion.

In the present study I found that $Ca^{2+}$ signaling through AMPARs at the postsynaptic sites of neuron-OPC synapse is important for modulation the differentiation and proliferation of OPCs. My data also suggest that non-ionotropic functions of AMPARs may play an essential role in regulating differentiation of OPCs. Therefore, activation of AMPARs may trigger several pathways which participate in regulation of differentiation and proliferation of OPCs. As reported previously, neuronal activity modulates development and function of oligodendrocyte lineage cells [18, 82, 94-96], suggesting that alterations at the presynaptic part of axon-OPC synapses may play an important role in these processes. I found that the properties of AMPARs at the postsynaptic sites can also influence the proliferation and differentiation of OPCs.

Understanding the mechanisms of GluA2-dependent regulation of proliferation and differentiation of OPCs under physiological condition is fundamentally important. Over the long-term, the results of my study may also be applied to the demyelinating disorders, and may be instructive for the development of new therapeutic strategies for these diseases.

## 7. Future perspectives.

In order to understand the relationship between axon-OPC AMPAR-mediated signaling, differentiation and proliferation of OPCs, and myelination by OL, in the future it would be interesting to investigate the following issues:

(1) The basic mechanisms of AMPARs trafficking in OPCs;

(2) The downstream cascades of AMPARs-mediated signaling, and expression of genes which are involved in regulation of differentiation and proliferation of OPCs;

(3) Relationship between different patterns of neuronal activities and function of different AMPARs subunits in OPCs.

## 8. Reference.


1. Perez-Cerda, F., M.V. Sanchez-Gomez, and C. Matute, *Pio del Rio Hortega and the discovery of the oligodendrocytes.* Front Neuroanat, 2015. **9**: p. 92.
2. Siegel, G.J. and B.W. Agranoff, *Basic neurochemistry : molecular, cellular, and medical aspects*. 1999, Philadelphia, Pennsylvania: Lippincott Williams & Wilkins.
3. Hille, B., *Ion channels of excitable membranes*. 2007, Sunderland, Mass.: Sinauer.
4. Poliak, S. and E. Peles, *The local differentiation of myelinated axons at nodes of Ranvier.* Nat Rev Neurosci, 2003. **4**(12): p. 968-80.
5. Nishiyama, A., et al., *Co-localization of NG2 proteoglycan and PDGF alpha-receptor on O2A progenitor cells in the developing rat brain.* J Neurosci Res, 1996. **43**(3): p. 299-314.
6. Ozerdem, U., et al., *NG2 proteoglycan is expressed exclusively by mural cells during vascular morphogenesis.* Dev Dyn, 2001. **222**(2): p. 218-27.
7. Hartmann, D.A., et al., *Pericyte structure and distribution in the cerebral cortex revealed by high-resolution imaging of transgenic mice.* Neurophotonics, 2015. **2**(4): p. 041402.
8. Rivers, L.E., et al., *PDGFRA/NG2 glia generate myelinating oligodendrocytes and piriform projection neurons in adult mice.* Nat Neurosci, 2008. **11**(12): p. 1392-401.
9. Psachoulia, K., et al., *Cell cycle dynamics of NG2 cells in the postnatal and ageing brain.* Neuron Glia Biol, 2009. **5**(3-4): p. 57-67.
10. Kang, S.H., et al., *NG2+ CNS glial progenitors remain committed to the oligodendrocyte lineage in postnatal life and following neurodegeneration.* Neuron, 2010. **68**(4): p. 668-81.
11. Zhu, X., R.A. Hill, and A. Nishiyama, *NG2 cells generate oligodendrocytes and gray matter astrocytes in the spinal cord.* Neuron Glia Biol, 2008. **4**(1): p. 19-26.
12. Dimou, L., et al., *Progeny of Olig2-expressing progenitors in the gray and white matter of the adult mouse cerebral cortex.* J Neurosci, 2008. **28**(41): p. 10434-42.
13. Zhu, X., D.E. Bergles, and A. Nishiyama, *NG2 cells generate both oligodendrocytes and gray matter astrocytes.* Development, 2008. **135**(1): p. 145-57.
14. Zhu, X., et al., *Age-dependent fate and lineage restriction of single NG2 cells.* Development, 2011. **138**(4): p. 745-53.
15. Zhang, S.C., *Defining glial cells during CNS development.* Nat Rev Neurosci, 2001. **2**(11): p. 840-3.
16. Reynolds, R. and G.P. Wilkin, *Development of macroglial cells in rat cerebellum. II. An in situ immunohistochemical study of oligodendroglial lineage from precursor to mature myelinating cell.* Development, 1988. **102**(2): p. 409-25.
17. Scolding, N.J., et al., *Myelin-oligodendrocyte glycoprotein (MOG) is a surface marker of oligodendrocyte maturation.* J Neuroimmunol, 1989. **22**(3): p. 169-76.
18. Nagy, B., et al., *Different patterns of neuronal activity trigger distinct responses of oligodendrocyte precursor cells in the corpus callosum.* PLoS Biol, 2017. **15**(8): p. e2001993.
19. Xiao, L., et al., *Rapid production of new oligodendrocytes is required in the earliest stages of motor-skill learning.* Nat Neurosci, 2016. **19**(9): p. 1210-1217.
20. Zhang, Y., et al., *An RNA-sequencing transcriptome and splicing database of glia, neurons, and vascular cells of the cerebral cortex.* J Neurosci, 2014. **34**(36): p. 11929-47.
21. Morita, J., et al., *Structure and biological function of ENPP6, a choline-specific glycerophosphodiester-phosphodiesterase.* Sci Rep, 2016. **6**: p. 20995.
22. Nishiyama, A., et al., *Polydendrocytes (NG2 cells): multifunctional cells with lineage plasticity.* Nat Rev Neurosci, 2009. **10**(1): p. 9-22.
23. Dawson, M.R., et al., *NG2-expressing glial progenitor cells: an abundant and widespread population of cycling cells in the adult rat CNS.* Mol Cell Neurosci, 2003. **24**(2): p. 476-88.

24. Raff, M.C., R.H. Miller, and M. Noble, *A glial progenitor cell that develops in vitro into an astrocyte or an oligodendrocyte depending on culture medium.* Nature, 1983. **303**(5916): p. 390-6.
25. Larson, V.A., Y. Zhang, and D.E. Bergles, *Electrophysiological properties of NG2(+) cells: Matching physiological studies with gene expression profiles.* Brain Res, 2016. **1638**(Pt B): p. 138-160.
26. Takumi, T., et al., *A novel ATP-dependent inward rectifier potassium channel expressed predominantly in glial cells.* J Biol Chem, 1995. **270**(27): p. 16339-46.
27. Lin, S.C. and D.E. Bergles, *Physiological characteristics of NG2-expressing glial cells.* J Neurocytol, 2002. **31**(6-7): p. 537-49.
28. Chittajallu, R., A. Aguirre, and V. Gallo, *NG2-positive cells in the mouse white and grey matter display distinct physiological properties.* J Physiol, 2004. **561**(Pt 1): p. 109-22.
29. Knutson, P., et al., *K+ channel expression and cell proliferation are regulated by intracellular sodium and membrane depolarization in oligodendrocyte progenitor cells.* J Neurosci, 1997. **17**(8): p. 2669-82.
30. Chittajallu, R., et al., *Regulation of Kv1 subunit expression in oligodendrocyte progenitor cells and their role in G1/S phase progression of the cell cycle.* Proc Natl Acad Sci U S A, 2002. **99**(4): p. 2350-5.
31. Kukley, M., A. Nishiyama, and D. Dietrich, *The fate of synaptic input to NG2 glial cells: neurons specifically downregulate transmitter release onto differentiating oligodendroglial cells.* J Neurosci, 2010. **30**(24): p. 8320-31.
32. Borges, K., et al., *Adult rat optic nerve oligodendrocyte progenitor cells express a distinct repertoire of voltage- and ligand-gated ion channels.* J Neurosci Res, 1995. **40**(5): p. 591-605.
33. Yuan, X., et al., *A role for glutamate and its receptors in the regulation of oligodendrocyte development in cerebellar tissue slices.* Development, 1998. **125**(15): p. 2901-14.
34. Ghiani, C.A., et al., *Voltage-activated K+ channels and membrane depolarization regulate accumulation of the cyclin-dependent kinase inhibitors p27(Kip1) and p21(CIP1) in glial progenitor cells.* J Neurosci, 1999. **19**(13): p. 5380-92.
35. Williamson, A.V., D.A. Compston, and A.D. Randall, *Analysis of the ion channel complement of the rat oligodendrocyte progenitor in a commonly studied in vitro preparation.* Eur J Neurosci, 1997. **9**(4): p. 706-20.
36. Karadottir, R., et al., *Spiking and nonspiking classes of oligodendrocyte precursor glia in CNS white matter.* Nat Neurosci, 2008. **11**(4): p. 450-6.
37. De Biase, L.M., A. Nishiyama, and D.E. Bergles, *Excitability and synaptic communication within the oligodendrocyte lineage.* J Neurosci, 2010. **30**(10): p. 3600-11.
38. Ge, W.P., et al., *Dividing glial cells maintain differentiated properties including complex morphology and functional synapses.* Proc Natl Acad Sci U S A, 2009. **106**(1): p. 328-33.
39. Nakanishi, S., *Metabotropic glutamate receptors: synaptic transmission, modulation, and plasticity.* Neuron, 1994. **13**(5): p. 1031-7.
40. Pin, J.P. and R. Duvoisin, *The metabotropic glutamate receptors: structure and functions.* Neuropharmacology, 1995. **34**(1): p. 1-26.
41. Conn, P.J. and J.P. Pin, *Pharmacology and functions of metabotropic glutamate receptors.* Annu Rev Pharmacol Toxicol, 1997. **37**: p. 205-37.
42. Barres, B.A., et al., *Ion channel expression by white matter glia: the O-2A glial progenitor cell.* Neuron, 1990. **4**(4): p. 507-24.
43. Steinhauser, C., R. Jabs, and H. Kettenmann, *Properties of GABA and glutamate responses in identified glial cells of the mouse hippocampal slice.* Hippocampus, 1994. **4**(1): p. 19-35.

44. Berger, T., *AMPA-type glutamate receptors in glial precursor cells of the rat corpus callosum: ionic and pharmacological properties.* Glia, 1995. **14**(2): p. 101-14.
45. Partin, K.M., et al., *Selective modulation of desensitization at AMPA versus kainate receptors by cyclothiazide and concanavalin A.* Neuron, 1993. **11**(6): p. 1069-82.
46. Patneau, D.K., L. Vyklicky, Jr., and M.L. Mayer, *Hippocampal neurons exhibit cyclothiazide-sensitive rapidly desensitizing responses to kainate.* J Neurosci, 1993. **13**(8): p. 3496-509.
47. Dingledine, R., et al., *The glutamate receptor ion channels.* Pharmacol Rev, 1999. **51**(1): p. 7-61.
48. Lu, W., et al., *Subunit composition of synaptic AMPA receptors revealed by a single-cell genetic approach.* Neuron, 2009. **62**(2): p. 254-68.
49. Wenthold, R.J., et al., *Evidence for multiple AMPA receptor complexes in hippocampal CA1/CA2 neurons.* J Neurosci, 1996. **16**(6): p. 1982-9.
50. Isaac, J.T., M.C. Ashby, and C.J. McBain, *The role of the GluR2 subunit in AMPA receptor function and synaptic plasticity.* Neuron, 2007. **54**(6): p. 859-71.
51. Burnashev, N., et al., *Divalent ion permeability of AMPA receptor channels is dominated by the edited form of a single subunit.* Neuron, 1992. **8**(1): p. 189-98.
52. Hollmann, M., M. Hartley, and S. Heinemann, *Ca2+ permeability of KA-AMPA--gated glutamate receptor channels depends on subunit composition.* Science, 1991. **252**(5007): p. 851-3.
53. Geiger, J.R., et al., *Relative abundance of subunit mRNAs determines gating and Ca2+ permeability of AMPA receptors in principal neurons and interneurons in rat CNS.* Neuron, 1995. **15**(1): p. 193-204.
54. Verdoorn, T.A., et al., *Structural determinants of ion flow through recombinant glutamate receptor channels.* Science, 1991. **252**(5013): p. 1715-8.
55. Donevan, S.D. and M.A. Rogawski, *Intracellular polyamines mediate inward rectification of Ca(2+)-permeable alpha-amino-3-hydroxy-5-methyl-4-isoxazolepropionic acid receptors.* Proc Natl Acad Sci U S A, 1995. **92**(20): p. 9298-302.
56. Kamboj, S.K., G.T. Swanson, and S.G. Cull-Candy, *Intracellular spermine confers rectification on rat calcium-permeable AMPA and kainate receptors.* J Physiol, 1995. **486 ( Pt 2)**: p. 297-303.
57. Bowie, D. and M.L. Mayer, *Inward rectification of both AMPA and kainate subtype glutamate receptors generated by polyamine-mediated ion channel block.* Neuron, 1995. **15**(2): p. 453-62.
58. Koh, D.S., N. Burnashev, and P. Jonas, *Block of native Ca(2+)-permeable AMPA receptors in rat brain by intracellular polyamines generates double rectification.* J Physiol, 1995. **486 ( Pt 2)**: p. 305-12.
59. Henley, J.M. and K.A. Wilkinson, *Synaptic AMPA receptor composition in development, plasticity and disease.* Nat Rev Neurosci, 2016. **17**(6): p. 337-50.
60. Liu, S.J. and R.S. Zukin, *Ca2+-permeable AMPA receptors in synaptic plasticity and neuronal death.* Trends Neurosci, 2007. **30**(3): p. 126-34.
61. Patneau, D.K., et al., *Glial cells of the oligodendrocyte lineage express both kainate- and AMPA-preferring subtypes of glutamate receptor.* Neuron, 1994. **12**(2): p. 357-71.
62. Cahoy, J.D., et al., *A transcriptome database for astrocytes, neurons, and oligodendrocytes: a new resource for understanding brain development and function.* J Neurosci, 2008. **28**(1): p. 264-78.
63. Yoshioka, A., et al., *Alpha-amino-3-hydroxy-5-methyl-4-isoxazolepropionate (AMPA) receptors mediate excitotoxicity in the oligodendroglial lineage.* J Neurochem, 1995. **64**(6): p. 2442-8.
64. Chew, L.J., et al., *Growth factor-induced transcription of GluR1 increases functional AMPA receptor density in glial progenitor cells.* J Neurosci, 1997. **17**(1): p. 227-40.
65. Kougioumtzidou, E., et al., *Signalling through AMPA receptors on oligodendrocyte precursors promotes myelination by enhancing oligodendrocyte survival.* Elife, 2017. **6**.

66. Itoh, T., et al., *AMPA glutamate receptor-mediated calcium signaling is transiently enhanced during development of oligodendrocytes.* J Neurochem, 2002. **81**(2): p. 390-402.
67. Hamilton, N., et al., *Axons and astrocytes release ATP and glutamate to evoke calcium signals in NG2-glia.* Glia, 2010. **58**(1): p. 66-79.
68. Liu, H.N., et al., *AMPA receptor-mediated toxicity in oligodendrocyte progenitors involves free radical generation and activation of JNK, calpain and caspase 3.* J Neurochem, 2002. **82**(2): p. 398-409.
69. Hossain, S., et al., *Agonist-induced down-regulation of AMPA receptors in oligodendrocyte progenitors.* Neuropharmacology, 2014. **79**: p. 506-14.
70. Harlow, D.E., et al., *Myelin Proteolipid Protein Complexes with alphav Integrin and AMPA Receptors In Vivo and Regulates AMPA-Dependent Oligodendrocyte Progenitor Cell Migration through the Modulation of Cell-Surface GluR2 Expression.* J Neurosci, 2015. **35**(34): p. 12018-32.
71. Gudz, T.I., H. Komuro, and W.B. Macklin, *Glutamate stimulates oligodendrocyte progenitor migration mediated via an alphav integrin/myelin proteolipid protein complex.* J Neurosci, 2006. **26**(9): p. 2458-66.
72. Ong, W.Y., et al., *A light- and electron-microscopic study of GluR4-positive cells in cerebral cortex, subcortical white matter and corpus callosum of neonatal, immature and adult rats.* Exp Brain Res, 1996. **110**(3): p. 367-78.
73. Rosenberg, P.A., et al., *Mature myelin basic protein-expressing oligodendrocytes are insensitive to kainate toxicity.* J Neurosci Res, 2003. **71**(2): p. 237-45.
74. Bergles, D.E., et al., *Glutamatergic synapses on oligodendrocyte precursor cells in the hippocampus.* Nature, 2000. **405**(6783): p. 187-91.
75. Kukley, M., E. Capetillo-Zarate, and D. Dietrich, *Vesicular glutamate release from axons in white matter.* Nat Neurosci, 2007. **10**(3): p. 311-20.
76. Ziskin, J.L., et al., *Vesicular release of glutamate from unmyelinated axons in white matter.* Nat Neurosci, 2007. **10**(3): p. 321-30.
77. Fremeau, R.T., Jr., et al., *The expression of vesicular glutamate transporters defines two classes of excitatory synapse.* Neuron, 2001. **31**(2): p. 247-60.
78. El Mestikawy, S., et al., *From glutamate co-release to vesicular synergy: vesicular glutamate transporters.* Nat Rev Neurosci, 2011. **12**(4): p. 204-16.
79. Lin, S.C., et al., *Climbing fiber innervation of NG2-expressing glia in the mammalian cerebellum.* Neuron, 2005. **46**(5): p. 773-85.
80. Muller, J., et al., *The principal neurons of the medial nucleus of the trapezoid body and NG2(+) glial cells receive coordinated excitatory synaptic input.* J Gen Physiol, 2009. **134**(2): p. 115-27.
81. Parri, H.R., T.M. Gould, and V. Crunelli, *Sensory and cortical activation of distinct glial cell subtypes in the somatosensory thalamus of young rats.* Eur J Neurosci, 2010. **32**(1): p. 29-40.
82. Mangin, J.M., et al., *Experience-dependent regulation of NG2 progenitors in the developing barrel cortex.* Nat Neurosci, 2012. **15**(9): p. 1192-4.
83. Gallo, V., et al., *Synapses on NG2-expressing progenitors in the brain: multiple functions?* J Physiol, 2008. **586**(16): p. 3767-81.
84. Passlick, S., et al., *The NG2 Protein Is Not Required for Glutamatergic Neuron-NG2 Cell Synaptic Signaling.* Cereb Cortex, 2016. **26**(1): p. 51-7.
85. Ge, W.P., et al., *Long-term potentiation of neuron-glia synapses mediated by Ca2+-permeable AMPA receptors.* Science, 2006. **312**(5779): p. 1533-7.
86. Koike, M., M. Iino, and S. Ozawa, *Blocking effect of 1-naphthyl acetyl spermine on Ca(2+)-permeable AMPA receptors in cultured rat hippocampal neurons.* Neurosci Res, 1997. **29**(1): p. 27-36.

87. Sciancalepore, M., et al., *Facilitation of miniature GABAergic currents by ruthenium red in neonatal rat hippocampal neurons.* J Neurophysiol, 1998. **80**(5): p. 2316-22.
88. Spitzer, S., et al., *Glutamate signalling: A multifaceted modulator of oligodendrocyte lineage cells in health and disease.* Neuropharmacology, 2016. **110**(Pt B): p. 574-585.
89. Kukley, M., et al., *Glial cells are born with synapses.* FASEB J, 2008. **22**(8): p. 2957-69.
90. Martin, D.L. and K. Rimvall, *Regulation of gamma-aminobutyric acid synthesis in the brain.* J Neurochem, 1993. **60**(2): p. 395-407.
91. Sahel, A., et al., *Alteration of synaptic connectivity of oligodendrocyte precursor cells following demyelination.* Front Cell Neurosci, 2015. **9**: p. 77.
92. Gautier, H.O., et al., *Neuronal activity regulates remyelination via glutamate signalling to oligodendrocyte progenitors.* Nat Commun, 2015. **6**: p. 8518.
93. Etxeberria, A., et al., *Adult-born SVZ progenitors receive transient synapses during remyelination in corpus callosum.* Nat Neurosci, 2010. **13**(3): p. 287-289.
94. Gibson, E.M., et al., *Neuronal activity promotes oligodendrogenesis and adaptive myelination in the mammalian brain.* Science, 2014. **344**(6183): p. 1252304.
95. Fannon, J., W. Tarmier, and D. Fulton, *Neuronal activity and AMPA-type glutamate receptor activation regulates the morphological development of oligodendrocyte precursor cells.* Glia, 2015. **63**(6): p. 1021-35.
96. Barres, B.A. and M.C. Raff, *Proliferation of oligodendrocyte precursor cells depends on electrical activity in axons.* Nature, 1993. **361**(6409): p. 258-60.
97. Demerens, C., et al., *Induction of myelination in the central nervous system by electrical activity.* Proc Natl Acad Sci U S A, 1996. **93**(18): p. 9887-92.
98. Hill, R.A., et al., *Modulation of oligodendrocyte generation during a critical temporal window after NG2 cell division.* Nat Neurosci, 2014. **17**(11): p. 1518-27.
99. Trapp, B.D., et al., *Cellular and subcellular distribution of 2',3'-cyclic nucleotide 3'-phosphodiesterase and its mRNA in the rat central nervous system.* J Neurochem, 1988. **51**(3): p. 859-68.
100. Hume, R.I., R. Dingledine, and S.F. Heinemann, *Identification of a site in glutamate receptor subunits that controls calcium permeability.* Science, 1991. **253**(5023): p. 1028-31.
101. Dingledine, R., R.I. Hume, and S.F. Heinemann, *Structural determinants of barium permeation and rectification in non-NMDA glutamate receptor channels.* J Neurosci, 1992. **12**(10): p. 4080-7.
102. Bassani, S., et al., *The GLUR2 subunit of AMPA receptors: synaptic role.* Neuroscience, 2009. **158**(1): p. 55-61.
103. Addgene. *Subcloning*. no date [cited 2017 June]; Available from: https://www.addgene.org/protocols/subcloning/.
104. Tashiro, A., C. Zhao, and F.H. Gage, *Retrovirus-mediated single-cell gene knockout technique in adult newborn neurons in vivo.* Nat Protoc, 2006. **1**(6): p. 3049-55.
105. Young, K.M., et al., *Oligodendrocyte dynamics in the healthy adult CNS: evidence for myelin remodeling.* Neuron, 2013. **77**(5): p. 873-85.
106. Kukley, M., A. Nishiyama, and D. Dietrich, *The fate of synaptic input to NG2 glial cells: neurons specifically downregulate transmitter release onto differentiating oligodendroglial cells.* J. Neurosci, 2010. **30**(24): p. 8320-8331.
107. Pernia-Andrade, A.J., et al., *A deconvolution-based method with high sensitivity and temporal resolution for detection of spontaneous synaptic currents in vitro and in vivo.* Biophys J, 2012. **103**(7): p. 1429-39.
108. Aguirre, A. and V. Gallo, *Reduced EGFR signaling in progenitor cells of the adult subventricular zone attenuates oligodendrogenesis after demyelination.* Neuron Glia Biol, 2007. **3**(3): p. 209-20.

109. Zbio.net. *DNA to Protein*. July 30 2013 [cited 2017 Nov]; Available from: http://www.molbiol.ru/eng/scripts/01_06.html.
110. Wang, R. and M.G. Brattain, *The maximal size of protein to diffuse through the nuclear pore is larger than 60kDa.* FEBS Lett, 2007. **581**(17): p. 3164-70.
111. Moshrefi-Ravasdjani, B., et al., *Changes in the proliferative capacity of NG2 cell subpopulations during postnatal development of the mouse hippocampus.* Brain Struct Funct, 2017. **222**(2): p. 831-847.
112. Frohlich, N., et al., *Fate of neuron-glia synapses during proliferation and differentiation of NG2 cells.* J Anat, 2011. **219**(1): p. 18-32.
113. Oliet, S.H., R.C. Malenka, and R.A. Nicoll, *Bidirectional control of quantal size by synaptic activity in the hippocampus.* Science, 1996. **271**(5253): p. 1294-7.
114. Choi, S. and D.M. Lovinger, *Decreased frequency but not amplitude of quantal synaptic responses associated with expression of corticostriatal long-term depression.* J Neurosci, 1997. **17**(21): p. 8613-20.
115. McNaughton, B.L., *Long-term synaptic enhancement and short-term potentiation in rat fascia dentata act through different mechanisms.* J Physiol, 1982. **324**: p. 249-62.
116. Atluri, P.P. and W.G. Regehr, *Determinants of the time course of facilitation at the granule cell to Purkinje cell synapse.* J Neurosci, 1996. **16**(18): p. 5661-71.
117. Swanson, G.T., S.K. Kamboj, and S.G. Cull-Candy, *Single-channel properties of recombinant AMPA receptors depend on RNA editing, splice variation, and subunit composition.* J Neurosci, 1997. **17**(1): p. 58-69.
118. Buck, S.B., et al., *Detection of S-phase cell cycle progression using 5-ethynyl-2'-deoxyuridine incorporation with click chemistry, an alternative to using 5-bromo-2'-deoxyuridine antibodies.* Biotechniques, 2008. **44**(7): p. 927-9.
119. Shi, S., et al., *Subunit-specific rules governing AMPA receptor trafficking to synapses in hippocampal pyramidal neurons.* Cell, 2001. **105**(3): p. 331-43.
120. Takahashi, T., K. Svoboda, and R. Malinow, *Experience strengthening transmission by driving AMPA receptors into synapses.* Science, 2003. **299**(5612): p. 1585-8.
121. Sudo, M., et al., *Postsynaptic expression of Ca2+-permeable AMPA-type glutamate receptor channels by viral-mediated gene transfer.* Brain Res Mol Brain Res, 1999. **65**(2): p. 176-85.
122. Soto, D., et al., *Stargazin attenuates intracellular polyamine block of calcium-permeable AMPA receptors.* Nat Neurosci, 2007. **10**(10): p. 1260-7.
123. Deng, W., et al., *Alpha-amino-3-hydroxy-5-methyl-4-isoxazole propionate receptor subunit composition and cAMP-response element-binding protein regulate oligodendrocyte excitotoxicity.* J Biol Chem, 2006. **281**(47): p. 36004-11.
124. Kohler, M., H.C. Kornau, and P.H. Seeburg, *The organization of the gene for the functionally dominant alpha-amino-3-hydroxy-5-methylisoxazole-4-propionic acid receptor subunit GluR-B.* J Biol Chem, 1994. **269**(26): p. 17367-70.
125. Shi, S.H., et al., *Rapid spine delivery and redistribution of AMPA receptors after synaptic NMDA receptor activation.* Science, 1999. **284**(5421): p. 1811-6.
126. Zhu, J.J., et al., *Postnatal synaptic potentiation: delivery of GluR4-containing AMPA receptors by spontaneous activity.* Nat Neurosci, 2000. **3**(11): p. 1098-106.
127. Kolleker, A., et al., *Glutamatergic plasticity by synaptic delivery of GluR-B(long)-containing AMPA receptors.* Neuron, 2003. **40**(6): p. 1199-212.
128. Stubblefield, E.A. and T.A. Benke, *Distinct AMPA-type glutamatergic synapses in developing rat CA1 hippocampus.* J Neurophysiol, 2010. **104**(4): p. 1899-912.

129. Panicker, S., K. Brown, and R.A. Nicoll, *Synaptic AMPA receptor subunit trafficking is independent of the C terminus in the GluR2-lacking mouse.* Proc Natl Acad Sci U S A, 2008. **105**(3): p. 1032-7.
130. Shepherd, J.D. and R.L. Huganir, *The cell biology of synaptic plasticity: AMPA receptor trafficking.* Annu Rev Cell Dev Biol, 2007. **23**: p. 613-43.
131. Rogawski, M.A., *AMPA receptors as a molecular target in epilepsy therapy.* Acta Neurol Scand Suppl, 2013(197): p. 9-18.
132. Gallo, V., et al., *Oligodendrocyte progenitor cell proliferation and lineage progression are regulated by glutamate receptor-mediated K+ channel block.* J Neurosci, 1996. **16**(8): p. 2659-70.
133. Toth, A.B., A.K. Shum, and M. Prakriya, *Regulation of neurogenesis by calcium signaling.* Cell Calcium, 2016. **59**(2-3): p. 124-34.
134. Yang, Q.K., J.X. Xiong, and Z.X. Yao, *Neuron-NG2 cell synapses: novel functions for regulating NG2 cell proliferation and differentiation.* Biomed Res Int, 2013. **2013**: p. 402843.
135. Blaschuk, K.L., E.E. Frost, and C. ffrench-Constant, *The regulation of proliferation and differentiation in oligodendrocyte progenitor cells by alphaV integrins.* Development, 2000. **127**(9): p. 1961-9.
136. Milner, R. and C. Ffrench-Constant, *A developmental analysis of oligodendroglial integrins in primary cells: changes in alpha v-associated beta subunits during differentiation.* Development, 1994. **120**(12): p. 3497-506.
137. Pozo, K., et al., *beta3 integrin interacts directly with GluA2 AMPA receptor subunit and regulates AMPA receptor expression in hippocampal neurons.* Proc Natl Acad Sci U S A, 2012. **109**(4): p. 1323-8.
138. Engl, E., et al., *Non-signalling energy use in the developing rat brain.* J Cereb Blood Flow Metab, 2017. **37**(3): p. 951-966.
139. Harris, J.J., R. Jolivet, and D. Attwell, *Synaptic energy use and supply.* Neuron, 2012. **75**(5): p. 762-77.
140. Follett, P.L., et al., *NBQX attenuates excitotoxic injury in developing white matter.* J Neurosci, 2000. **20**(24): p. 9235-41.
141. Pitt, D., P. Werner, and C.S. Raine, *Glutamate excitotoxicity in a model of multiple sclerosis.* Nat Med, 2000. **6**(1): p. 67-70.
142. Matute, C., et al., *The link between excitotoxic oligodendroglial death and demyelinating diseases.* Trends Neurosci, 2001. **24**(4): p. 224-30.
143. Li, S. and P.K. Stys, *Mechanisms of ionotropic glutamate receptor-mediated excitotoxicity in isolated spinal cord white matter.* J Neurosci, 2000. **20**(3): p. 1190-8.
144. Tekkok, S.B. and M.P. Goldberg, *Ampa/kainate receptor activation mediates hypoxic oligodendrocyte death and axonal injury in cerebral white matter.* J Neurosci, 2001. **21**(12): p. 4237-48.
145. Temple, S. and M.C. Raff, *Clonal analysis of oligodendrocyte development in culture: evidence for a developmental clock that counts cell divisions.* Cell, 1986. **44**(5): p. 773-9.